Portofoliu de lucrări relevante pentru domeniul de doctorat Ingineria Autovehiculelor

Prof.dr.ing. Stelian Ţârulescu

1. Taus N., Ţârulescu S., Idomir M., Taus R., Respiratory exposure to air pollutants, Journal of Environmental Protection and Ecology 9, No 1, 15-25 (2008), ISSN 1311-5065, ISI indexed Factor de Impact 2008 = 0.102, SCOPUS indexed SJR 0.035, SNIP 0.051, WOS:000255086100002
https://www.webofscience.com/wos/woscc/full-record/WOS:000255086100002

2. Ţârulescu S., Tarulescu R., Soica A., Mathematical model of pollution compounds calculus in function of traffic capacity from urban areas, Proceedings of the 1st WSEAS International Conference on Multivariate Analysis and its Application in Science and Engineering (MAASE 08), Istanbul, Turcia, 27-30 mai 2008, ISSN: 1790-5117, ISBN: 978-960-6766-65-7, ISI Thomson Reuters. https://www.webofscience.com/wos/woscc/full-record/WOS:000257948800018

3. Ţârulescu, S., Ţârulescu, R., Leahu, CI. (2020). On-Board Measurement of Emissions from Spark Ignition Engine Vehicle for Urban Routes. In: Dumitru, I., Covaciu, D., Racila, L., Rosca, A. (eds) The 30th SIAR International Congress of Automotive and Transport Engineering. SMAT 2019. Springer, Cham. https://doi.org/10.1007/978-3-030-32564-0_29, WOS:000528526600029, https://www.webofscience.com/wos/woscc/full-record/WOS:000528526600029

4. Ţârulescu S., Ţârulescu R., Şoica A., Leahu C. I., Smart Transportation CO2 Emission Reduction Strategies, IOP Conference Series: Materials Science and Engineering, Volume 252, Conference 1, indexare ISI 2018, WOS:000419817200051, https://www.webofscience.com/wos/woscc/full-record/WOS:000419817200051

5. Ţârulescu S., Ţârulescu R., Researches on Combustion Quality for a Single Cylinder Diesel Engine, 12th International Congress of Automotive and Transport Engineering (CONAT), DOI: 10.1007/978-3-319-45447-4_48, ISBN:978-3-319-45447-4, indexare ISI 2017, WOS:000390821400048, https://www.webofscience.com/wos/woscc/full-record/WOS:000390821400048

6. Țârulescu S., Țârulescu R., Urban Transportation Solutions for the CO2 Emissions Reduction Contributions, 12th International Congress of Automotive and Transport Engineering (CONAT), DOI: 10.1007/978-3-319-45447-4_49, ISBN:978-3-319-45447-4, indexare ISI 2017, WOS:000390821400049, https://www.webofscience.com/wos/woscc/full-record/WOS:000390821400049

7. Țârulescu R., Țârulescu S., Electronic Control Systems of E-Smart Vehicle, 12th International Congress of Automotive and Transport Engineering (CONAT), DOI: 10.1007/978-3-319-45447-4_49, ISBN:978-3-319-45447-4, indexare ISI 2017, WOS:000390821400056, https://www.webofscience.com/wos/woscc/full-record/WOS:000390821400056

8. Leahu, CI., Țârulescu, S., Radu S., Steady state engine efficiency specific to series hybrid electric vehicles, Ingineria Autovehiculului, (50), pp.19-22, martie 2019, WOS:000486368200008, https://www.webofscience.com/wos/woscc/full-record/WOS:000486368200008

9. Șoica A., Țârulescu S., "Impact phase in frontal vehicle-pedestrian collisions ", International Journal Of Automotive Technology, 2016, Volume: 17 Issue: 3 Pages: 387-397 DOI: 10.1007/s12239-016-0040-y 2016, ISSN: 1229-9138, WOS:000375449200004, https://www.webofscience.com/wos/woscc/full-record/WOS:000375449200004

10. Țârulescu, R., Țârulescu, S., Soica, A. (2019). Optimization of Cooling System for Internal Combustion Engines. In: Burnete, N., Varga, B. (eds) Proceedings of the 4th International Congress of Automotive and Transport Engineering (AMMA 2018). AMMA2018 2018. Proceedings in Automotive Engineering. Springer, Cham. https://doi.org/10.1007/978-3-319-94409-8_62, WOS:000578264900062, https://www.webofscience.com/wos/woscc/full-record/WOS:000578264900062

Brașov, 8.10.2024 **Prof.dr.ing. Stelian ȚÂRULESCU**

[redacted]

Journal of Environmental Protection and Ecology 9, No 1, 15–25 (2008)

RESPIRATORY EXPOSURE TO AIR POLLUTANTS

N. TAUS*, S. TARULESCU, M. IDOMIR, R. TAUS

Transilvania University of Brasov, 29 Eroilor Blvd., 500 036 Brasov, Romania
E-mail: *nicoletataus@yahoo.com*

Abstract. Mobile source emissions are important contributors to ambient air pollution. Exposure to ambient particulate matter has been associated with cardiopulmonary morbidity and mortality, including asthma. Causal biological mechanisms about health effects of air pollution are only partly understood. Air pollution exposure has been associated with compromised pulmonary immune defence mechanisms in both animals and humans. Exposure to polycyclic aromatic hydrocarbons – especially benzopyrene – can cause immune suppression, increases the risk of infection and disease, and increases the risk of lung and other types of cancers. Acute exposures to oxides of nitrogen and sulphur have been associated with increased bronchial reactivity and susceptibility to bacterial and viral infections. Our aim with this article is to review the prevalence of mobile source emissions in Brasov and Constanta. In this study, combustion particles from vehicle exhaust (CH_4, NO, CO, COU) were analysed with MX 21 PLUS (OLDHAM) in August 2005 and June 2006. Air pollution contains complex mixtures of many pollutants, which vary overtime and from place to place. Traffic-related exposure shows a light pollution between 15-16 o'clock. This study has shown ambient air pollution increase with proximity to roadways. This study provides important insights into the physicochemical components of engine emissions that most strongly influence the toxicity of inhaled emissions.

Keywords: air pollutant, acute exposures, MX 21 PLUS.

AIMS AND BACKGROUND

In recent years, much attention has been given to review reports on the early effects of air pollution on health[1–3].

Air pollution exposure has been associated with compromised pulmonary immune defense mechanisms in both animals and humans[4–7].

Air pollution induces a systemic inflammatory response involving stimulation of the bone marrow, which can contribute to cardiorespiratory morbidity. Exposure to polycyclic aromatic hydrocarbons – especially benzopyrene – induces immune suppression and can increase the risk of infection and disease[8–11].

Benzopyrene can increase the risk of lung and other types of cancers.

Acute exposures to oxides of nitrogen and sulphur have been associated with increased bronchial reactivity and susceptibility to bacterial and viral infections[12–15].

* For correspondence.

Mobile sources pollute the air through combustion and fuel evaporation. These emissions contribute greatly to air pollution nationwide and are the primary cause of air pollution in many urban areas.

Our aim with this article is to review the prevalence of mobile source emissions in Brasov and Constanta.

EXPERIMENTAL

In this study, combustion particles from vehicle exhaust (CH_4, NO, CO, COU) were analysed with MX 21 PLUS (OLDHAM) in August 2005 and June 2006.

RESULTS

Intersection – Castanilor street + Iuliu Maniu street + 13 Decembrie street. This intersection is signalled by traffic light (3-phase traffic light), having three access ways (entries), while the road fluxes corresponding to these entries differ in terms of their size and structure, from the point of view of vehicle categories. The busiest acces way is Iuliu Maniu street, more exactly the transit of vehicles from the civic center towards the historical center of the city. The values of vehicle fluxes are presented for each access way in Tables 1-4.

Table 1. Flux of vehicles in the access way Iuliu Maniu street

Cars			Common transportation vehicles			Trucks		
left	forward	right	left	forward	right	left	forward	right
237	1773	321	0	79	9	3	9	2

Table 2. Flux of vehicles in the access way 13 Decembrie street

Cars			Common transportation vehicles			Trucks		
left	forward	right	left	forward	right	left	forward	right
0	780	615	0	18	33	0	8	6

Table 3. Flux of vehicles in the access way Castanilor street

Cars			Common transportation vehicles			Trucks		
left	forward	right	left	forward	right	left	forward	right
186	597	0	0	37	0	6	16	0

Table 4. Total flux of vehicles in the intersection

Cars	Common transportation vehicles	Trucks
4509	50	176

In a hour's time (15.00-16.00), the intersection has been crossed by approximately 4500 cars, approximately 175 common transportation vehicles (jointed and nonjointed buses and trolleybuses), and approximately 50 trucks. Because the authorities built the traffic lane to the right in 2005, the vehicle capacity of the intersection in the access way 13 Decembrie street has increased as compared to previous years.

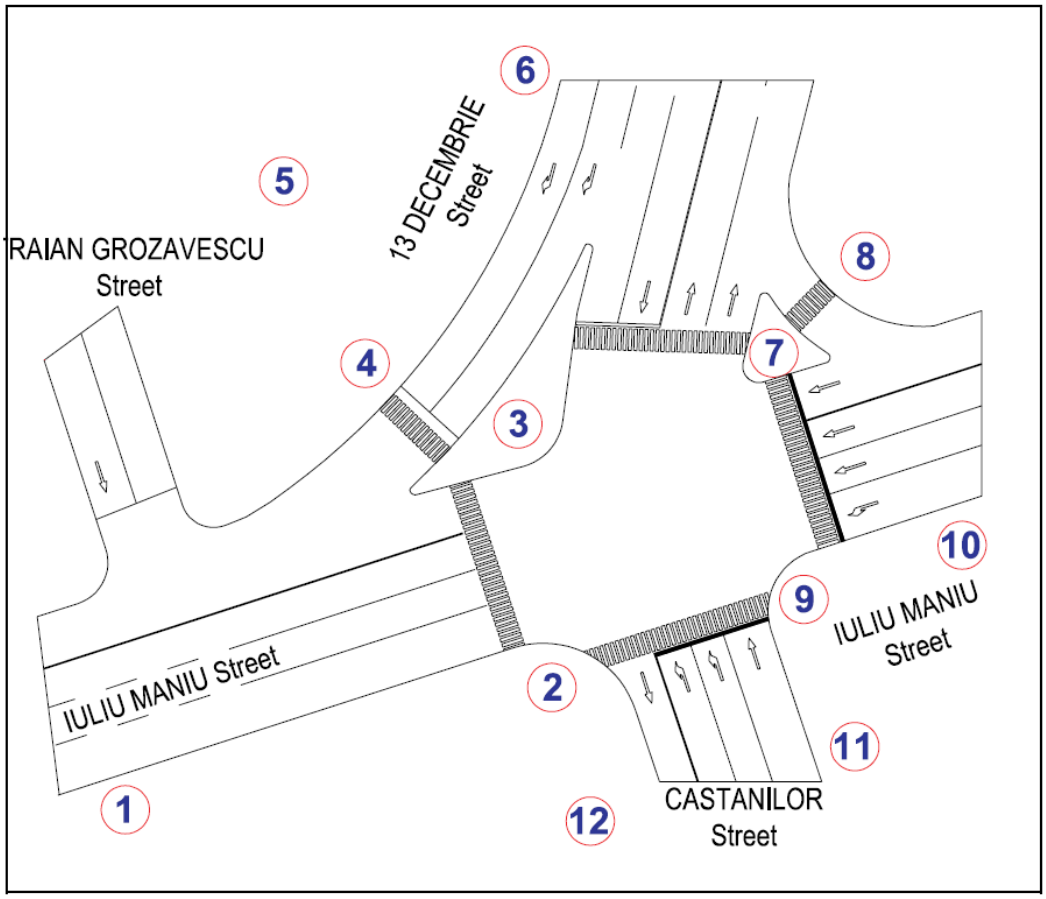

Fig. 1. Measurement points intersection – Castanilor street + Iuliu Maniu street + 13 Decembrie street

The concentrations of nitrogen monoxide, volatile organic compounds and carbon monoxide in the measurement points intersection (Fig. 1) have been registered and the data are shown in Table 5.

Table 5. Concentrations of nitrogen monoxide, volatile organic compounds and carbon monoxide

No*	CH_4 (%)	NO (ppm)	CO (ppm)	VOC (ppm)
1	63	2	4	2
2	63	2	7	8
3	63	2	1	3
4	63	2	2	2
5	63	2	1	2
6	63	3	4	5
7	63	2	4	2
8	63	2	4	7
9	63	2	6	7
10	63	2	4	5
11	63	2	4	5
12	63	2	1	2

* Measurement points inleresection as shown in Fig. 1; CH_4 – indicates the atmosphere security level (LEL); NO – indicates the nitrogen monoxide level; CO – indicates the carbon monoxide level; VOC – indicates the level of volatile organic compounds.

The concentration of CH_4 has been registered by an explosive gas cell. The range of this cell is from 0 to 100% and for a hazardous area the level of LEL CH_4 exceeds 75%. The level of nitrogen monoxide for most of the points of the measured interval is 2 ppm. Only for point 6 this value is 3 ppm, and the reason for that is the high concentration of vehicles for this road section (access to 13 Decembrie street).

The carbon monoxide level is 4 ppm for most of the measurement points. The concentration of CO for measurement points 2 and 9 is 7 and 6 ppm, respectively. The level of CO is higher for these points because these are situated on the main access of the intersection (Iuliu Maniu street).

The level of volatile organic compounds is different for all measurement points. The concentration of VOC for point 2 is 8 ppm and for points 8 and 9 - 7 ppm. The reason for these higher values of VOC is due to the fact that these 3 points are situated on the main access of the intersection (Iuliu Maniu street). For the rest of the point the level of VOC varies between 2 and 5 ppm.

Intersection – Nicolae Balcescu street + Dobrogeanu Gherea street. This intersection is signalled by traffic light (2-phase trafffic light), having two access ways (entries) and the road fluxes corresponding to these entries differ in terms of their size and structure from the point of view of vehicle categories. The busiest access way is Nicolae Balcescu street – coming from Piata Unirii, that is the transit of vehicles coming from the historical center towards the civic center of the city.

Table 6. Flux of vehicles in the access way Nicolae Balcescu street – coming from Teatrul Dramatic

Cars			Common transportation vehicles			Trucks		
left	forward	right	left	forward	right	left	forward	right
129	0	174	0	0	0	2	0	0

Table 7. Flux of vehicles in the access way Nicolae Balcescu street – coming from Poarta Schei

Cars			Common transportation vehicles			Trucks		
left	forward	right	left	forward	right	left	forward	right
358	945	87	0	51	0	9	7	2

Table 8. Total flux of vehicles in the intersection

Cars	Common transportation vehicles	Trucks
1692	51	20

In a hour's time (15.00-16.00), the intersection has been crossed by approximately 1700 cars, approximately 50 common transportation vehicles (jointed and nonjointed buses and trolleybuses), and 20 trucks. The traffic in the intersection is made difficult by the taxi station which is positioned very close to Dobrogeanu Gherea street, towards the Prefecture of the city of Brasov and by the highly heavy flux of pedestrians. There are several commercial, cultural and administrative objectives in this area. These are: the Prefecture of the Brasov city, the Museum of History, UNIREA Highschool, the Building of the University of 'Transilvania' of Brasov, the comercial complex STAR, etc. Because all these buildings are positioned so close to the road, the intersection can not be geometrically modified, but it can be optimised as far as the traffic light system is concerned.

The concentrations of nitrogen monoxide, volatile organic compounds and carbon monoxide have been monitored in the measurement points intersection (Fig. 2) and are given in Table 9.

Table 9. Registrations of concentration of nitrogen monoxide, the volatile organic compounds and carbon monoxide

No*	CH_4 (%)	NO (ppm)	CO (ppm)	VOC (ppm)	Obs.
1	62	1	1	3	
2	62	1	1	3	
3	62	1	2	8	
4	62	1	1	13	
5	62	1	2	10	
6	62	2	3	15	
7	62	1	1	5	
8	62	2	2	11	

* Measurement points interesection as shown in Fig. 2.

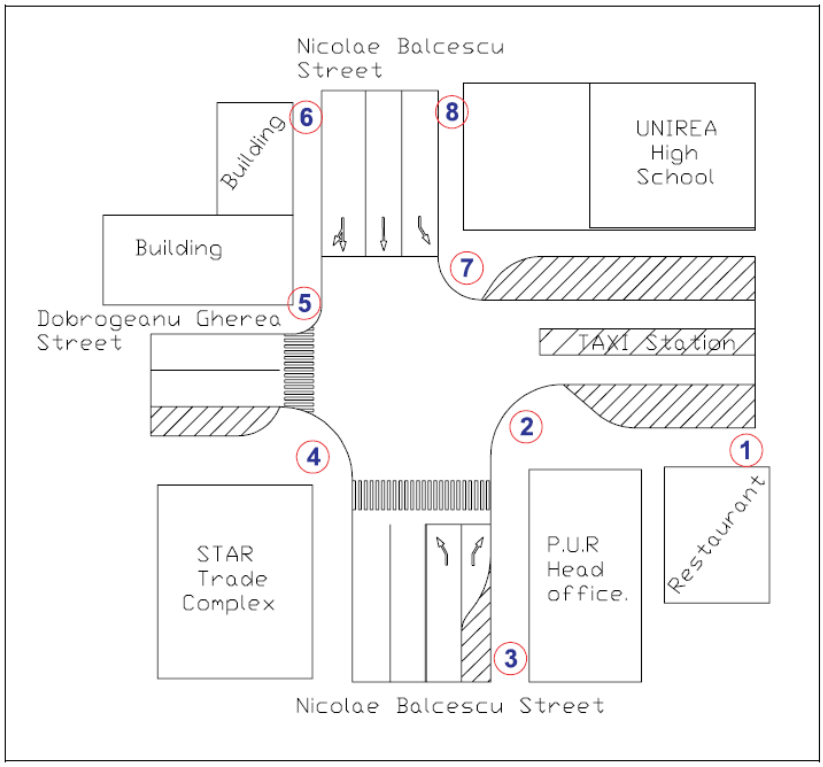

Fig. 2. Measurement points intersection – Nicolae Balcescu street + Dobrogeanu Gherea street

The level of nitrogen monoxide for most of the measurement points is 1 ppm. Only for measurement points 6 and 8 it is 2 ppm. The carbon monoxide level varies between 1 and 3 ppm for this measurement points intersection. Higher values are registered in points 3, 5, 6 and 8, because these are situated on the main road access (Nicolae Balcescu street), where at the rush hours a big lane of vehicles is formed. The level of volatile organic compounds is different for all measurement points. The concentration of VOC for point 6 is 15 ppm and for points 4, 5 and 8 – 13, 10 and 10 ppm, respectively. This result is due to the fact that these 3 points are situated on the main access of the intersection (Nicolae Balcescu street). For the rest of the point the level of VOC varies between 3 and 8 ppm. The high level of VOC is caused by the big percentage of trucks and buses registered for this intersection.

Intersection – Garii boulevard + Victoriei boulevard. This intersection is signalled by a traffic light (4-phase traffic light), having four access ways (entries), while the road fluxes corresponding to these entries differ in their size and structure from the point of view of the vehicles categories. The busiest access ways are the two entries from the Garii boulevard, the transit of heavy vehicles between the points of entrance into and exit out of the city. The values of vehicle fluxes are presented for each access way in Tables 10-14.

Table 10. Flux of vehicles in the access way Garii boulevard coming from Al. Vlahuta street

Cars			Common transportation vehicles			Trucks		
left	forward	right	left	forward	right	left	forward	right
130	633	64	2	31	3	1	163	1

Table 11. Flux of vehicles in the access way Victoriei boulevard

Cars			Common transportation vehicles			Trucks		
left	forward	right	left	forward	right	left	forward	right
126	168	129	10	18	13	1	0	1

Table 12. Flux of vehicles in the access way Garii boulevard coming from Aurel Vlaicu street

Cars			Common transportation vehicles			Trucks		
left	forward	right	left	forward	right	left	forward	right
136	774	265	15	33	3	1	123	1

Table 13. Flux of vehicles in the access way Gara

Cars			Common transportation vehicles			Trucks		
left	forward	right	left	forward	right	left	forward	right
247	146	175	1	12	2	4	1	5

Table 14. Total flux of vehicles in the intersection

Cars	Common transportation vehicles	Trucks
2993	143	302

In one hour's time (15.00-16.00), the intersection was crossed by approximately 3000 cars, approximately 143 common transportation vehicles (jointed and nonjointed buses and trolleybuses), and approximately 300 trucks. The registered values of chemical pollution were high, especially the compounds given out by heavy vehicles (Table 15).

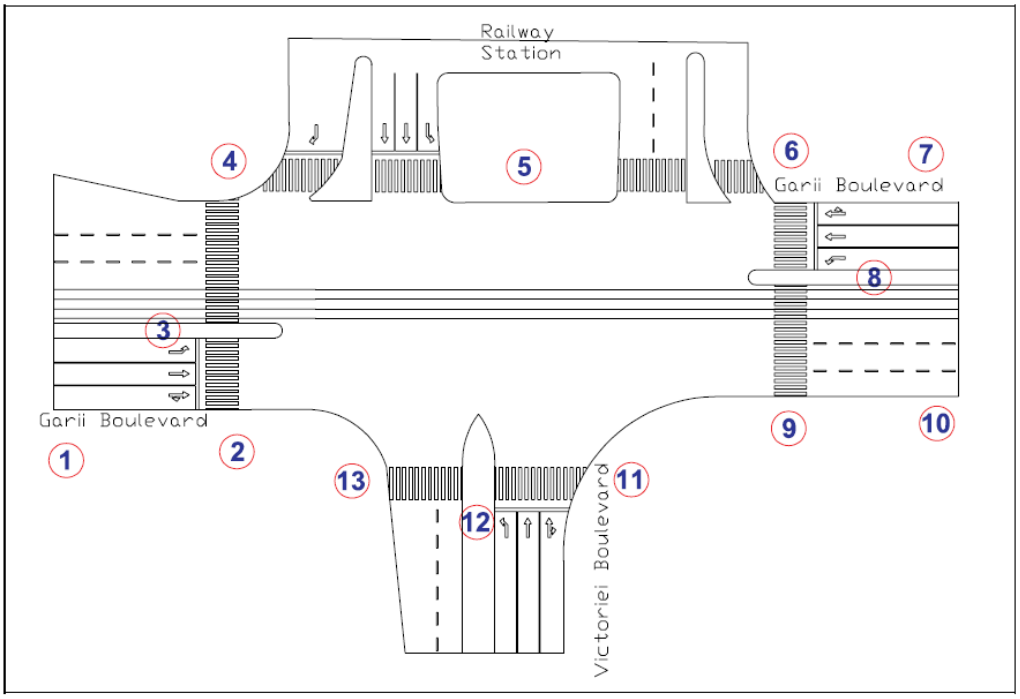

Fig. 3. Measurement points intersection – Garii boulevard + Victoriei boulevard

Table 15. Data on the concentration of nitrogen monoxide, volatile organic compounds and carbon monoxide

No*	CH_4 (%)	NO (ppm)	CO (ppm)	VOC (ppm)
1	62	1	7	11
2	62	1	7	23
3	62	1	1	7
4	62	1	1	3
5	62	1	4	15
6	62	1	7	8
7	62	1	10	27
8	62	1	19	32
9	62	1	1	7
10	62	1	2	11
11	62	1	1	3
12	62	1	1	4
13	62	1	1	4

* Measurement points interesection as shown in Fig. 3.

The level of nitrogen monoxide for all points of the measured interval is 1 ppm. The carbon monoxide level for this intersection varies between 1 and 19 ppm. The concentration of CO for measurement points 7 and 8 is 10 and 19 ppm, respec-

tively and for measurement points 1, 2 and 6 – 7 ppm. The level of CO is higher for these points because these are situated on the main access of the intersection (Garii boulevard). For the rest of the point the level of CO varies between 1 and 4 ppm. The level of volatile organic compounds is different for all measurement points being maximum for point 8, i. e. 32 ppm. Also, for points 1, 2, 5, 7 and 10, the concentration of VOC is very high: 11, 23, 15, 27 and 11 ppm, respectively, and the reason is because these 3 points are situated on the main access of the intersection (Garii boulevard). For the rest of the point the level of VOC varies between 3 and 8 ppm. The high level of VOC is caused by the big percentage of trucks and buses registered for this intersection.

The measurements were made within the interval 27-29 June 2006, between 15-16 o'clock at the following atmospherical conditions:

- weather condition: good/wind
- T_{atm} = 30-32 °C,
- humidity = 45-57%,
- wind velocity = 11-17 km/h (N, NV),
- atmospheric pressure = 101.50 – 102.40 KPa.

The device used for measurements was an Oldham MX21 PLUS (Fig. 4). It is a portable device for gas detection. It can be used for the simultaneous detection of the concentration of four different gases found in air. The device is provided with specific cells for the determination of each gas type.

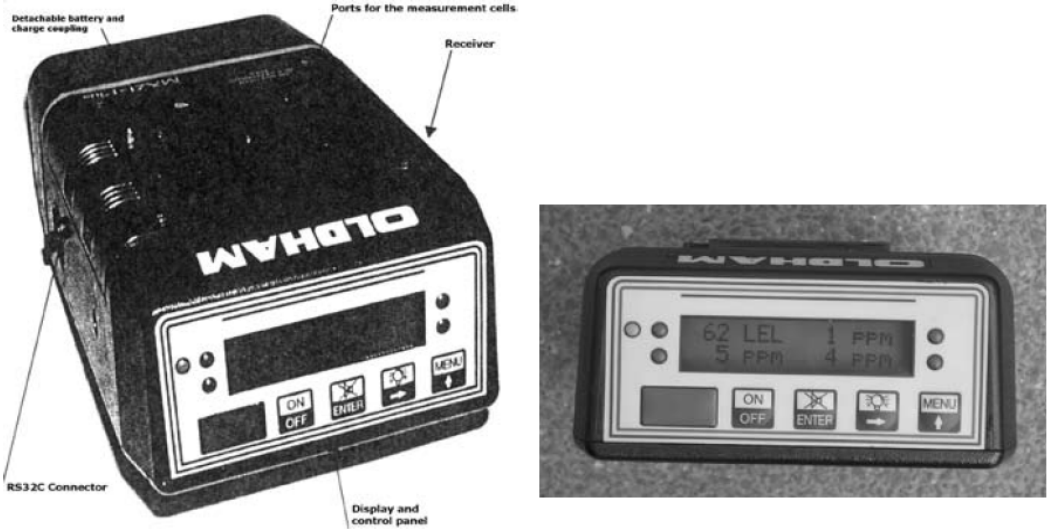

Fig. 4. Presentation of the MX21 PLUS device

In the Constanta town measurements of exhausts fumes have been taken at the following crossroads: 1 Decembrie + Bratianu street, 1 Decembrie + Ferdinand street, I.G. Duca + Ferdinand street, 1 Soveja + Tomis street, 1 Mamaia + Tomis street.

Traffic volume has been registered at different hours (periods of time) in a day time and they decided to take the measurements from 9.00 to 10.00 a.m., 3.00 to 4.00 p.m., and 6.00 to 7.00 p.m.

High amounts (quantities) of concentrations of volatiles organic compounds and carbon monoxide have been registered. The nitrogen oxides concentrations are quite low, with few exception when its level exceeds with 1 ppm.

The ligh registrations of the concentration of the volatiles organic compounds are due to the heavy vehicles working and supplying the shopping centre (in all area).

The public transport using buses that produce exhaust fumes are the cause of this high level of pollution, too. Most of them are old (MAZ model).

The high concentration of carbon monoxide is caused by the heavy traffic of the private light vehicle, too.

In conclusion, the highest figures of exhaust fumes (emissions) registered at the crossroads I.G. Duca + Ferdinand street, were measured at the crossroads I.G. Duca from 9.00 to 10.00 a.m. In this area, high values of carbon oxide and volatile organic compounds have been registred. The most polutted area of the crossroads is proved to be the RAT, bus stop, on I.G. Duca street, having been registered the highest values of carbon oxide 37 ppm, volatile organic compounds – 42 ppm and nitrogen oxide –4 ppm.

CONCLUSIONS

This study has shown ambient air pollution increase with proximity to roadways.

This study provides important insights into the physicochemical components of engine emissions that most strongly influence the toxicity of inhaled emissions.

Traffic-related exposure shows a light pollution between 15-16 o'clock in Brasov and Constanta.

The light registrations of the concentration of the volatiles organic compounds are due to the heavy vehicles working and supplying the shopping centre (in all area).

REFERENCES

1. F. LADEN, L. M. NEAS, D. W. DOCKERY, J. SCHWARTZ: Association of Fine Particulate Matter from Different Sources with Daily Mortality in Six U.S. Cities. Environ. Health Perspect, **108** (10), 941 (2000).
2. W. J. GAUDERMAN, E. AVOL, F. GILLILAND, H. VORA, D. THOMAS, K. BERHANE et al.: The Effect of Air Pollution on Lung Development from 10 to 18 Years of Age. N. Engl. J. Med., **351**, 1057 (2004).

3. A. PETERS, H. E. WICHMANN, T. TUCH, J. HEINRICH, J. HEYDER: Respiratory Effects are Associated with the Number of Ultrafine Particles. Am. J. Respir. Crit. Care Med.,**155**(4), 1376 (1997).
4. B. BRUNEKREEF, N. A. JANSSEN, J. de HARTOG, H. HARSSEMA, M. KNAPE, P. van VLIET: Air Pollution from Truck Traffic and Lung Function in Children Living near Motorways. Epidemiology, **8**(3), 298 (1997).
5. Y. L. GUO, Y. C. LIN, F. C. SUNG, S. L. HUANG, Y. C. KO, J. S. LAI, H. J. SU, C. K. SHAW, R. S. LIN, D. W. DOCKERY: Climate, Traffic-related Air Pollutants, and Asthma Prevalence in Middle-school Children in Taiwan. Environ. Health Perspect., **107** (12), 1001 (1999).
6. J. SCHWARTZ: Assessing Confounding, Effect Modification, and Thresholds in the Association between Ambient Particles and Daily Deaths. Environ. Health Perspect., **108** (6), 563 (2000).
7. D. M. GLOVER, P. K. HOPKE, S. J. VERMETTE, S. LANDSBERGER, D. R. D'AUBEN: Source Apportionment with Site Specific Source Profiles. J. Air Waste Manage. Assoc., **41** (3), 294 (1991).
8. A. BIGGERI, P. BELLINI, B. TERRACINI: Meta-analysis of the Italian Studies on Short-term Effects of Air Pollution – MISA 1996-2002. Epidemiol. Prev., **28** (4-5 Suppl) 4 (2004). Italian; Http://www.epa.gov/OMS/invntory/overview/pollutants/carbonmon.htm
9. N. KULKARNI, N. PIERSE, L. RUSHTON, J. GRIGG: Carbon in Airway Macrophages and Lung Function in Children. NEJM, **355**, 21 (2006).
10. J. MOLITOR, N.-T. MOLITOR, M. JERRETT, R. MCCONNELL, J. GAUDERMAN, K. BERHANE, D. THOMAS: Bayesian Modeling of Air Pollution Health Effects with Missing Exposure Data. Am. J. Epidemiol., **164**, 69 (2006).
11. B. CHAIX, S. GUSTAFSSON, M. JERRETT, H. KRISTERSSON, T. LITHMAN, A. BOALT, J. MERLO: Children's Exposure to Nitrogen Dioxide in Sweden: Investigating Environmental Injustice in an Egalitarian Country. J. Epidemiol. Community Health, 234 (2006).
12. R. M. EFFROS, R. CASABURI, J. SU, M. DUNNING, J. TORDAY, J. BILLER, R. SHAKER: The Effects of Volatile Salivary Acids and Bases on Exhaled Breath Condensate pH. Am. J. Respir. Crit. Care Med., **173**, 386 (2006).
13. T. SANDSTROM, D. NOWAK, L. van BREE: Health Effects of Coarse Particles in Ambient Air: Messages for Research and Decision-making. Eur. Respir. J., **26**, 187 (2005).
14. A. S. BERNSTEIN, H. T. ABELSON: PM 2.5-A Killer in Our Midst. Arch. Pediatr. Adolesc. Med., **159**, 786 (2005).
15. A. H. LOCKWOOD, P. J. F. M. MERKUS, G. A. TETRAULT, W. J. GAUDERMAN, E. AVOL, F. GILLILAND: Air Pollution and Lung Function. NEJM, **351**, 2652 (2004).

Received 18 October 2006
Revised 12 December 2006

Mathematical model of pollution compounds calculus in function of traffic capacity from urban areas

Article *in* WSEAS Transactions on Environment and Development - May 2008

CITATIONS
11

READS
941

3 authors:

Stelian Tarulescu
Universitatea Transilvania Brasov
68 PUBLICATIONS 111 CITATIONS
SEE PROFILE

Radu Tarulescu
Universitatea Transilvania Brasov
78 PUBLICATIONS 102 CITATIONS
SEE PROFILE

Adrian Solea
Universitatea Transilvania Brasov
48 PUBLICATIONS 103 CITATIONS
SEE PROFILE

Mathematical model of pollution compounds calculus in function of traffic capacity from urban areas

STELIAN TARULESCU, RADU TARULESCU, ADRIAN SOICA
Department of Mechanical Engineering
Transilvania University of Brasov
Eroilor Boulevard, No 29, Brasov
ROMANIA
s.tarulescu@unitbv.ro

Abstract: - The Brasov city is one of the biggest towns in Romania. In the central area of the Brasov city can be found the biggest concentration of the carbon monoxide, nitrogen oxides, the ozone and the volatile organic compounds. For intersection's analysis there were collected data about the road traffic and data about the chemical pollution in the neighborhood of the road. In order to realize the model there were made tables with the traffic values and the values of the three pollutants, in function of the intersections of the analyzed route. For calculus were used the equations corresponding to the determined polynomial curves, for each pollutant, using the values obtained experimentally. The working page of the mathematical model was made grouping the four analyzed situations.

Key-Words: - Chemical, pollution, traffic, mathematical, model, etalon vehicle

1 Introduction

The human activity generates the emission of many gaseous pollutants into the atmosphere. The vehicles give many pollutants, and the studies made at international level allow quantification of the pollutants from the traffic flow. From all the primary pollutants made by the internal combustion engines, there are distinguished seven significant atmospheric pollutants, brought under regulation in Europe:

- sulphur dioxide (SO_2);
- particles (with a diameter <10 μm);
- lead (Pb);
- nitrogen oxide (NO_x);
- carbon monoxide (CO);
- unburned hydrocarbons (H_nC_m) – benzene;
- the ozone (O_3) from atmosphere, in concentrations of 0.5-10[ppm] [5].

A synthesis of the traffic flow development shows three significant travel phases:

- daily travels to and from work;
- afternoon travels to different centers (commercial, social-cultural, of individual or group meetings);
- going to and especially coming back from the week-end, generally outside the city, in order to relax.

The simple enunciation of these three main phases of travel present in city's life can prove the variety of the urban traffic flow structure and intensity, where the vehicle has the main role, having the purpose to assure the maximum comfort of the travels, by its accessibility from "door to door".

The essence of the problem is the mutual accommodation city-vehicle, its solution not being the sacrifice of one for the other.

If at the big traffic flow volume of the small vehicles we add the common transportation (which in many cities has the first place in order to satisfy the travel necessary of the habitants) and the transportation of goods and services, it can be said that the traffic flow needs two categories of measures in the urban areas:

- the adequate arrangement of a main road network, which can satisfy the traffic flow which is increasing continuously, but also which does not disturb the urban ambience;
- the organization, regulation and control of the traffic flow in intersections, which represents for the urban traffic real intake and exhaust valves, being for the streets network their strangulation points, the ones which determine the intrinsic capacity of the traffic flow [6].

The region of Brasov is situated in a mountainous area in the centre of Romania. In Brasov County there are 4 municipalities and 5 towns, 43 communes and 150 villages. The county population registered is 626499 inhabitants, from which in the urban environment 472620 inhabitants and in rural environment 153879 inhabitants.

In the central area of the Brasov City can be found the biggest concentration of the carbon monoxide, where the majority in traffic is composed by the vehicles equipped with gasoline engines, where the

traffic conditions are admitting their functioning frequently at uneconomical regimes, with partial loads, low engine speeds and uncompleted burnings of the fuel [4].

The nitrogen oxides, the ozone and the VOC are usually specific to the peripheral urban areas, where it can be noticed a high volume of heavy vehicles, which have diesel engines.

The following list describes the potential health risks associated with these emissions:

- Carbon Monoxide (CO): An odorless and colorless gas which is highly poisonous. CO can reduce the blood's ability to carry oxygen and can aggravate lung and heart disease. Exposure to high concentrations can cause headaches, fatigue and dizziness.
- Nitrogen Oxides (NO_x) and Nitrogen Dioxide (NO_2): These chemicals form the yellowish-brown haze seen over dirty cities. When combined with oxygen from the atmosphere, NO becomes NO_2, a poisonous gas that can damage lung tissue [2].
- Hydrocarbons (HC): This is a group of pollutants containing hydrogen and carbon. Hydrocarbons can react to form ozone. Some are carcinogenic and other can irritate mucous membranes. Hydrocarbons include: Volatile organic compounds (VOC); Volatile organic gases (VOG); Reactive organic gases (ROG); Reactive organic compounds (ROC); Non-methane hydrocarbons (NMHC); Non-methane organic gases (NMOG).
- Ozone (O_3): This is the white haze or smog seen over many cities. Ozone is formed in the lower atmosphere when NMOG and NO_x react with heat and sunlight. Ozone can irritate the respiratory system, decrease lung function and aggravate chronic lung disease such as asthma [5].

2 The studied area

For the pollution level measurement it was chosen the Brasov's historical center area. In this area there are many commercial, cultural and touring objectives: institutions (City Hall, Prefecture, University's buildings, high schools and schools), shops, hotels, churches, museums, theatres, monuments and parks. These objectives bring on each day a high number of pedestrians which are exposed to the pollution caused by road traffic from this area.

The analyzed route was: Lunga Street, Eroilor Boulevard, 15 Noiembrie Street, Castanilor Street, Iuliu Maniu Street, Nicolae Iorga Street.

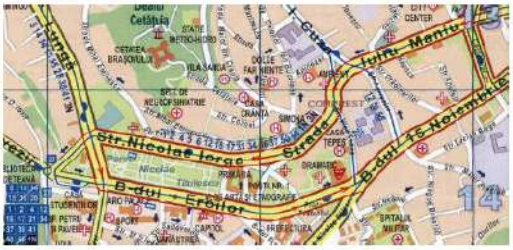

Fig.1 The studied area of Brasov city (the historical centre)

Fig.2 The objectives from the studied area of Brasov city

The objectives from this picture are: 1- The City Hall; 2- Prefect Hall; 3- Building N of the Transilvania University; 4- Unirea High School; 5- Capitol Hotel; 6- Aro Palace Hotel; 7- Casa Armatei Building; 8- Sica Alexandrescu Theatre; 9- Building M of the Transilvania University; 10- Comercial Area; 11- C.F.R. Hospital; 12- Lecture Room of the Transilvania University; 13- Mihail Eminescu Hospital; 14- Romano-Catholic Church; 15- Offices and Banks Area.

The route includes six intersections, from which four are with traffic lights and two are marked with traffic signs.

The six intersections are:

Intersection 1 - Castanilor Street + Iuliu Maniu Street;

Intersection 2 - Alexandru Ioan Cuza Street + Agrişelor Street + Iuliu Maniu Street;

Intersection 3 - Nicolae Iorga Street + Lungă Street;

Intersection 4 - Lungă Street + Eroilor Boulevard + Mureşenilor Street;

Intersection 5 - Eroilor Boulevard + Vlad Ţepeş Street + Nicolae Bălcescu Street + 15 Noiembrie Boulevard;

Intersection 6 - 15 Noiembrie Boulevard + Castanilor Street.

On three of those the access of the road traffic is made from the residential areas to the historical center (intersections 1, 2 and 3), and on the other three there is an opposed flux.

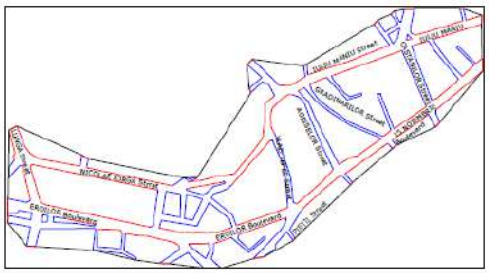

Fig. 3 Analyzed route: Iuliu Maniu Street, Nicolae Iorga Street, Lunga Street, Eroilor Boulevard, 15 Noiembrie Boulevard and Castanilor Street.

3 Road traffic and chemical pollution data measurement methodology

For intersection's analysis there were collected data about the road traffic and data about the chemical pollution in the neighborhood of the road (the values of some pollutants resulted from the fuel combustion).

The most common and handy method is the manual collecting of the road traffic data, with the help of an observer team, each member of this team writing down a specific element of the road traffic.

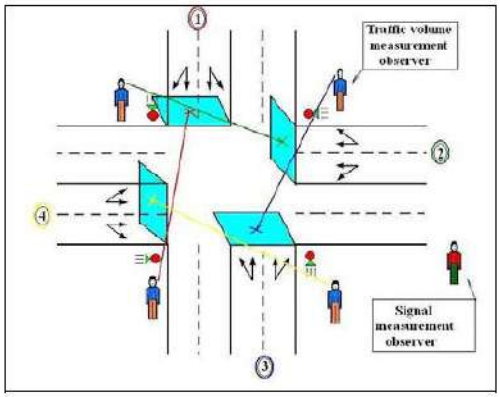

Fig. 4 Measuring a regular intersection with four phases.

For a certain input with variable time signals it is established the following data measurement in order to analyze the intersection: traffic volume, number of vehicles which are passing the stop line, for each traffic direction (forward, left, right), for each vehicle category. In the figure above it is presented a regular intersection with four phases, with observers placed so that to obtain a minimum number of them.

In this case, with special turning moves there are necessary more persons, the maximum number being of 5: one for each entrance and the 5th one to measure the time interval [4], [5].

The volume of the traffic flow was determined by counting the total number of the vehicles, which passed through the intersection during one hour (8.00-9.00 and 15.00-16.00) in all ways.

The volumes of the traffic flows from the studied intersections are presented in the next picture:

Inter-section number	Etalon Vehicles	Light vehicles	Trucks	Buses and Troleys
4	2969	2428	50	118
8	3245	2776	27	127
9	3657	3075	28	151
3	4678	4173	36	119
2	4905	4471	13	124
1	5451	4629	69	182

Fig. 5 The registered values for the 8.00-9.00 hour interval, for one intersection

For measuring the concentration of the chemical pollutants from the studied area it will be used a team of two persons. The two persons will use the necessary equipment (portable gas analyzer) and will write the specific values of the measurement points [7].

The MX21 Plus is a portable multi-gas monitor which can detect up to four gasses simultaneously and includes features such as: data logging, interchangeable pre-calibrated sensor blocks, instantaneous, STEL and TWA alarms. The unit is programmable via serial link from a PC or via a user-friendly menu interface and is approved for use in hazardous areas. By the use of intelligent plug-in sensor modules the device has one of the largest range of toxic sensors (20 plus) including CO_2, CO, H_2S, SO_2, CL_2, NO, NO_2, HCN, HF, PH_3, O_3, H_2, solvents etc.

Another unique feature of the MX21 Plus is the ability to measure CH_4 in percentage volume as well percentage LEL with a library of 32 pre-programmed flammable gasses to allow for more accurate monitoring of specific flammable gasses by

simply selecting the target gas CH_4, H_2, butane, petrol vapors etc., from a menu.

Fig. 6 The OLDHAM MX21 Plus portable multi-gas detector

The measurement cells:

- Oxygen and toxic gases measurement cells;
- Anemometric cell;
- Carbon dioxide measurement cell;
- Explosive gases measurement cell.

Fig. 7 The OLDHAM MX21 measurement cells

Advantages:

- Simple to use. The MX 21 PLUS incorporates a self-diagnostic function, which indicates any irregularities in its operation thereby providing complete confidence measurement.
- Clear messages. Without having to calibrate the MX 21 PLUS, you can select the gas you wish to measure from any of the 16 preprogrammed flammable gases or vapors from its international library, thereby ensuring a direct reading in % LEL. If the concentration exceeds the LEL range, the instrument will display over range in compliance with "non-ambiguity readout"
- Reliable oxygen measurement. The oxygen sensor manufactured in OLDHAM's modern laboratories provides accurate and reliable measurement [8].

The user can carry the MX21 PLUS apparatus in housing. The apparatus is designed so that the measurement cells are oriented to exterior. This fact makes that the holes for the measurement cells are visible during measurements.

The MX21 PLUS apparatus must be put in vertical position, with the battery downwards. Depending on the gas types that are measured, the apparatus must be placed:

- on ground, for heavy gases measurement (H_2S, CO);
- on medium height (about 1 meter above the ground) or at the exhaust of some ventilation tubes from the industrial zone (for the general measurement of the maximum number of gases or for oxygen supervise).

Fig. 8 Measurement with the OLDHAM MX21 Plus portable multi-gas detector

Next is presented as an example the scheme of an intersection, with the chosen measurement points in order to make the measurements.

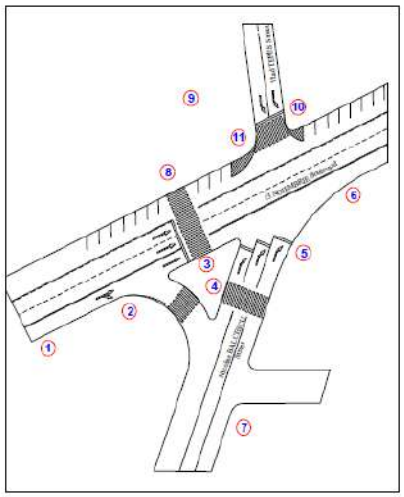

Fig. 9 The points where the measurements were done

The measurements were made for each of the 6 intersections of the route. Simultaneously there were taken the values of traffic flow and the values of main chemical compounds pollutants. The four distinct situations, in function of season and time interval in which the measurement was made are:

- cold season (winter), morning rush hour (8.00-9.00);
- cold season (winter), evening rush hour (15.00-16.00);
- warm season (summer), morning rush hour (8.00-9.00);
- warm season (summer), evening rush hour (15.00-16.00).

From the six pollutants for which were made measurements, there were analyzed only three and these are: carbon monoxide (CO), volatile organic compounds (VOC) and ozone (O_3). The rest of the pollutants were not analyzed for the following reasons:

Nitrogen monoxide (NO) – the values of the NO concentration are for most of the intersections minimum (1 [ppm])

Sulphuretted hydrogen (H_2S) – the values of the H_2S concentration varies very little from one season to another, and is not specific to vehicles.

Nitrogen dioxide (NO_2) – the values of the NO_2 concentration varies depending on the season and on the time interval when the measurements were made. The values are between 0.1 and 0.2 [ppm] for most of the cases. Though, it could not be established a dependency of the NO_2 concentration in function of the etalon vehicle number. The values measured varies randomly in function of the weight of different categories of vehicles from the road traffic, but also in function of geometrical parameters of each intersection. For exemplification it was chosen the route 2, in the summer, for the evening rush hour.

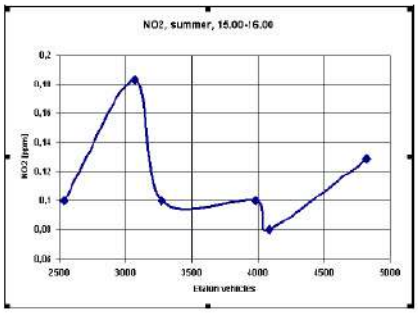

Fig. 10 The concentration variation of NO_2 [ppm] for one intersection

The concentration variation of three chemical pollutants (CO [ppm], VOC [ppm], O_3 [ppm]), specific to the areas near the road' infrastructure for the two analyzed time intervals is presented in the next graphics (for one intersection):

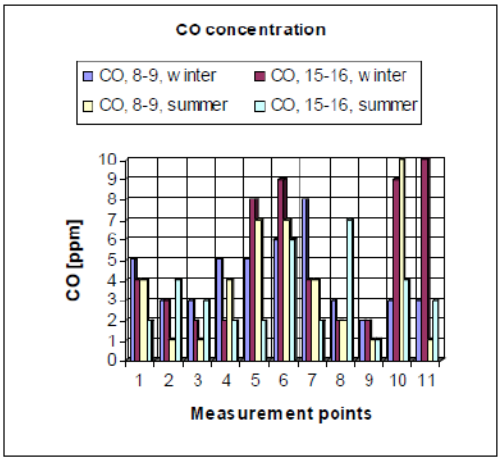

Fig. 11 The concentration variation of CO [ppm] for Intersection 5 - Eroilor Boulevard + V. Ţepes Street + N. Bălcescu Street + 15 Noiembrie Bvd.

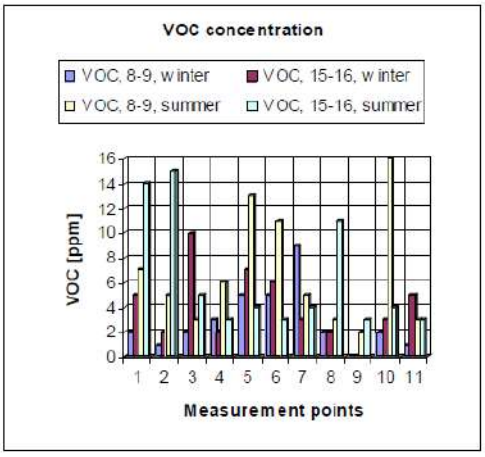

Fig. 12 The concentration variation of VOC [ppm] for Intersection 5 - Eroilor Boulevard + Vlad Ţepes Street + 15 Noiembrie Boulevard

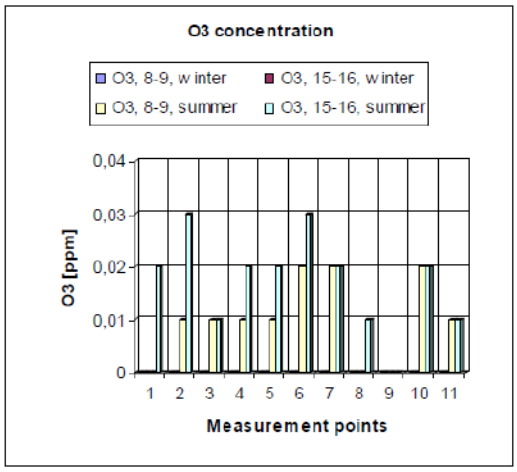

Fig. 13 The concentration variation of O_3 [ppm] for Intersection 5 - Eroilor Boulevard + Vlad Ţepeş Street + Nicolae Bălcescu Street + 15 Noiembrie Boulevard

4 Accomplishment of the mathematic model

Using the measured data from the intersections, it can be established an average pollution level for each of these ones. For each intersection it will be analyzed only the points which are near the road, excluding the points which are far from the road or placed after green areas or other objectives. For each pollutant it will be established an average value, expressed in the corresponding measuring unit. The average will be a rounded arithmetical mean, which will contain all the values obtained in the measurement points, but without the maximum and the minimum value.

$$X_{medie} = \frac{\sum_{i=1}^{n} p_i - \min(p_i) - \max(p_i)}{n-2} \quad (1)$$

where: $X_{average}$ = the average value of the analyzed pollutant; p_i = the value of the pollutant in each of the analyzed points; n = the number of analyzed points for each intersection.

In order to realize the model there were made tables with the traffic values and the values of the three pollutants, in function of the intersections of the analyzed route. For calculus were used the equations corresponding to the determined polynomial curves, for each pollutant, using the values obtained experimentally.

Season	Interval	The average value CO [ppm]
winter	8.00-9.00	5,4286
	15.00-16.00	4,1429
summer	8.00-9.00	4,0000
	15.00-16.00	4,2857

Season	Interval	The average value VOC [ppm]
winter	8.00-9.00	4,2857
	15.00-16.00	3,7143
summer	8.00-9.00	7,4286
	15.00-16.00	4,8571

Season	Interval	The average value NO_2 [ppm]
winter	8.00-9.00	0,1000
	15.00-16.00	0,1000
summer	8.00-9.00	0,2000
	15.00-16.00	0,1000

Season	Interval	The average value O_3 [ppm]
winter	8.00-9.00	0,0129
	15.00-16.00	0,0143

Fig. 14 Tables with the chemical pollutant values for one intersection

The working page of the mathematical model was made grouping the four analyzed situations, for each of the analyzed route. For each of these situations, the intersections were sorted increasingly by the number of etalon vehicles. For each of the studied pollutants there were determined their variations in function of the etalon vehicles number.

The taken values vary randomly in function of weight of the different vehicles' categories from the road traffic, but also in function of the geometrical parameters of each intersection.

For each of the four situations, the intersections were arranged increasingly after the number of etalon

Manuscript received Sep. 17, 2007; revised Mar. 24, 2008

vehicles. Next to each intersection there were written the average values of the two pollutants, to represent in a chart the dependence between these two and the number of etalon vehicles. The obtained curves were calculated for each representation of the experimental values (obtained from measurements), obtaining a theoretical curve given by a polynomial equation. It was whished to obtain a theoretical curve very closed to the curves obtained with the experimental values. For each situation, the resulted theoretical curves will be described through polynomial equations of 2nd and 3rd degree [1], [3].
Next it will be presented the resulted curves and equations from the analysis, for each of the three studied pollutants, for a single situation. For exemplification there will be presented the variation curves for CO, VOC and O_3 in the warm season, at he morning rush hour.

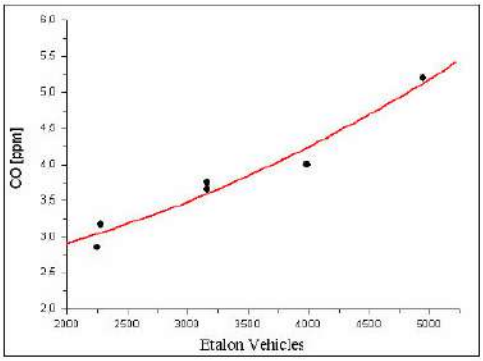

Fig. 15 The variation of the CO concentration in function of the etalon vehicles number

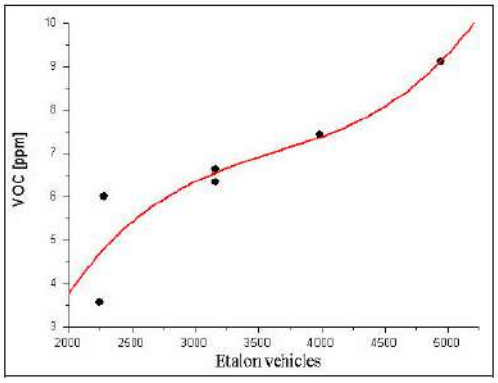

Fig. 16 The variation of the VOC concentration in function of the etalon vehicles number

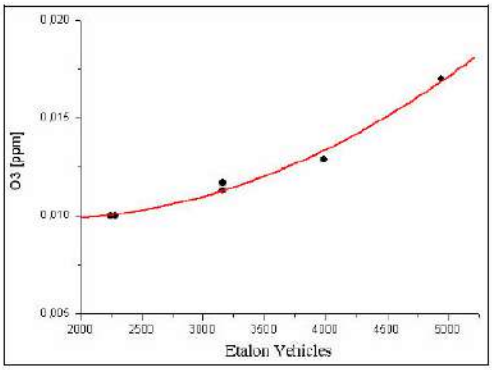

Fig. 17 The variation of the O_3 concentration in function of the etalon vehicles number

For this analyzed chemical compounds, in order to realize a unitary mathematical model, it can be written equations of pollution concentration variation depending on etalon vehicles number measured in one hour time interval.

$$CO_{theoretical} = 2{,}32428 + 1{,}09063 \cdot 10^{-4} \cdot V_E + \\ + 9{,}27022 \cdot 10^{-8} \cdot V_E{}^2 \quad (2)$$

$$VOC_{theoretical} = -15{,}45515 + 0{,}01672 \cdot V_E - \\ - 4{,}3480 \cdot 10^{-6} \cdot V_E{}^2 + 3{,}9856 \cdot 10^{-10} \cdot V_E{}^3 \quad (3)$$

$$O_{3\ theoretical} = 0{,}01179 - 2{,}2649 \cdot 10^{-6} \cdot V_E + \\ + 6{,}65935 \cdot 10^{-10} \cdot V_E{}^2 \quad (4)$$

Where: $CO_{theoretical}$, $VOC_{theoretical}$ and $O_{3theoretical}$ = the theoretical values of the CO, VOC and O_3 concentrations which describes the variations of the mathematical model curves; V_E = The number of etalon vehicles;
These equations can be generalized, using for all situations representative constants.

$$CO_{theoretical} = A_{CO} + B_{CO} \cdot V_E + C_{CO} \cdot V_E{}^2 + \\ + D_{CO} \cdot V_E{}^3 \quad (5)$$

$$VOC_{theoretical} = A_{VOC} + B_{VOC} \cdot V_E + \\ + C_{VOC} \cdot V_E{}^2 + D_{VOC} \cdot V_E{}^3 \quad (6)$$

$$O_{3theoretical} = A_{O3} + B_{O3} \cdot V_E + C_{O3} \cdot V_E{}^2 + \\ + D_{O3} \cdot V_E{}^3 \quad (7)$$

Where: A_{VOC}, B_{VOC}, C_{VOC}, D_{VOC}, A_{CO}, B_{CO}, C_{CO}, D_{CO}, A_{O3}, B_{O3} and C_{O3} = Representative constants for

each analyzed situation.

After the introduction of the formulas and the graphical representation of the three pollutants, result the theoretical curves corresponding to the used equations.

In figure 18 are presented the table and the corresponding diagrams for route, in the warm season and the morning rush hour (8.00-9.00). In the table are presented: the corresponding number for each intersection, the traffic values (etalon vehicles), the average values for the chemical pollutants concentration (determined using the data obtained experimentally) and the pollutants' values obtained through calculus, using the polynomial equation of each pollutant compound.

The three diagrams represent the variation of the three pollutants in function of the measured traffic volumes in the route's intersections. The blue spots represents the values determined experimentally, from the measurements and corresponds to the values from the table (written also in blue), from columns C, E and G. The red curves represent the pollutants variations with the etalon vehicle number, using the values obtained mathematically using the polynomial equations corresponding to each pollutant. These values are written in red and they are situated in columns D, F and H of the table.

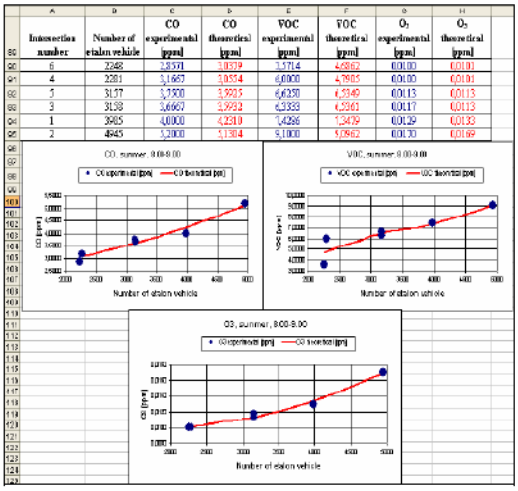

Intersection number	Number of etalon vehicle	CO experimental [ppm]	CO theoretical [ppm]	VOC experimental [ppm]	VOC theoretical [ppm]	O_3 experimental [ppm]	O_3 theoretical [ppm]
6	2248	3,8571	3,8719	3,1714	4,2862	0,0100	0,0101
4	2281	3,9665	3,8934	4,0000	4,2985	0,0100	0,0101
5	3137	3,7300	3,7935	4,6250	4,5349	0,0113	0,0113
3	3138	3,6667	3,7932	4,3333	4,2963	0,0117	0,0113
1	3905	4,0000	4,2310	4,4286	4,2479	0,0129	0,0133
2	4945	5,2000	5,1304	5,1000	5,0562	0,0130	0,0169

Fig. 18 Presentation of mathematical model results for one of the four situations, for the analyzed route

Each studied pollutant it had variations in relation with the season and the time interval in which the measurement were made. So, the variation curves of the CO, VOC and O_3 differs in function of the atmospheric conditions. For exemplification are presented the variation curves of the carbon monoxide (CO), for the four studied situations. In the four figures it can be noticed the visible differences of the etalon vehicles number from the intersections for the measurement time interval, but also of the variation curves' shape.

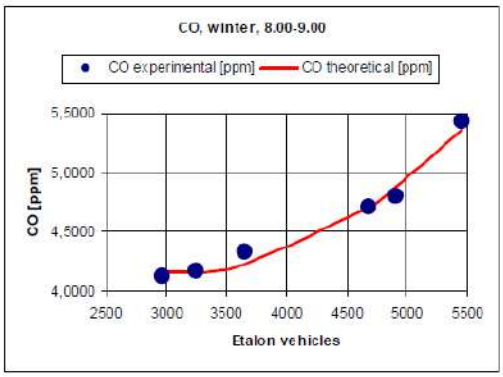

Fig. 19 The variation of the CO concentration for the 8.00-9.00 hour interval and for the winter season

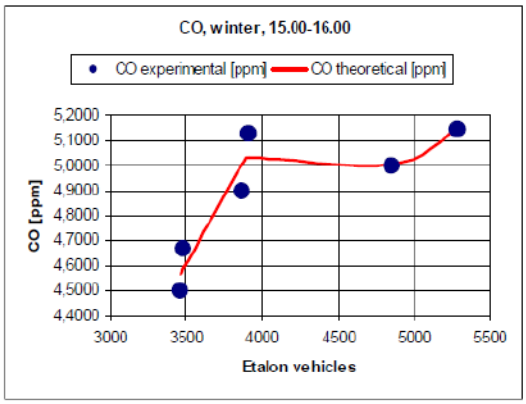

Fig. 20 The variation of the CO concentration for the 15.00-16.00 hour interval and for the winter season

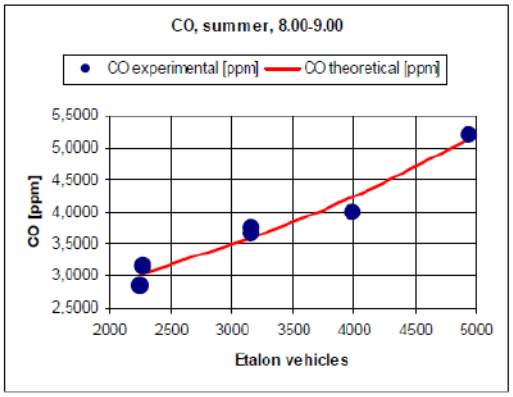

Fig. 21 The variation of the CO concentration for the 8.00-9.00 hour interval and for the summer season

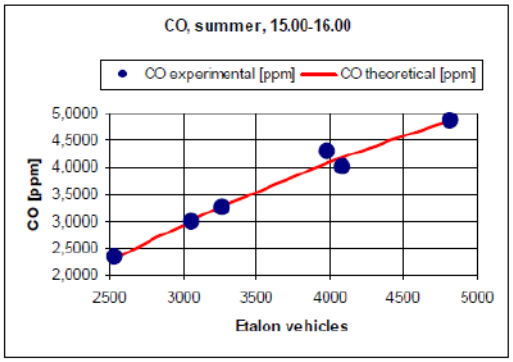

Fig. 22 The variation of the CO concentration for the 15.00-16.00 hour interval and for the summer season

4 Conclusion

The mathematical model can be used for different routes and situations and introducing a number of etalon vehicles for an intersection can be estimated the pollution level for three chemical pollutants.

In the case of the cold season (winter), on the morning rush hour (8.00-9.00), the CO and VOC concentration variations are after two ascending curves, given by the 2nd degree polynomial equations. For CO the curve is convex and for VOC the curve is concave.

In the case of the cold season (winter), on the evening rush hour (15.00-16.00), the CO concentration variation is after one ascending curve, given by the 3rd degree polynomial equation and the VOC concentration variation is after one ascending concave curve given by the 2nd degree polynomial equation.

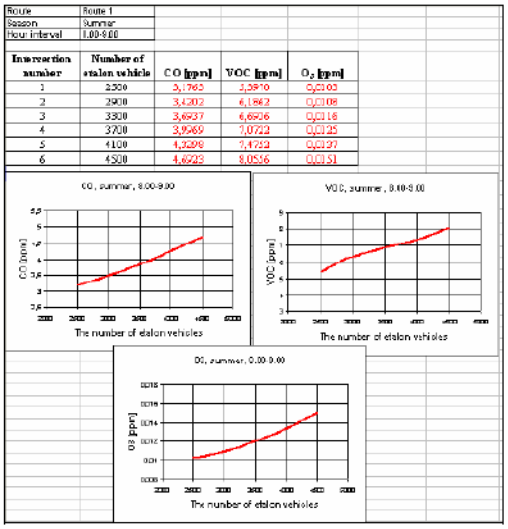

Fig.23 Utilization of mathematical model for CO, VOC and O_3 concentration estimation, in function of etalon vehicle number for a route

In the case of the hot season (summer), on the morning rush hour (8.00-9.00), the CO and O_3 concentration variations are after ascending convex curves given by the 2nd degree polynomial equations, and the VOC concentration variation is after an ascending curve given by a 3rd degree polynomial equation. For all three pollutant compounds, their concentration variation in function of the etalon vehicle number is similar.

In the case of the hot season (summer), on the evening rush hour (15.00-16.00), the CO and O_3 concentration variations are after concave ascending curves given by 2nd degree polynomial equations, and the VOC concentration variation is after an ascending curve given by the 3rd degree polynomial equation. For all three pollutant compounds, their concentration variation in function of the etalon vehicle number is, as in the case of the morning rush hour, similar.

From this study which as realized on the base of the data obtained experimentally can be observed some characteristics of the pollution made by traffic flow:

- Substantial increments of the chemical compounds concentrations resulted from the fossil fuels burning are in the case of transitory functioning of internal combustion engines.
- The time interval and the season influence visibly the chemical pollutant compounds.
- The meteorological conditions (temperature, wind's speed and direction, humidity, air pressure) influence the pollutants' values.
- The traffic's flow composition (cars, trucks, buses, trolleybuses) but also the traffic volume values (expressed by the Traffic capacity = etalon vehicles \ hour) have a determinant role over the city's pollution level.
- Intersection's and main street's geometry on which is developing the city's transitory traffic influences significantly the pollution level.
- The biggest impact over the air quality, from the areas designated to pedestrians, is given by the traffic road; the pollutant emissions from the vehicles being maximal near the roads, at the height of the human respiratory organs.

The main contributions given by this research about the chemical pollution from the road traffic are the following:

- There were identified the major problems about the organization of the road traffic from Brasov District which contributes to the chemical and noise pollution from the urban areas.
- There were made road traffic and environment measurements, aiming to locate the levels of chemical and noise pollution from the traffic road.
- There was analyzed the local vehicles park, its structure, perspectives, the level of pollutant emissions from this one and the causes of the pollutant emissions generation.
- It was realized a complex data base, which includes the values of the traffic road, the chemical pollutants and the noise levels. The data base will be updated with the values measured in the next years.
- It was identified the current and the future international and the national legislation regarding the maximum allowed levels of the chemical and noise pollution caused by road traffic.
- It was realized a mathematical model of estimation of the chemical and noise pollution levels in function of the time interval for the two routes studied.

References:

[1] ESCHELBECK, G., Th. Moser: Distributed Traffic - Monitoring and Evaluation by Means of a Client - Server Architectures. The 13th World Computer Congress 94 IFIP, vol.2.

[2] SHISHIR, L., PATIL, S., "Monitoring of atmospheric behavior of NO_x from vehicular traffic", Environmental Monitoring Assessment, Vol. 68, Springer, Netherlands, 2001.

[3] BERKOWICZ R., KETZEL, M., VACHON, G., „Examination of Traffic Pollution Distribution in a Street Canyon Using the Nantes'99 Experimental Data and Comparison with Model Results" Water, Air, & Soil Pollution: Focus, Vol. 2, Springer, Netherlands, 2002

[4] ZABALZA, J., OGULEI, D., "Study of urban atmospheric pollution in Navarre", Environmental Monitoring and Assessment, Vol. 134, Springer, Netherlands, 2007.

[5] COFARU, C., *"Pollution legislation in road transportation"*, Transilvania University of Brasov, 2002.

[6] FLOREA, D., COFARU, C., ŞOICA, A., *"Traffic management"*, Transilvania University of Brasov 1998.

[7] UZUREANU, K., "The monitoring and air quality diagnosis", Technical editor, Bucuresti 2007.

[8] OLDHAM MX 21 PLUS, Technical Documentation

On-Board Measurement of Emissions from Spark Ignition Engine Vehicle for Urban Routes

Stelian Ţârulescu(✉), Radu Ţârulescu, and Cristian-Ioan Leahu

Transilvania University of Brasov, Eroilor Boulevard No. 29, Braşov, Romania
s.tarulescu@unitbv.ro

Abstract. Currently, testing the ecological performance of light vehicles is made using the New European Drive Cycle. Taking into account the problems of the last years, related to the efficiency of the testing procedures and approval of the motor vehicles on the stand, new testing and approval strategies are required. Our research aims to develop a methodology for measuring on-board emissions from vehicles, for different urban and extra-urban routes. For the present paper, the emission measurement system was tasted on the vehicle equipped with a spark ignition engine. There were 5 routes, of which 4 urban and one combined (urban and extra-urban). The results will help to prepare a methodology for testing on-board vehicles.

Keywords: Vehicle · Engine · Pollution · Emissions · Urban

1 Introduction

In recent years are developed various systems and equipments used for on board vehicle pollutant emissions evaluation. This paper presents experimental methodology for an on-road emissions measurement strategy (using a portable measuring equipment). The collected data from measurements can help the development of an emission inventories methodology.

In order to evaluate and control air pollution produced by the transport sector, it is essential to identify the pollution sources and environmental impact. In present, the assessment of the emission factor is determined using the dynamometer testing. Dynamometer testing is a methodology in which the pollutant emissions of the vehicle are measured in laboratory conditions, using a cycle that simulates road conditions (urban and extra-urban). This cycle is a sequence of stops, starts, rolling at constant speed, accelerations and brakes. Nowadays, different test cycles are used to simulate different running conditions. The problem is that the dynamometer tests are affected from shortcomings associated with non-representativeness of actual driving conditions. On-board measurements represents a more efficient alternative to quantifying vehicle emissions, because the data are collected under real conditions, on any route we want [1].

The light vehicles are tested under controlled laboratory conditions using a standardized cycle. For the pollutant emissions evaluation, the test conditions are well

I. Dumitru et al. (Eds.): SMAT 2019, *The 30th SIAR International Congress of Automotive and Transport Engineering*, pp. 241–248, 2020.
https://doi.org/10.1007/978-3-030-32564-0_29

known and there could be a risk of a configuration of the engine's operating mode for passing the emission tests when operating under test conditions [2].

Most studies at EU level show that the emissions measured in real road conditions were higher than in the case of stand testing with at least 60% and 30% for diesel vehicles and respectively, for almost all pollutants. Also, the carbon dioxide emissions measured on the stand were lower by 10% to 50% compared to the actual emissions measured on board, for different vehicles [3].

In order to resolve these problems, on-board pollution evaluation is needed. Investigation of vehicle emissions with on-board measurement systems is a more efficient alternative in order to understand how these emissions contribute to air pollution [4].

2 Methodology

Our research aims to develop a methodology for measuring on-board emissions from vehicles, for different urban and extra-urban routes. For the present paper, the emission measurement system was tasted on the vehicle equipped with a spark ignition engine. There were 5 routes, of which 4 urban and one combined (urban and extra-urban). The results will help to prepare a methodology for testing on-board vehicles.

The measurements ware made using a portable analyzer, GA-21 plus, an equipment produced by Madur Austria. The GA-21 plus is a flue gas analyzer which can measure the emissions of: Oxygen - O_2, Carbon monoxide - CO, Nitric oxide - NO, Sulphur dioxide - SO_2, Carbon dioxide - CO_2, Nitrogen oxides - NO_x [5].

Experimental research has been made using a light vehicle, Dacia Sandero, equipped with a 1390 cm^3 spark ignition engine. Engine vehicle Power is 55 kW at 5500 rpm [6].

The pollutant emission measurement equipment has been fixed in the vehicle. Its probe was mounted on the vehicle exhaust as instructed in the operating manual of the equipment, as shown in Fig. 1.

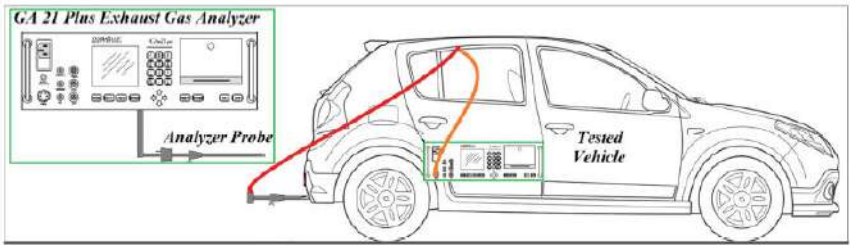

Fig. 1. GA-21 plus Analyzer placement inside tested vehicle.

The 5 routes that were run were chosen as representative for road transportation daily journeys in urban areas in Brasov City: the connection between residential areas and the historic centre, the connection between residential areas and industrial areas, connections between the historical centre and the civic centre or commercial areas, connections between the mall area and new residential neighbourhoods, etc.

The routes were numbered from 1 to 5, as follows:

Route 1 – Transilvania University Institute (Institutului Str.) + Făgărașului Street + Cristianului Street + Lungă Street + Livada Poștei (see Fig. 2);

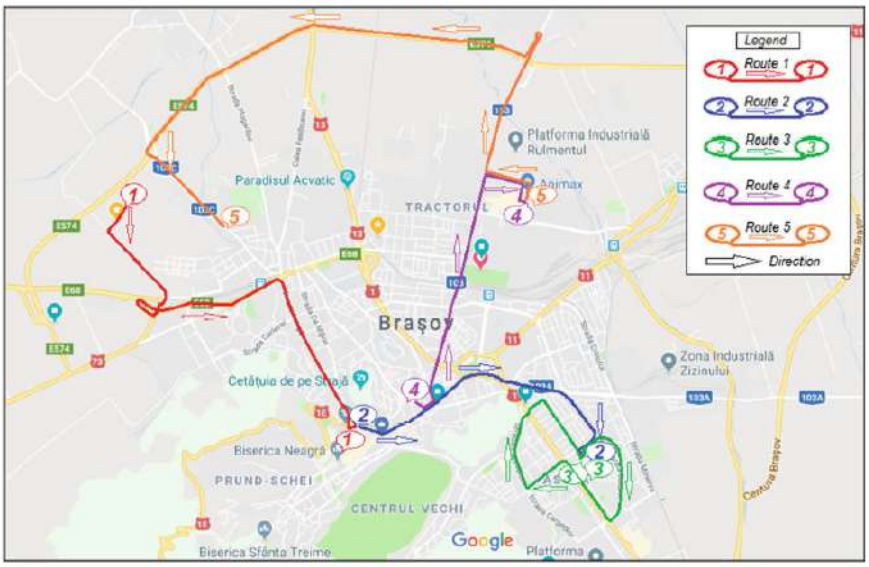

Fig. 2. The 5 analyzed routes from Brasov City.

Route 2 – Livada Poștei + Eroilor Boulevard + 15 Noiembrie Str. + Civic Centre + Zizinului Str. + Gemenii Intersection + Saturn Boulevard + Orizont Shopping Center (see Fig. 2);

Route 3 – Orizont Shopping Center + Saturn Boulevard + Calea București Str. + Zorilor Str. + Carpaților Str. + County Hospital + Traian Str. + Orizont Shopping Center (see Fig. 2);

Route 4 – Grădinarilor Str. + 15 Noiembrie Boulevard + Castanilor Str. +- 13 Decembrie Str. + Henri Coandă Str. + Coresi Mall (see Fig. 2);

Route 5 – Coresi Mall + Henri Coandă Str. + 13 Decembrie Str. + Brasov Bypass Road - Bartolomeu Residence + Lânii Str. (see Fig. 2).

All five routes were configured to be traveled within 10 min, depending on street categories, intersections, priorities, and road traffic. Every 10 s values for emissions (CO, CO_2, NO, NO_2, NO_x) was stored.

3 Research Results

The results resulted after the five tests were downloaded and it was created a database in order to analyze them [7].

For every report following parameters are saved: parameters values (CO, NO, NO_2, SO_2, H_2S, H_2) measured by the equipment cells and expressed in (ppm); calculated parameters values (O_2 (%), CO_2 (%), NO_x (ppm)); calculated parameters values (CO, NO, NO_2, SO_2, H_2S, H_2) expressed in (mg/m^3); flue gas temperature, T_{gas} (°C); ambient temperature T_{amb} (°C); excess air factor λ [5].

Pollution data stored after recording the tests (for all routes) are presented as charts (see Fig. 3).

Route 1 - It is a route that connects an institution (the Transylvania University Institute) and the historical centre of the city, more precisely with the main public transport terminal in this area (Livada Postei Terminal).

Route 2 - It is a route that connects the historical centre of the city (the terminus point of Route 1) and an important commercial area of Brasov (Orizont Shopping Center), passing through the civic centre of the city.

Route 3 - It is a route that has the same start and end point, starting from a commercial area (Orizont Shopping Center, the terminus point of Route 2) and passing through several residential areas and the area where the Brasov County Hospital is located.

Route 4 - It is a route that connects one of the limitrophic areas of the historical centre (Patria area) and the main shopping area of the city (Coresi Mall), passing one of the busiest streets of Brasov (13 Decembrie Street).

Route 5 - It is a route that connects the city's main shopping area (Coresi Mall) and an expanding residential district (Bartolomeu) through the bypass road of the city.

Each route has peculiarities, but it can be assimilated by the majority of the metropolitan urban routes.

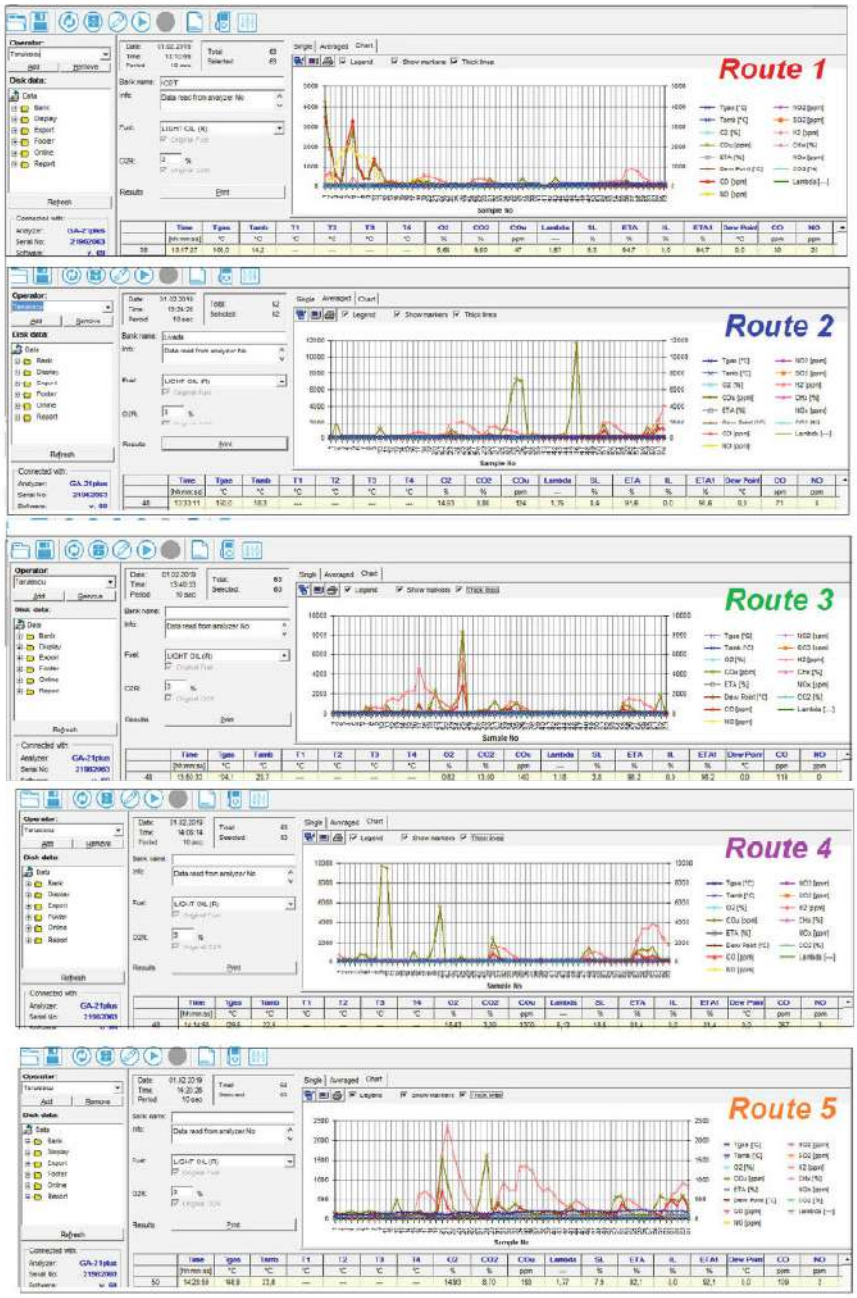

Fig. 3. Pollution data stored from GA21Plus analyzer, for all routes.

In order to compare the values registered for all 5 routes, CO, NO_x and CO_2 concentrations ware analyzed. These values are presented as charts in Figs. 4, 5 and 6.

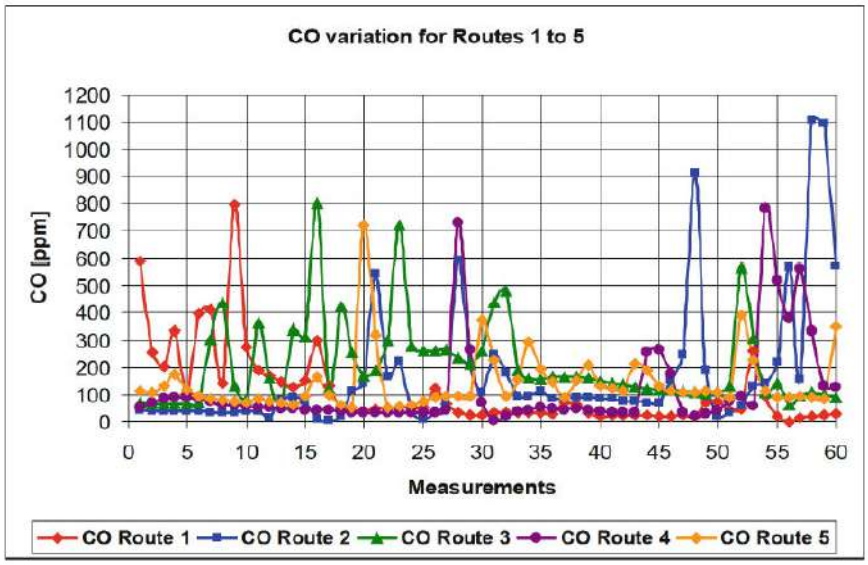

Fig. 4. The variation of CO at vehicle's exhaust pipe, for routes 1, 2, 3, 4 and 5.

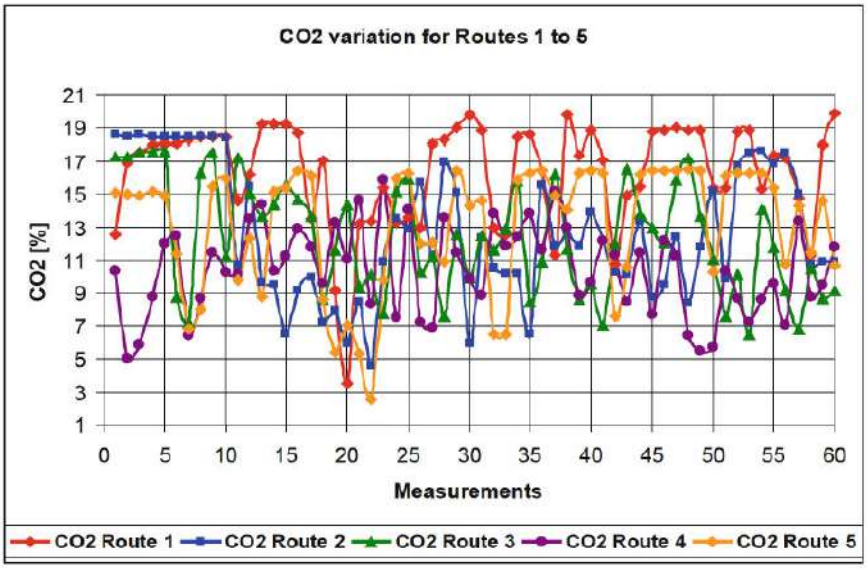

Fig. 5. The variation of CO_2 at vehicle's exhaust pipe, for routes 1, 2, 3, 4 and 5.

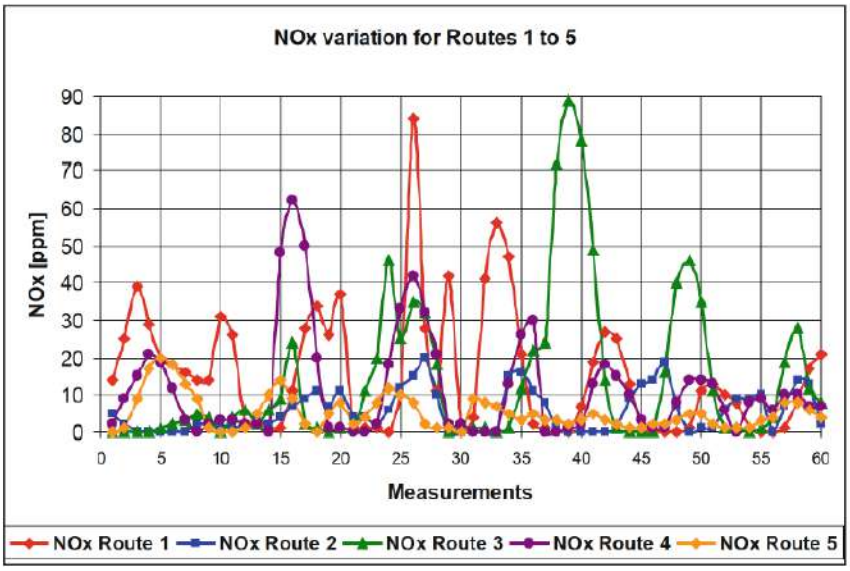

Fig. 6. The variation of NO_x at vehicle's exhaust pipe, for routes 1, 2, 3, 4 and 5.

For carbon monoxide the highest values were recorded for all routes in areas where unstable engine regimes were used: departure, intersections, crowded areas, and areas where a parking space was sought. By comparison, the highest values (peaks or mean values) were recorded for Route 2, Route 3 and Route 4.

In the case of carbon dioxide, the values varied substantially for all routes. By comparison, the highest values (peaks or mean values) were recorded for Route 1 and Route 5, on speed corridors. In the case of Route 1, the highest values were recorded in the starting area, on the Institutului Street and Fagarasului Street, but also in the case of the main arteries with one sense, Lunga Street. For Route 5, the maximum values were recorded when we were on the bypass road of the city.

In the case of nitrogen oxides, the values varied in areas of use of the engine to unstable modes: intersections, turns, pedestrian crossings, crowded areas. The highest values were recorded for Route 1 and Route 3. These two routes are also most fragmented by intersections, pedestrian crossings and priority losses.

4 Conclusions

The on board measurement for vehicles emission is an optimal strategy compared to the strategies based on static measurements, under laboratory conditions. Measurement of emissions on board provides data at any time and location, resulting in a more representative database than can be obtained classically.

The paper presents a methodology for performing tests of emissions from exhaust gases of vehicle in urban and urban/ extra urban environment. To be relevant, tests have to be done on routes showing general elements specific to certain types of cities. In this case, the routes were chosen to be representative of metropolis in Europe. Short trips of about 10 min have been simulated to cover the usual destinations of those that use personal vehicles.

The values of carbon monoxide, carbon dioxide and nitrogen oxides, specific to spark ignition engines, have been analyzed. The highest values were recorded for all routes in areas where unstable engine regimes were used: departure, intersections, crowded areas, and areas where a parking space was sought.

The next step of the research is to find a route that will faithfully simulate the current European test cycle and determine the differences between the values recorded in laboratory and real-time conditions when going through the real route. The research will be made according to the RDE legislative requirements laid down in Regulations (EU) 2017/1151, 2016/467, 2016/626, and 2017/1154 (collectively referred to in this document as the RDE LDV regulations) [8].

References

1. Frey, H.C., Unal, A.: Use of on-board tailpipe emissions measurements for development of mobile source emission factors. Department of Civil Engineering North Carolina State University, Raleigh, NC 27695-7908
2. Rubino, L., Bonnel, P., Hummel, R., Krasenbrink, A., Manfredi, U.: Mobile measurement of pollutant emissions and fuel consumption of road vehicles in real-world driving situations using portable emission measurement systems (PEMS), JRC REF N°28555-2005-08 A1CO ISP
3. Saâdane, C., Boughedaoui, M., Kerbachi, R., Joumard, R.: On-board measurement of emissions from liquefied petroleum gas, gasoline and diesel powered passenger cars in Algeria. HAL Id: hal-01250461. https://hal.archives-ouvertes.fr/hal-01250461
4. North, R.J., et al.: Development of a vehicle emissions monitoring system. Transp.: Proc. Inst. Civ. Eng. **158**(3), 167–177 (2005)
5. Flue Gas Analyser GA-21 plus: Operating manual, Madur Electronics, Vienna - Austria (2013)
6. Ţârulescu, S., Şoica, A.: Emissions level approximation at cold start for spark ignition engine vehicles. Appl. Mech. Mater. **555**(2014), 375–384 (2014)
7. Cofaru, C.: Pollution legislation in road transportation. Transilvania University of Brasov (2002)
8. Valverde Morales, V., Bonnel, P.: JRC technical report, on-road testing with portable emissions measurement systems (PEMS) (2017). https://ec.europa.eu/jrc

Smart Transportation CO_2 Emission Reduction Strategies

Smart Transportation CO_2 Emission Reduction Strategies

S Tarulescu[1], R Tarulescu[1], A Soica[1] and C I Leahu[1]
[1]Transilvania University of Brasov, Eroilor Boulevard Nr. 29, Romania

Abstract. Transport represents the sector with the fastest growing greenhouse gas emissions around the world. The main global objective is to reduce energy usage and associated greenhouse gas emissions from the transportation sector. For this study it was analyzed the road transportation system from Brasov Metropolitan area. The study was made for the transportation route that connects Ghimbav city to the main surrounding objectives. In this study ware considered four optimization measures: vehicle fleet renewal; building the detour belt for the city; road increasing the average travel speed; making bicycle lanes; and implementing an urban public transport system for Ghimbav. For each measure it was used a mathematical model to calculate the energy consumption and carbon emissions from the road transportation sector. After all four measures was analyzed is calculated the general energy consumption and CO_2 reduction if this are applied from year 2017 to 2020.

1. Introduction

The cities from Europe are centres of many activities: economic, social and innovation. Many of them face many challenges to their mobility systems: traffic jams, poor air quality, noise pollution, green house gases emissions and road accidents. All of these have significant negative impacts over the environment, human health and economic performance of cities. These problems will increase in intensity in the future, because, the cities continue to grow [1].

Urban transport systems are important elements of the European transport system and are a concern for the European Common Transport Policy. The 2011 Transport White Paper sets very ambitious targets to address these challenges, especially for Central European Countries. In this case, there is a wide range of instruments available to implement the policy efforts: efficient land usage, urban planning, pricing policy, infrastructure for non-motorised vehicles, charging/refuelling of clean vehicles to reduce emissions, 100% green transportation systems and infrastructure upgrades. These instruments should be part of a meaningful strategy in order to develop cost-effective interventions.

The target is the year 2030, in order to meet the Transport White Paper objectives for urban transportation [1].

The development of the roadmaps helps to recognise that different types of policy measures are appropriate for different types of cities. The analysis of scenarios and roadmaps help to assess the impact of the European urban mobility policies in the long term [1].

In Romania transport policy aims to align the national transport system continues to Community Transport Policy principles defined in the Transport White Paper (with corresponding updates) and the requirements of sustainable development of Romania [2].

For this study it was analyzed the road transportation system from Brasov Metropolitan area. The study was made for the transportation route that connects Ghimbav city to the main surrounding objectives. This region faces many mobility problems, because is situated in the centre of Romania, at the junction of several main transportation routes. This mobility problems affect Brasov city and all

communities from the metropolitan zone. The city of Ghimbav is an important industrial, economic and residential city, despite its size (5200 inhabitants).

2. The analyzed area

For this study it was analyzed the transportation modes from Brasov Metropolitan Area, especially in the surroundings of Ghimbav city. The city of Ghimbav is located in the west of Brasov County, with the following geographic coordinates: 45 degrees 39 minutes wide. N; 25 degrees 36 minutes long. E. The road connections with these areas are insured by the national road network (DN1 and DN73B) and county road (DJ 103C).

This area is an important industrial zone, but also is an expanding residential zone. In the future in this area will be developed some important objectives, such as: International Airport Ghimbav-Brasov, Brasov-Comarnic highway, an agreement zone and more residential districts. The connections between the Ghimbav city centre and all this objectives will be made by road transportation (passengers and freights). In the figure 1 is presented the Ghimbav zone and its connections with actual and future objectives.

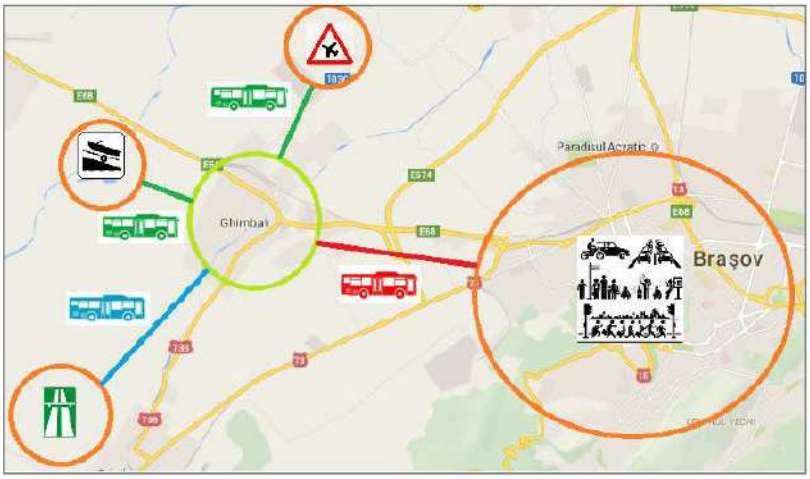

Figure 1. Analyzed area - Ghimbav city and its connections with actual and future objectives (Google Maps)

3. Energy consumption and CO_2 mitigation model for

3.1. Mathematical model for Ghimbav transportation system

For the city of Ghimbav it was made a prediction model in order to estimate the energy consumption diminish and the CO_2 amount resulted from road transportation. Three optimization measures ware considered: vehicle fleet renewal; making bicycle lanes; and green public transportation system implementation.

There were calculated the proportions of decrease for the following:

- Final energy consumption [MWh].
- Total CO_2 Emissions / CO_2 equivalent [6].

The study was start from initial data: Ghimbav vehicle fleet composition during 2008 - 2012; values expressed in tones of CO_2 produced in the 2008 -2012 period.

The prediction model uses traffic volumes data from 2010 - 2015 period in order to predict the traffic flows for the 2016 - 2020 period. Using existing data on vehicle fleet, the total energy consumption and CO_2 emissions for Ghimbav we can calculate the total energy and CO_2 emissions for 2016 - 2020

period. Following the mathematical modelling results the dependence of total energy consumption and amount of emitted CO_2 over the vehicle fleet evolution [6].
Without applying any measures, the energy consumption will increase in the following years. Equation (1) described by polynomial second degree regression curve, represents Energy consumption evolution up to 2020, for transportation sector (also in Figure 2):

$$X_{Energy} = 25{,}432 \cdot V_E^2 - 10217 \cdot V_E + 10^8 \quad (1)$$

Where: X_{Energy} is the approximate amount of the total energy consumed, and V_E is the number of etalon vehicles. For this function, the standard deviation (R^2) is 0.9963.

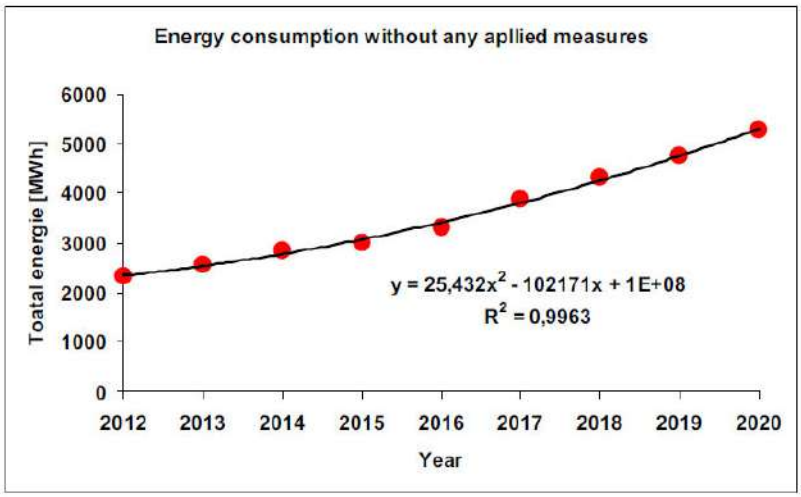

Figure 2. Energy consumption prevision for 2020 without any transportation applied measures

The CO_2 emission values will increase directly proportional with energy consumption. In order to decrease energy consumption and CO_2 emission values it is necessary to implement the measures mentioned above [8].
The standard emissions factors applied in this study are:

- 0.249 [tones CO_2 / MWh] - for spark ignition engines;
- 0.267 [tones CO_2 / MWh] - for compression ignition engines;
- 0.000 [tones CO_2 / MWh] - for biofuels [6].

For the transportation sector, data for each fuel and vehicle were calculated using the formula:

$$X_{UsedFuel} = D \cdot C_{average} \cdot Y \quad (2)$$

Where: $X_{UsedFuel}$ - Energy consumption for road transportation [kWh]; D - route distance [km]; $C_{average}$ - average fuel consumption [liters/km]; Y - conversion factor for each fuel [kWh/liters]. Y = 9.2 for gasoline and Y = 10 for Diesel [8].

3.2. Vehicle fleet renewal

This measure can only be applied to the municipal and local transport fleet. Using the data on the number of municipal vehicles fleet of Ghimbav city and from related fuel consumptions, result the following [6].
Fleet renewal for municipal fleet will lead to a consumption decrease for: from 10 liters/100 km to 8 liters/100 km for light vehicles and from 30 liters/ 00 km to 25 liters/100 km for heavy vehicles. After applying these measures will have a reduction: 448.97 [MWh] and 117,84 [tones CO_2].

3.3. Bicycle lanes implementation

Cycling has a major role for mobility quality in metropolitan areas. By using non-motored vehicles, congestions will be lighter and local air pollution and emissions of greenhouse gases will decrease. About 20% of car trips are less than 3 kilometres, a distance that can be easily made by the bike in less than 15 minutes [5]. The study is based on approximate traffic volumes decrease by creating bicycle lanes in Ghimbav city and on the main roads that connects Ghimbav with the stranding cities (Brasov, Codlea and Cristian).

Figure 3. Bicycle lanes implantation strategy: bicycle lane example (left); bicycle lanes strategy in Ghimbav city for 2020

According to the analyzed data in this study for bicycle lanes, resulted a decrease of 8% road traffic volumes after the construction of a bicycle lane in Ghimbav. After applying this percentage reduction for total vehicle we have a reduction of: 1015.28 [MWh] and 260,82 [tones CO_2] [6].

According to the analyzed data in this study for bicycle lanes, resulted a decrease of 8% road traffic volumes after the construction of a bicycle lane in Ghimbav. After applying this percentage reduction for total vehicle we have a reduction of: 1015.28 [MWh] and 260,82 [tones CO_2] [6].

3.4. Implementing a green urban public transport system for Ghimbav

Public transportation systems, including electric buses, contributes to cleaner air and quality of life in cities and reduces green house gas emissions, as it uses up fewer resources and emits less CO_2 than other transportation modes. Compared to private motorised mobility, public transportation makes the most efficient and equitable use of scarce resources, such as fuel and public space. By occupying less space and generating fewer emissions per passenger, public transport enhances the quality of life in cities. The full potential can be exploited in the right conditions, when buses operate on reserved priority lanes and with prioritization measures [3].
Also, implementing a public transportation with electric buses will lead to a noise level diminish in city area. Road traffic noise may depend by several parameters: the traffic volume, the traffic flow typology, the vehicles typology, the road and pavement features, the speed. The influence of the speed on the noise is determined by two main factors: the interaction between tires and road and the power train noise, influenced by the engine speed. The power train noise will be significant decrease if electric buses are used [7].
For Ghimbav city was proposed two public buses routes. First route will cover the Ghimbav city centre, connections to schools, City Hall, commercial objectives and residential areas. The second route will cover residential areas, City Hall, industrial areas, Ghimbav Industrial Park, Aerotec an Airbus (in the perimeter of future International Airport) and commercial objectives.
For this paper it will be presented Route 1. The public transportation system parameters are presented in the following paragraphs:

- The total length of the route: 5,50 km.

- Total journey time: 30 minutes.
- Number of bus stations (stops) on the route: 11.
- The average bus stop time in stations: 1,2 minutes.
- Number of intersections (without priority) on the route: 7.
- The average stop time at intersections is 30 seconds.
- Buses speed limit on the route: 50 km/h.
- Cruising speed (average) of the route: 25 km/h.
- Peaks of passenger demand: Monday - Friday (working days): between 6:00 h – 10:00 h and 14:00 h – 18:00 h; Saturday: between 18:00 h – 22:00 h; Sunday: between 18:00 h – 22:00 h.
- Necessary buses: 3 peaces.

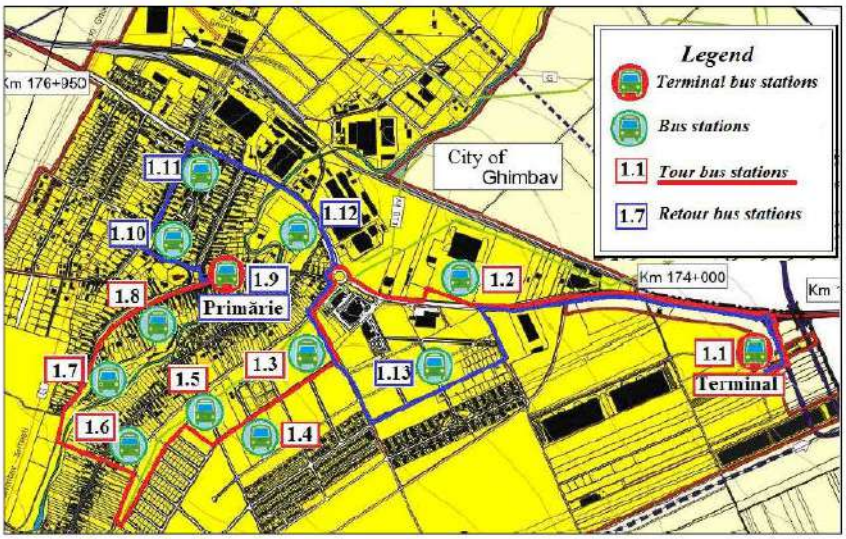

Figure 4. Electric public transportation system for Ghimbav - Route 1 presentation

Figure 5. Electric bus Route 1 length (Google Maps)

The arrival frequency of bus stops in weekly hours is shown in the Table 1.

Table 1. Frequency buses arrival in station (hourly intervals)

Weekdays	*Hour interval*	*Time frame between consecutive arrivals*
Monday - Friday	22:00 h – 6:00 h 10:00 h – 14:00 h și 18:00 h – 22:00 h 6:00 h – 10:00 h și 14:00 h – 18:00 h	60 minutes 20 minutes 10 minutes
Saturday	22:00 h – 6:00 h 6:00 h - 22:00 h	60 minutes 20 minutes
Sunday	22:00 h – 6:00 h 6:00 h - 22:00 h	60 minutes 20 minutes

The transportation system will have an integrated management system in order to control very efficient the network. It can be used as an example the public transportation management system from Brasov. Necessary infrastructure for electric buses will be needed. Also, two terminal stations and 15 bus stations will be made.

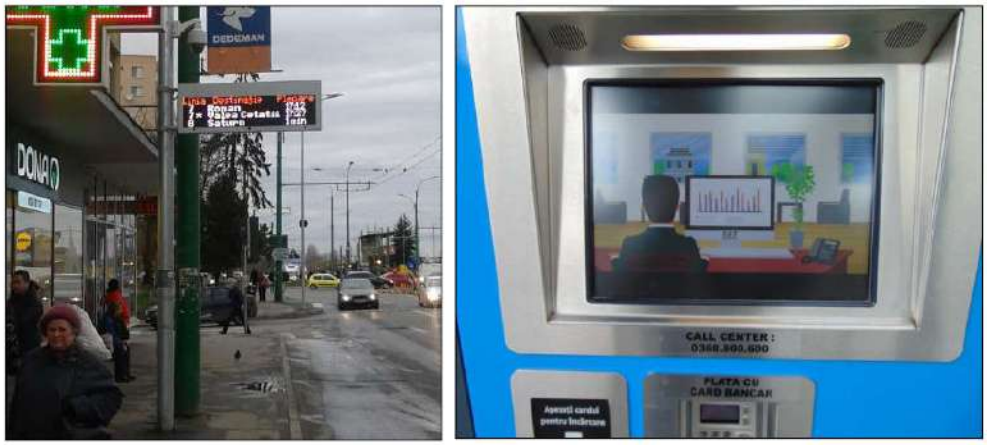

Figure 6. The public transportation management system from RAT Brasov

The implementation of an urban public transport system serving the Ghimbav population will reduce the number of daily journeys made with personal cars in the following years as follows:

Table 2. The decrease percentage of local road traffic

Year	*2016*	*2017*	*2018*	*2019*	*2020*
The decrease percentage of local road traffic after public transportation implementation:	5 %	15 %	30 %	40 %	50 %

After applying this measure, we will have a reduction of: 1785,35 [MWh] and 458,64 [tones CO_2].

3.5. Estimated impact of analyzed measures in the future

In order to estimate the impact of implementing the proposed long-term measures, a calculation resource used in the European Union was used. This resource is Urban Transport Roadmaps framework (it is one of the tools used by the metropolitan development agencies). Using this framework, we can estimate the benefits of implementing the three measures for reducing energy consumption for Ghimbav, up to year 2030 (Figure 7, 8, 9 and 10) [4].

In Figure 7 is presented the evolution of carbon dioxide emissions after the implementation of the measures (reference year - 2017). On the left is anticipated the quantitative reduction of CO_2 from 2015 to 2030, after the implementation of the measures in 2017. On the right is the evolution of the CO_2 level produced by the studied region from 2015 to 2030, after applying the measures in 2017 (cumulated CO_2 level).

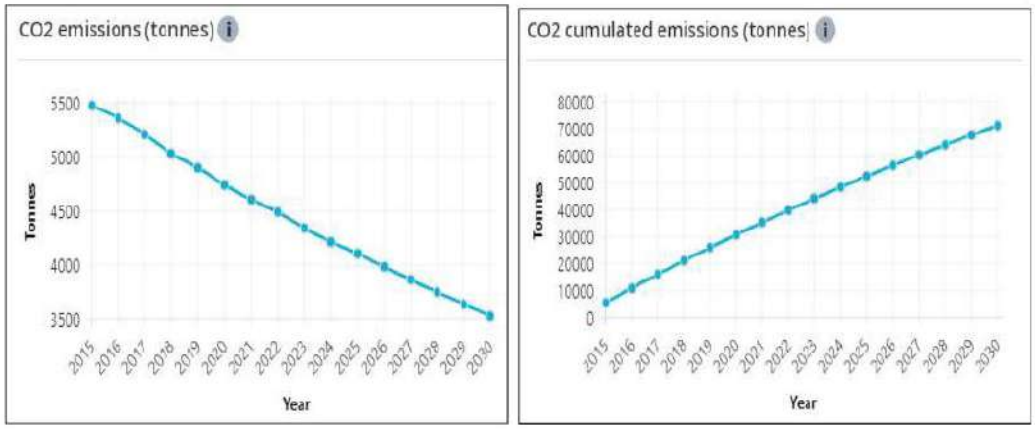

Figure 7. CO_2 emissions reduction after smart measures implementation [4]

In Figure 8 is presented the evolution of carbon monoxide pollution level after the implementation of the measures. On the left is anticipated the quantitative reduction of CO from 2015 to 2030, and on the right is the evolution of the CO level produced by the studied region, after applying the measures in 2017 (cumulated CO level).

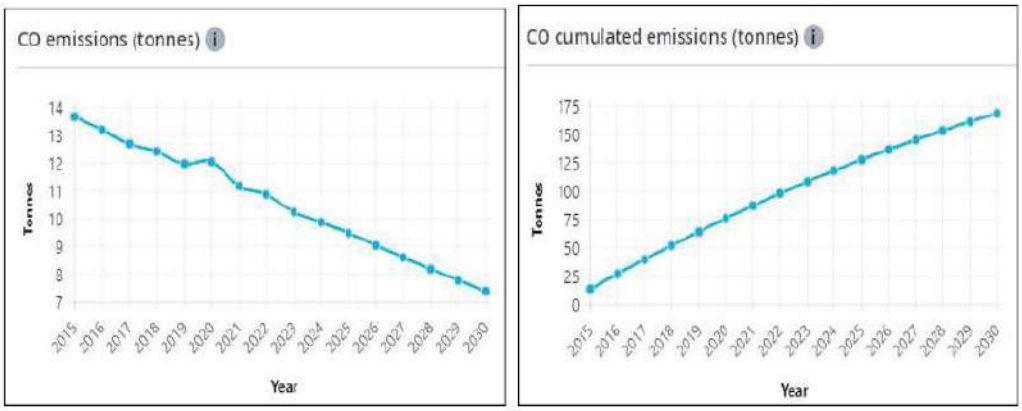

Figure 8. CO emissions reduction after smart measures implementation [4]

In Figure 9 is presented the evolution of particulate matter (PM) pollution level after the implementation of the measures. On the left is anticipated the quantitative reduction of PM from 2015 to 2030, and on the right is the evolution of the PM level produced by the studied region, after applying the measures in 2017 (cumulated PM level).

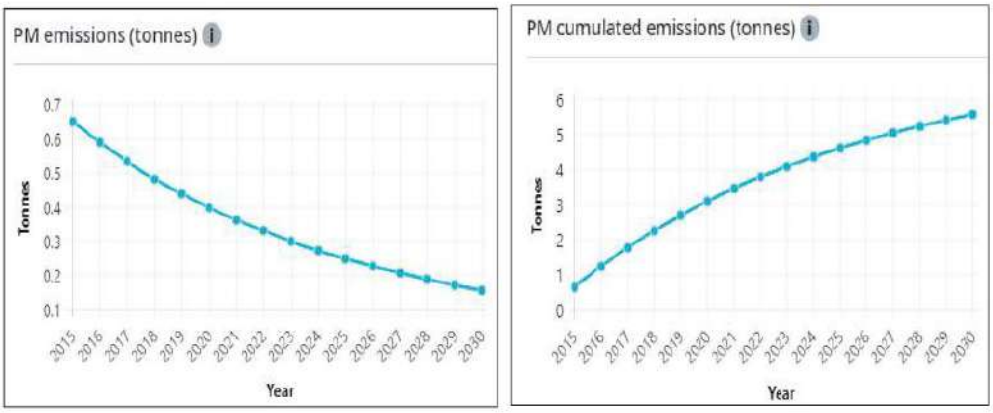

Figure 9. Particulate Matter (PM) emissions reduction after smart measures implementation [4]

The economy output after vehicle fleet renewal, making bicycle lanes and green public transportation system implementation is expressed in the Figure 10.

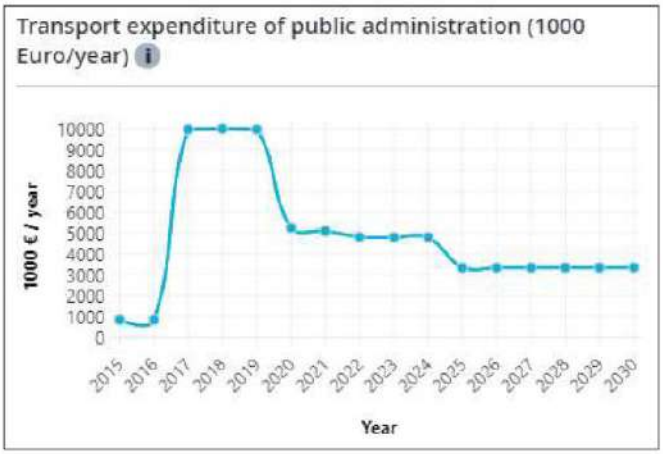

Figure 10. Transport expenditure of public administration after smart measure implementation for Ghimbav city [4]

4. Conclusions

For this study were analyzed three measures that can be adopted in order reduce energy consumption and CO_2 emissions: vehicle fleet renewal; making bicycle lanes; and green public transportation system implementation. The most effective measure, implementing a green urban public transport system for Ghimbav, will result in a decrease in energy consumption and CO_2 emissions by 19.71%. Making bicycle lanes will lead to lower energy consumption and CO_2 emissions by 11,21%. Vehicle fleet renewal strategy will lead to lower energy consumption and CO_2 emissions by 5%.

Using Urban Transport Roadmaps framework, we can estimate the benefits of implementing the three measures for reducing energy consumption for Ghimbav, up to year 2030. It can by noticed a substantial reduction of the CO_2, CO and PM emissions after implementation of the smart measures at

Ghimbav City. Also, the pollution level of the analyzed area will increase less after the implementation of these measures.

5. References

[1] C. de Stasio (TRT), D. Fiorello (TRT), F. Fermi (TRT), G. Hitchcock (Ricardo Energy & Environment), S. Kollamthodi (Ricard Energy & Environment), *Study On European Urban Transport Roadmaps 2030, Urban transport policy roadmaps*, European Platform on Sustainable Urban Mobility Plans, Ref: MOVE/C1/2013-188-2, March 2016.

[2] E.Vasile, M. Balan, I. Grabara, S. Balan, *Measures to Reduce Transportation Greenhouse Gas Emissions in Romania*, Polish Journal of Management Studies, 2012.

[3] The International Association of Public Transport (UITP), *Bus systems in Europe: Towards a higher quality of urban life and a reduction of pollutants and CO_2 emissions*, June 2015, Bruxelles.

[4] G. Hitchcock, *European Urban Transport Roadmaps to 2030, A policy support tool for small and medium size cities,* Ricardo-AEA, *http://www.urban-transport-roadmaps.eu/scenario/2bc5e0cf#*

[5] Protected Bicycle Lanes, *New York City Department of Transportation – Polly Trottenberg*, Commissioner September 2014.

[6] U.A.T. Ghimbav, *Action Plan for Sustainable Energy Of Ghimbav City*, *http://primaria-ghimbav.ro/docs/2016/2016-09-16-PAED-Ghimbav-2016.pdf,* September 2016.

[7] D. Covaciu, D. Florea, J. Timar, *Estimation of the noise level produced by road traffic in roundabouts*, Applied Acoustics, Volume 98, November 2015, Pages 43-51.

[8] S. Tarulescu Stelian, R. Tarulescu, *Urban Transportation Solutions for the CO_2 Emissions Reduction Contributions*, 12th International Congress of Automotive and Transport Engineering (CONAT), DOI: 10.1007/978-3-319-45447-4_49, ISBN:978-3-319-45447-4, 2016.

Acknowledgments

We hereby acknowledge the national project "*Introducere sistem de transport urban inteligent și ecologic în orașul Ghimbav. Trasee și infrastructură pentru transport electric*", 1755/16.02.2017 and Transilvania University of Brasov for providing the infrastructure used in this work.

Also, we hereby acknowledge the structural founds project PRO-DD (POS-CCE. O.2.2.1.. ID 123. SMIS 2637. ctr. No 11/2009) and Transilvania University of Brasov for providing the infrastructure used in this work.

Researches on Combustion Quality for a Single Cylinder Diesel Engine

Conference Paper · October 2016

DOI: 10.1007/978-3-319-45447-4_48

2 authors:

Stelian Tarulescu
Universitatea Transilvania Brasov
68 PUBLICATIONS 111 CITATIONS

SEE PROFILE

Radu Tarulescu
Universitatea Transilvania Brasov
78 PUBLICATIONS 102 CITATIONS

SEE PROFILE

Researches on Combustion Quality for a Single Cylinder Diesel Engine

Stelian Tarulescu(✉) and Radu Tarulescu

Transilvania University of Brasov, Brasov, Romania
{s.tarulescu, radu.tarulescu}@unitbv.ro

Abstract. The present paper presents researches on combustion quality for a Diesel single cylinder engine. The tests ware made on an AVL single cylinder test bed for gasoline and diesel engines. In this case, it was used an AVL 510 cc Single Cylinder Engine Type 5402. The quality of the combustion for this engine was analyzed and compared with the theoretical principles. During the test was noticed that the main engines parameters are variable for 100 engine cycles. The variation occurs in function of the air temperature, air/fuel mixture formation, cooling system variation, combustion start moment and several engine design parameters. In order to increase the combustion quality, some measures can be applied: using different injection strategies; varying the advance angle of the spark related to TDC; varying the quantity of fuel injected per engine cycle; optimization of combustion chambers.

Keywords: Diesel · Combustion · Quality · Engine · Mixture

1 Introduction

In order to obtain data and optimize solutions for GDI engines, a research program was developed at Transilvania University of Brasov, ICDT - Research & Development Institute. The research stand is an AVL single cylinder test bed for gasoline and Diesel engines. For the present paper, the tests was made on a AVL CR Diesel Single Cylinder Research Engine 5402. The single cylinder can be setup in several configurations (with multipoint injection, with direct injection, with turbocharger). The mixture formation and combustion processes of the fuel can be monitored through the test bed component software, AVL FIRE Commander 7.06c - IAV [2].

2 Combustion Quality Evaluation for Diesel Engines

In Fig. 1 is presented the typical data for cylinder pressure, fuel injector needle lift and fuel pressure in the nozzle gallery through the compression and expansion strokes of a direct injection Diesel engine. The rate of fuel injection can be obtained from the fuel pressure, cylinder pressure, nozzle geometry, and needle lift profiles by considering the injector as one or more flow restrictions. There is a delay between the start of injection and start of combustion. The pressure rises rapidly for a few crank angle degrees, then more slowly to a peak value. Injection continues after the start of combustion. The general

A. Chiru and N. Ispas (eds.), *CONAT 2016 International Congress of Automotive and Transport Engineering*, DOI 10.1007/978-3-319-45447-4_48

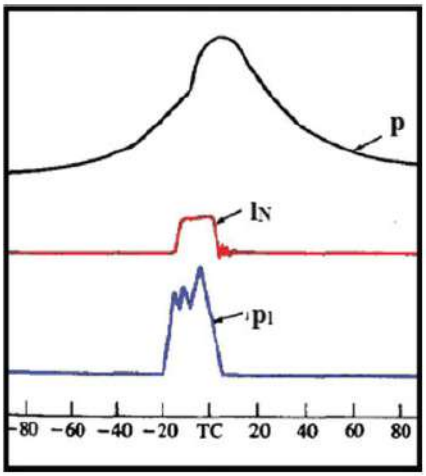

Fig. 1. Cylinder pressure p, injector needle lift I, and injection system fuel line pressure p_i, as functions of crank angle for small DI diesel engines (Source: B. Heywood, Internal Combustion Engine Fundamentals, p. 503)

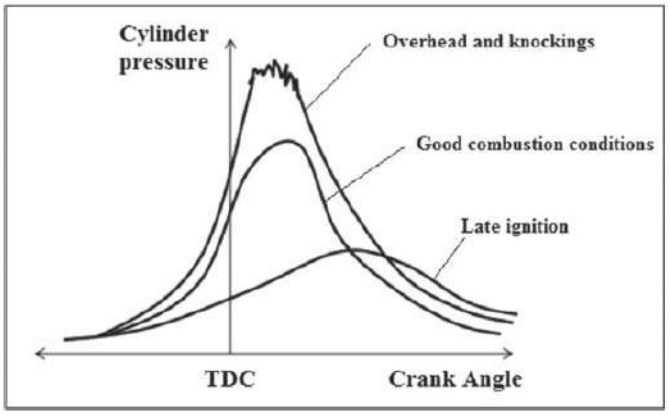

Fig. 2. Cylinder pressure variation in function of combustion quality (Source: W. Pulkrabek)

shape of the rate of heat release curve is typical of this type of DI engine over its load and speed range [5].

Estimates of the rate at which fuel and air mixture with composition within the combustible limits is produced in Diesel sprays under typical engine conditions, based on a variety of turbulent jet models of the spray show that mixing rates and burning rates are comparable in magnitude. Estimates of characteristic times for the turbulent jet

mixing processes in diesel combustion chambers show these to be comparable to the duration of the heat release process, and much longer than characteristic times for evaporation and the combustion chemical kinetics (Fig. 2) [3, 4].

3 Used Equipments

The researches presented in the present paper ware made on a AVL CR Diesel Single Cylinder Research Engine 5402 with following specifications:

- Bore: 85 mm; Stroke: 90 mm.
- Displacement: 510 cm^3.
- Max. speed: 4200 rpm.
- Max. firing pressure: 180 bar.
- Max. BMEP: 14 bar at 2300 rpm supercharged.
- Max. output: 19 kW at 4200 rpm supercharged.
- Compression ratio: 17:1.

The test bed have some other components and systems: AVL Engine Control Unit (AVL ETU 427); Coolant and conditioning Unit 577; AVL Fuel mass flow meter - Type Flex Fuel; AVL Fuel temperature control; Intake Air Consumption Measurement Device; Particle Evaluation - Micro Soot Sensor Continuous Measurement of Soot Concentration; AVL PUMA Open Test bed Automation (Fig. 3) [1].

Fig. 3. Engine parameters read from the AVL PUMA Open Test bed Automation

The used software for intake and combustion process optimization is AVL FI2RE Commander 7.06c – IAV. AVL FIRE was developed to solve the most demanding flow problems in respect to geometric complexity and chemical and physical modelling. FIRE offers a comprehensive computational fluid dynamics solution: a powerful set of modules, features and capabilities, pre-and post-processing integrated in a common environment and workflows and methods effectively supporting the use of the software to solve any problem accurately [2].

The software used for engine parameters monitoring is AVL Indicom software. During cycle based data acquisition the value of cycle time must vary all the time.

4 Research Methodology

The engine was tested in controlled laboratory conditions. The used fuel was Diesel Petrom Standard. The atmospheric temperature was constant maintained at 18°C.

The test was made for 50 % load and for 1500, 2000, 2500, 3000 and 3500 rpm engine speeds. The intake parameters are controlled by set the number of injections. In this case it was used only two injection phases (first pilot injection and main injection) from a maximum of for possible phases. The fuel mixture was adjusted by varying the amount of fuel injected per cycle (injection period - μs). The ignition time was set in crank angle degrees before top dead centre. The engine combustion quality was tested for 100 engine cycles.

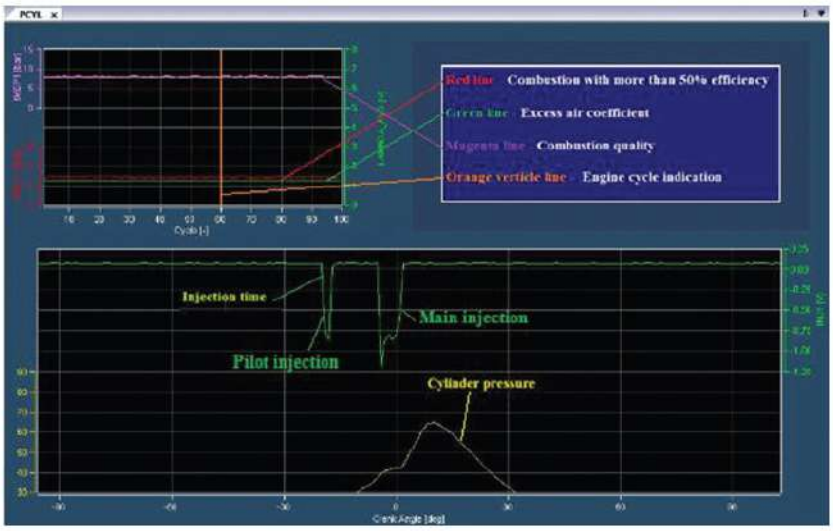

Fig. 4. The intake and combustion features for AVL CR Diesel Single Cylinder Research Engine 5402, for 50 % Load and 1500 rpm

The parameters changes were made to obtain an optimal single cylinder pressure curve and more optimal combustion (no detonations). In the Fig. 4 are presented the intake and combustion features for AVL CR Diesel Single Cylinder Research Engine 5402. The upper window presents the parameters for intake and combustion quality: combustion quality, combustions with more than 50 % efficiency and excess air coefficient (mixture quality).

The main window presents the injection time (in function of engine crank angle and TDC) and engine cylinder pressure.

The paper presents researches on combustion quality for an experimental single cylinder Diesel engine. The tests ware made on a AVL single cylinder test bed for single cylinder engines. In this case, it was used a AVL 510 cc Single Cylinder Engine Type 5402. The quality of the combustion for this engine was analyzed and compared with the theoretical principles. During the test was noticed that the main engines parameters are variable for 100 engine cycles.

In the following diagrams are presented the variation of engine cylinder pressure for 100 engine cycles.

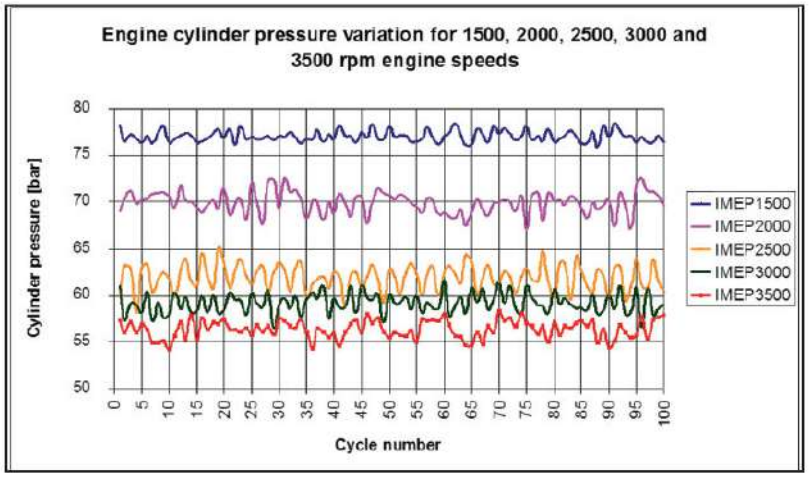

Fig. 5. Variation of engine cylinder pressure for 100 cycles, for 1500, 2000, 2500, 3000 and 3500 rpm engine speeds

From Fig. 5 results that the cylinder pressure varies for all tested regimes for all 100 cycles. The biggest variations are registered when engine runs at 2000 and 2500 rpm.

We can connect this variations with air/fuel mixture inside of combustion chamber. The mixture (lambda) is expressed as an electric parameter (an electric impulse value - expressed in Volts).

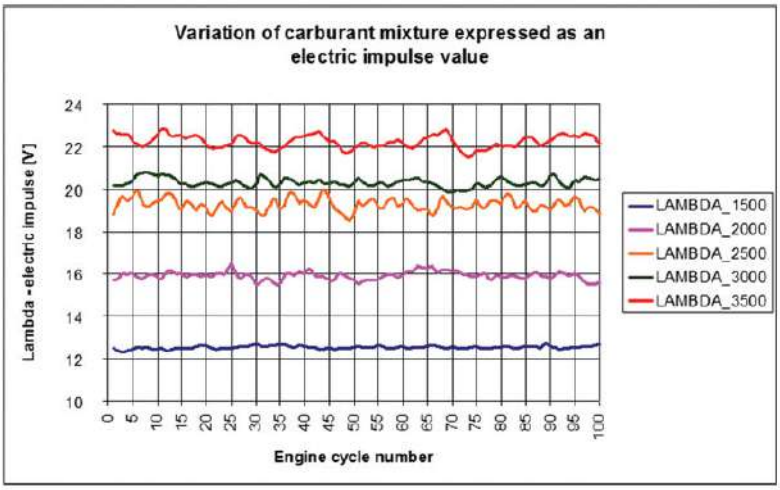

Fig. 6. Variation of carburant mixture for 100 cycles, for 1500, 2000, 2500, 3000 and 3500 rpm engine speeds

Figure 6 presents the variation of fuel/air mixture for all 100 engine cycles and for the same engine regimes (50 % load and 1500, 2000, 2500, 3000 and 3500 rpm engine speeds).

It results that the cylinder pressure varies for all tested regimes for all 100 cycles. The biggest variations are registered when engine runs at 2500, 3000 and 3500 rpm.

In this condition we can conclude that the fuel/air mixture can influence the quality of combustion for the analyzed engine.

5 Conclusions

In the research tests made on the experimental engine, a large set of data were collected for the analysis of combustion quality and efficiency. The combustion quality can be expressed by a set of graphical parameters, among which the most important is the engine cylinder pressure. For functional conditions there were recorded 100 engine cycles, at different engine regimes. It was observed a variation of cylinder pressure curve in function of the excess air coefficient and indicated mean effective pressure.

In order to optimize engine operation and for a high quality of combustion we can take the following measures:

- using an injection strategy with three or four phases;
- varying the advance angle of the spark related to TDC;
- varying the quantity of fuel injected per engine cycle;
- optimization of combustion chambers.

All these strategies can be tested using the software component AVL FI2RE Commander 7.06c – IAV.

Another set of measures can be related to modelling the combustion chambers. There has always been extensive debate over the optimum Diesel engine combustion chamber design. There are a large number of options for cylinder head and piston crown shape, spark plug location, size and number of valves, and intake port design.

The major combustion chamber design objectives which relate to engine performance and emissions are:

- a fast combustion process, with low cycle-by-cycle variability, over the full engine operating range;
- a high volumetric efficiency at wide-open throttle;
- minimum heat loss to the combustion chamber walls;
- a high fuel cetane requirement [6].

Acknowledgements. We hereby acknowledge the structural founds project PRO-DD (POS-CCE, O.2.2.1., ID 123, SMIS 2637, ctr. No 11/2009) and Transilvania University of Brasov for providing the infrastructure used in this work.

References

1. AVL - Tutorials and books for Engines Test Cell equipments usage (2013)
2. Fritz, O.: GDI engine development according EU 6, AVL Tutorials and books for Engines Test Cell (2013)
3. Pulkrabek, W.: Engineering Fundamentals of the Internal Combustion Engine, University of Wisconsin, Platteville (2004)
4. Gatowski, J.A., Balles, E.N., Chun, K.M., Nelson, F.E., Ehchian, J.A., Heywood, J.B.: Heat release analysis of engine pressure data, SAE paper 841359, SAE Trans., **93** (1984)
5. Heywood, J.B.: Internal Combustion Engine Fundamentals, edn. McGraw-Hill, Inc., New York (2000). ISBN:0-07-028637-X
6. Ţârulescu, S., Ţârulescu, R., Şoica, A.: Researches on Combustion Quality for a GDI Experimental Engine. In: AFASES Conference, Brasov (2016)

Urban Transportation Solutions for the CO2 Emissions Reduction Contributions

Conference Paper · October 2016

DOI: 10.1007/978-3-319-45447-4_49

CITATIONS
3

READS
1,315

2 authors:

Stolian Tarulescu
Universitatea Transilvania Brasov
68 PUBLICATIONS 111 CITATIONS
SEE PROFILE

Radu Tarulescu
Universitatea Transilvania Brasov
78 PUBLICATIONS 102 CITATIONS
SEE PROFILE

Urban Transportation Solutions for the CO_2 Emissions Reduction Contributions

Stelian Tarulescu(✉) and Radu Tarulescu

Transilvania University of Brasov, Brasov, Romania
{s.tarulescu, radu.tarulescu}@unitbv.ro

Abstract. Consumption of electricity and greenhouse gas production represents the actual global issues. To reduce energy consumption and the amount of CO_2 specific local measures need to be adopted. For this study it was analyzed the urban transportation system from Brasov Metropolitan Area. The study was made for the transportation route that connects Brasov city and Săcele city. For Săcele city it was made a prediction model in order to the decrease the energy consumption and the CO_2 amount resulted from road transportation. For this study ware considered four optimization measures: vehicle fleet renewal; increasing the average travel speed; making bicycle lanes; and students mobility management. There were calculated the proportions of decrease for the following: final energy consumption [MWh] and total CO_2 Emissions / CO_2 equivalent for each implemented measure.

Keywords: Transportation · CO_2 · Measures · Mitigation

1 Introduction

Many countries around the world have adopted very stringent regulations to monitor and control urban traffic emissions. Energy use and carbon emissions are influenced by how electricity is produced, use of energy in buildings and to move around the city. Urban density and spatial organization are the key factors that influence energy consumption, especially in the transportation and building sectors. The expansion of built-up areas through suburbanization has been particularly prominent among the metropolitan areas. Climate action over the urban level happens through local regulations, urban services, programme administration, city purchasing and property management, and convening of local stakeholders [1].

Dealing with climate changes will require many instruments and strategies implemented for local conditions. If we want to meet the objective of cutting emission by at least 30 % by 2050, the level generally agreed on to prevent dangerous anthropogenic interference, and minimize the costs involved, a number of strategies must be implemented or expanded in order to diminish the overall pollution level [1].

In the last three decades, emissions of greenhouse gases have increased by an average of 1.6 % CO_2 in fossil fuel use, reaching 1.9 %/year. In the absence of policy action, it is expected that these patterns of emissions growth to continue. For Romania, green house gases (GHG) resulted from different sectors also highlights the major

A. Chiru and N. Ispas (eds.), *CONAT 2016 International Congress of Automotive and Transport Engineering*, DOI 10.1007/978-3-319-45447-4_49

contribution to energy and transport sector, which means that they are areas on which are necessary to implement measures and actions to reduce CO_2 emissions [2].

In terms of environmental impact, there is a wide range of factors influencing high level of CO_2 emissions from road transport, such as supply and demand for road vehicles, individual mobility needs, availability/lack of availability of alternative public transport services common and associated costs of having a private vehicle. Although the energy efficiency of vehicles was and is still growing, this is offset by increased average length of travel, the increase of the fleet, and other variables, such as driving style, traffic jams etc., which translates into an increase in the intensity of emissions of GHG. In Romania transport policy aims to align the national transport system continues to Community Transport Policy principles defined in the Transport White Paper (with corresponding updates) and the requirements of sustainable development of Romania [2].

2 The Analyzed Area

For this study it was analyzed the urban transportation system from Brasov Metropolitan Area. The study was made for the transportation route that connects Brasov city and Săcele city.

The city of Săcele is located in the south-eastern county of Brasov, the historic region of Bârsa, on the river Tărlung. Being located to the southeast of the Brasov city, Săcele is one of 18 municipalities that are part of Brasov Metropolitan Area (as we can see in Fig. 1). The road connections with these areas are insured by the national road network (DN1 and DN1A) and county roads (DJ 103A, 103B, 102I).

Fig. 1. The analyzed area - Brasov city and Săcele city (Source: Google Maps)

Statistical data for Săcele city:
- The city area is 32,000 ha.
- Population: 32 185 inhabitants.
- Population density: 122 inhabitants/square km.

Săcele city, the second highest city of Brasov Metropolitan Area in terms of population, is also the only city after Brasov that have his own public passenger road transportation system [5].

3 Energy Consumption and CO_2 Mitigation Model for Săcele

3.1 Mathematical Model for Săcele Transportation System

For Săcele city it was made a prediction model in order to the decrease the energy consumption and the CO_2 amount resulted from road transportation. For this study ware considered four optimization measures: vehicle fleet renewal; increasing the average travel speed; making bicycle lanes; and students mobility management.

There were calculated the proportions of decrease for the following:

- Final energy consumption [MWh].
- Total CO_2 Emissions / CO_2 equivalent [6].

For this study we start from initial data: Săcele vehicle fleet composition during 2008–2013; values expressed in tones of CO_2 produced in the 2008–2012 period.

There were grouped the Săcele traffic volumes data for period 2009–2013 in order to predict the traffic values for the 2014–2020 period. There results values for Săcele fleet evolution for all vehicle categories for 2014–2020 period.

Using existing data on vehicle fleet, the total energy consumption and CO_2 emissions for Sacele in the 2008–2013 period and the resulting approximating fleet evolution data during 2014–2020 we can calculate the total energy and CO_2 emissions for 2014–2020 period.

Following the mathematical modeling results the dependence of total energy consumption and amount of emitted CO_2 over the vehicle fleet evolution. Two equations are described by polynomial second degree regression curves (also in Fig. 2):

$$X_{Energy} = 52,822 \cdot V_E^2 - 145,17 \cdot V_E + 22493 \quad (1)$$

Where: X_{Energy} is the approximate amount of the total energy consumed, and V_E is the number of etalon vehicles. For this function, the standard deviation (R^2) is 0.9743.

$$X_{CO2} = 14,897 \cdot V_E^2 - 61,213 \cdot V_E + 5725,3 \quad (2)$$

Where: X_{CO2} is the approximate amount of CO_2 emitted, and V_E is the number of etalon vehicles. For this function, the standard deviation (R^2) is 0.9601 (also in Fig. 3).

In order to decrease energy consumption and CO_2 emission values it is necessary to implement the following measures: vehicle fleet renewal; increasing the average travel speed; making bicycle lanes; students mobility management.

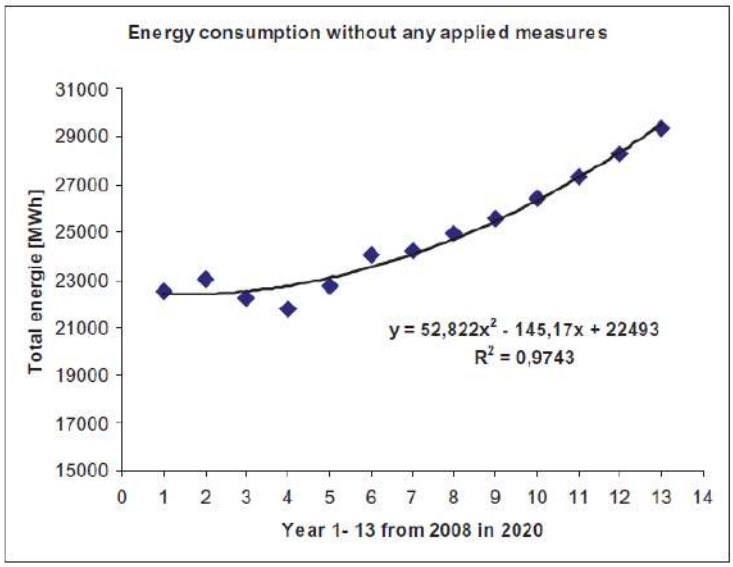

Fig. 2. Energy consumption prevision for 2020 without any transportation applied measures

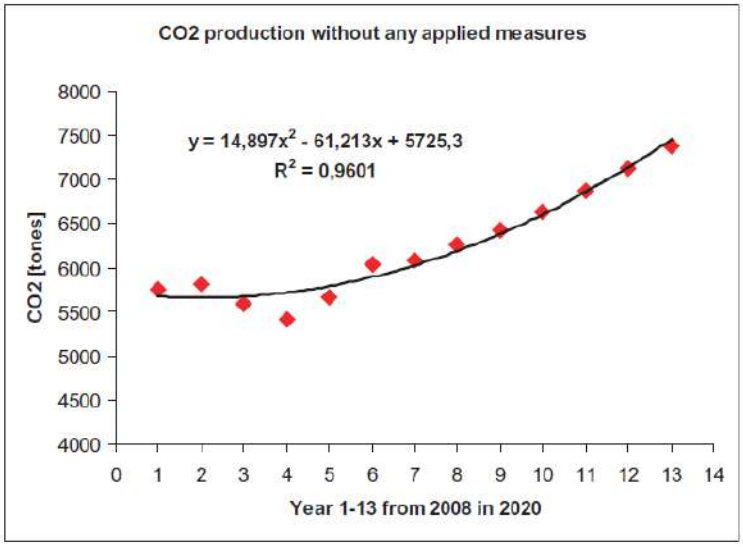

Fig. 3. CO_2 resulted from transportation activities prevision for 2020 without any applied measures

These measures can be grouped into measures that will have direct results in the reduction of fuel consumption and measures that will have a direct impact over the traffic flows in the urban area of Săcele.

The standard emissions factors applied in this study are:

- 0.249 [tones CO_2 / MWh] - for spark ignition engines;
- 0.267 [tones CO_2 / MWh] - for compression ignition engines;
- 0.000 [tones CO_2 / MWh] - for biofuels.

For the transportation sector, data for each fuel and vehicle were calculated using the formula:

$$X_{UsedFuel} = D \cdot C_{average} \cdot Y \tag{3}$$

Where: $X_{UsedFuel}$ - Energy consumption for road transportation [kWh]; D - route distance [km]; $C_{average}$ - average fuel consumption [liters/km]; Y - conversion factor for each fuel [kWh/liters]. Y = 9.2 for gasoline and Y = 10 for Diesel.

3.2 Vehicle Fleet Renewal

This measure may be applied to the municipal and local public transport fleet. The proposed solutions are based on actions for greening public transportation system between Săcele and Brasov.

Using the data on the number of municipal vehicles fleet, public transportation Săcele fleet and from related fuel consumptions, the following measures are proposed:

- Fleet renewal for municipal fleet and public transportation fleet will lead to a consumption decrease from 11.25 L/100 km to 7 L/100 km for light vehicles and from 27 L/100 km to 24 L/100 km for buses.
- By reevaluating and improving the transportation system management and fuel consumption monitoring the fuel consumption can be redused by 5 %. If this scenario is adopted, will result a reduction in fuel consumption of municipal fleet from 11.25 L/100 km to 10.69 L/100 km, and for local public transportation fleet from 27 L/100 km to 25.65 L/100 km.
- Replacing 50 % of public transportation fleet with green vehicles (using 100 % biofuel or electric buses).

After applying these measures will have a reduction: 627.95 [MWh] and 540.71 [tones CO_2].

3.3 Increasing the Average Travel Speed

The level of service of the road network (expressed as average travel speeds) is generally low. Average travel speeds are 66 km/h for the national road network, 34 % less than the target of 100 km/h. Similarly, the average speed of traffic in urban areas is between 15 km/h and 40 km/h.

Measurements on test cycles that are close to actual traffic conditions showed a slight influence of travel speed limits over the pollutant emissions. In general, the lowers speeds increase pollutant emissions, but due to turbulence generated behind the vehicle quickly dispersed into the atmosphere pollutants are avoiding their local concentration.

In the case of the Municipality of Săcele was made a dependency calculating average fuel consumption in function of average speed of the vehicles. It has been determined fuel consumption equation depending on the vehicle speed. The graphical representation is given by Fig. 4 [3].

It has been determined that the rate of decrease of the fuel consumption with the increase of average speed of vehicle travel is 7.35 % for a speed increase from 35 to 40 km/h and 13.45 % for a speed increase from 35 to 45 km/h.

It was established an average speed for Săcele by making measurements at peak morning and evening hours. The analyzed route was from Brasov Boulevard to George Moroianu Avenue, in both directions, from 8.00–9.00 and 17.00–18.00.

It results that an increasing of average travel speed (on 7.8 km route) from 35 km/h to 45 km/h will result a decrease in fuel consumption of 13.45 %. Thus we have a reduction: 3106.33 [MWh] and 785.59 [tones CO_2].

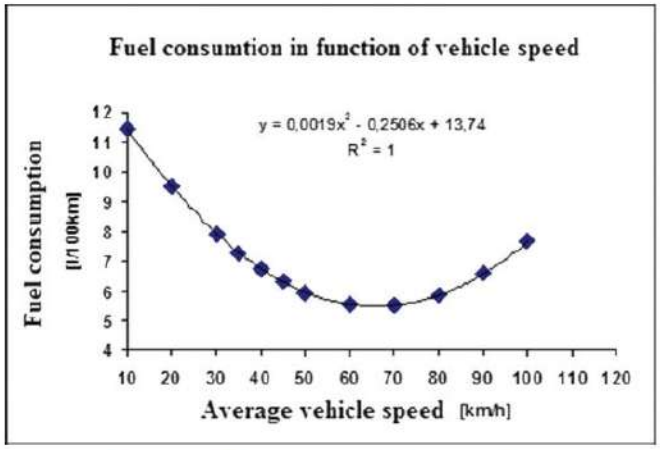

Fig. 4. Fuel consumption equation depending on the vehicle speed (Source: [3] Mitran Gabriela, a.a, A model for determining the average speed of light duty vehicles in urban traffic in terms of minimum pollution and fuel consumption)

3.4 Bicycle Lanes for Săcele

Cycling has a major role in the metropolitan urban transport. It helps reduce congestions, local air pollution and emissions of greenhouse gases. About 20 % of car journeys are less than 3 km, a distance that can be traveled easily by bike in less than 15 min. If people choose to make some of those trips by bike, we could have a

considerable impact on local congestion and road pollution. The study is based on approximate traffic volumes decrease by creating bicycle tracks in Săcele. According to the analyzed data in this study for cyclists routes, resulted a decrease of 7.8 % road traffic volumes after the construction of a bicycle lane in Săcele. After applying this percentage reduction for total vehicle we have a reduction of: 2455.28 [MWh] and 651.86 [tones CO_2] [4].

3.5 Students Mobility Management

The target group of this study are students in primary and secondary schools. If they would use much often the public transportation (existing system or special routes), from the approximately 8,000 etalon vehicles of Săcele fleet, we will have about 1000 etalon vehicles less in the first year of implementation at peak morning and evening rush hours. It is anticipated that for each year the number of vehicles will be reduced by 500 cars. After applying this reduction we will have a reduction in energy consumption and CO_2 emissions: 570.63 [MWh] and 178.07 [tones CO_2].

4 Conclusions

For this study were analyzed four measures that can be adopted in order reduce energy consumption and CO_2 emissions: vehicle fleet renewal; increasing the average travel speed; making bicycle lanes; and students mobility management. The most effective measure, increasing average travel speed of 7.8 km route from about 35 km/h to 45 km/h will result in a decrease in fuel consumption of 13.45 % and a decrease in

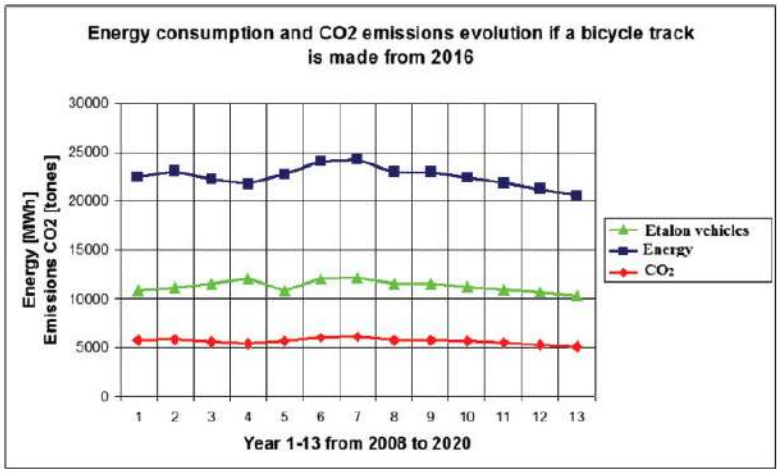

Fig. 5. The evolution of energy consumption and CO_2 production by building a bicycle track

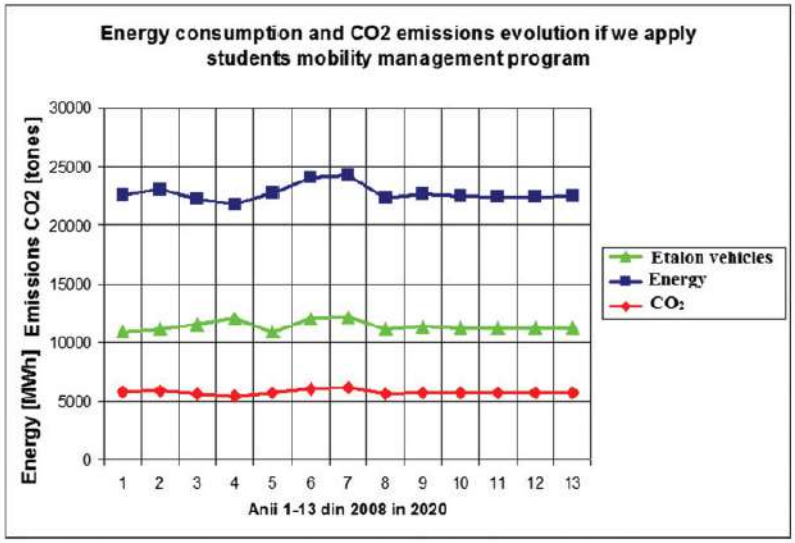

Fig. 6. The evolution of energy consumption and CO_2 production if is applied students mobility management program

energy consumption and CO_2 emissions by 13.50 %. Making bicycle lanes will lead to lower energy consumption and CO_2 emissions by 11 %.

In Fig. 5 is presented the evolution of energy consumption and CO_2 production by building a bicycle track. Municipal and public transportation fleet renewal, fuel consumption monitoring program and replacement of 50 % of a fleet of public transport vehicles with green vehicles will lead to a 3 % lower energy consumption and 9.3 % less CO_2 emissions. Mobility management program for students in Săcele will lead to a decrease in energy consumption and CO_2 emissions by 3 %. Figure 6 shows the evolution of energy consumption and CO_2 production by students mobility management program.

Acknowledgements. We hereby acknowledge the structural founds project "Plan de acțiune privind energia durabilă pentru Municipiul Săcele", 2964/13.03.2015 and Transilvania University of Brasov for providing the infrastructure used in this work.

References

1. Kamal-Chaoui, L., Robert, A.: Competitive Cities and Climate Change, OECD Regional Development Working Papers No. 2, OECD Publishing, © OECD (2009)
2. Vasile, E., Balan, M., Grabara, I., Balan, S.: Measures to reduce transportation greenhouse gas emissions in Romania. Pol. J. Manage. Stud. (2012)

3. Gabriela, M., Ion, T., Florian, I., Sorin, I., Viorel, N., Alexandru, B.: A model for determining the average speed of light duty vehicles in urban traffic in terms of minimum pollution and fuel consumption, CAR Pitesti (2011)
4. Protected Bicycle Lanes, New York City Department of Transportation – Polly Trottenberg, Commissioner, September 2014
5. Stadiul implementării măsurilor din responsabilitatea R.A.T. Brașov din PLANUL DE ACȚIUNE PENTRU ENERGIE DURABILĂ 2010–2020
6. Strategia de dezvoltare a Municipiului Săcele 2014–2020

Electronic Control Systems of E-Smart Vehicle

Conference Paper · October 2016

DOI: 10.1007/978-3-319-45447-4_50

2 authors:

Radu Tarulescu
Universitatea Transilvania Brasov
78 PUBLICATIONS 102 CITATIONS

SEE PROFILE

Stelian Tarulescu
Universitatea Transilvania Brasov
68 PUBLICATIONS 111 CITATIONS

SEE PROFILE

Electronic Control Systems of E-Smart Vehicle

Radu Tarulescu(✉) and Stelian Tarulescu

Transilvania University of Brasov, Brasov, Romania
{radu.tarulescu, s.tarulescu}@unitbv.ro

Abstract. In this paper the authors present the electronic control systems used to manage the driving performances and optimize the energy supply for E-Smart electric vehicle. E-Smart is an electric vehicle obtained through conversion, of a Smart ForTwo City vehicle, from the internal combustion propulsion system to a system that uses a three-phase asynchronous motor. The requirement of the electric vehicle entire control system is to have a controller able to accomplish the submission tasks from the driver.

AQ1

AQ2

Keywords: Electric vehicle · Curtis controller · Sensor

1 Introduction

Referring to electric vehicles, the global automotive industry is undergoing a significant transformation. Electric vehicles are an emerging technology that manufacturers are increasingly turning towards. Increasingly more vehicle manufacturers are at various different stages of electric vehicle development and commitment. The environmental benefit of electric vehicles over fossil fuel powered vehicles is that they don't produce any polluting emissions.

Driving an electric vehicle produces no carbon dioxide or any other environmentally damaging emissions at the source [1]. The average price of an electric vehicle is higher than a conventional fossil fuel powered vehicle, because of the high production costs of the electric vehicle's battery, but savings are made from electricity prices being cheaper than gasoline or Diesel fuels [2].

In this article will be presented E-Smart electric vehicle's electronic systems. E-Smart (Fig. 1) is a vehicle obtained by converting a Smart ForTwo City Coupe

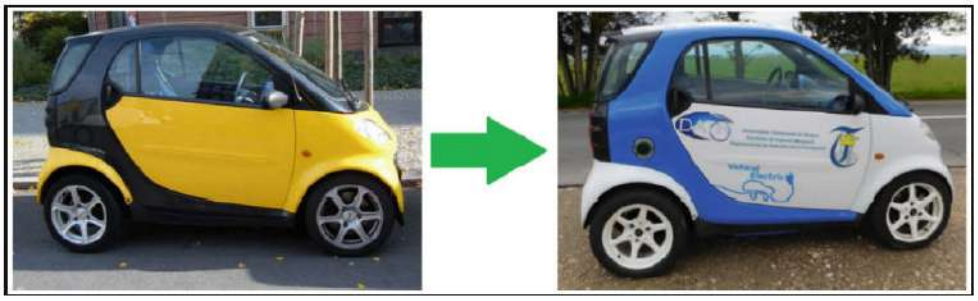

Fig. 1. From 1999 Smart ForTwo City Coupe to 2016 E-Smart electric vehicle

A. Chiru and N. Ispas (eds.), *CONAT 2016 International Congress of Automotive and Transport Engineering*, DOI 10.1007/978-3-319-45447-4_56

vehicle manufactured in 1999 and fueled by gasoline, with an electric propulsion system. The old gasoline engine of 33 kW power was replaced with an electric three-phase asynchronous motor of 22 kW power, model N50D2.

2 E-Smart Vehicle Electronic Devices

2.1 Electronic Control Module

The engine control unit (ECU) of the old gasoline engine was replaced with an electronic control unit E-Car-Box based on a Curtis 1238 controller (Fig. 2). Al of the commands from the vehicle's driver are processed in this controller and given to the electric motor.

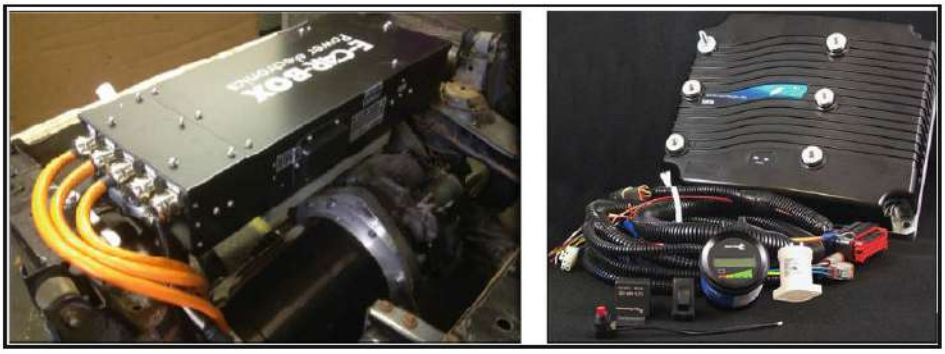

Fig. 2. E-Car-Box electronic control unit and Curtis 1238 controller

Curtis 1238 controller has advanced pulse width modulation technology for efficient use of battery voltage, low motor harmonics, low torque ripple, and minimized switching losses.

Fig. 3. The 1314 PC programming station and software

Also, power limiting maps allow performance customization for reduced motor heating and consistent performance over varying battery state of charge. Powerful operating system of this controller allows parallel processing of vehicle control tasks and motor control tasks. Curtis 1238 controller is easily programmable through the 1314 PC programming station (Fig. 3).

Fig. 4. Curtis 840 display for main parameters

Curtis 840 display (Fig. 4) show all important information from the Curtis controller. It can show motor power and temperature, battery status, motor speed in rpm, motor torque in Nm, vehicle speed in km/h and total voltage at the controller.

Fig. 5. Emus Evgui application for smart phone

That parameters can be displayed also on the smart phone using an android free application named Emus Evgui (Fig. 5). In addition, it can display more information about the state of battery, discharge voltages of individual battery cells and the highest, lower and medium cell voltage. Curtis 1238 controller communicate with mobile phone through a Bluetooth device.

2.2 System Electronic Interface (SEI)

The System Electronic Interface (SEI) is an interface between E-Smart vehicle and Curtis controller. SEI (Fig. 6) is a board which generate a signal of type "charger on" and a signal of type "neutral/drive" for the Curtis 1238 controller.

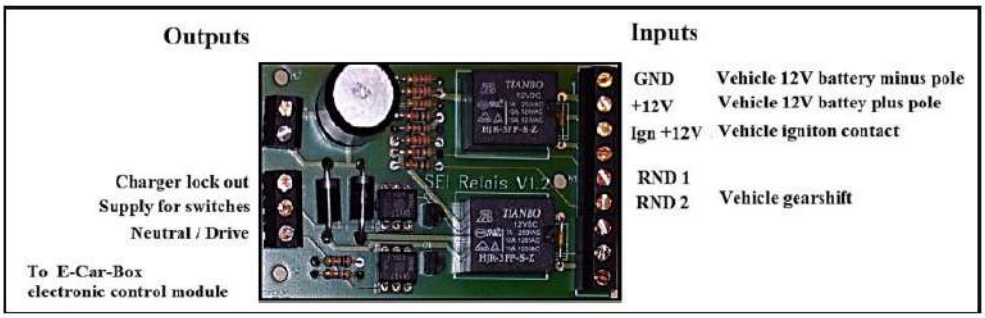

Fig. 6. Inputs and outputs signals for System Electronic Interface (SEI)

The SEI board gives to the Curtis controller a signal that there is a power of 230 V available because the charging cable is plugged into the vehicle. Having this information, the Curtis controller inhibits drive mode, showing "Charger" on the Curtis 840 display and the driver is not able to drive away with the charging cable plugged. This is the safety function of the SEI board. The other function is to enable vehicle's driving, being generate a signal "neutral/drive" to the Curtis controller. If the signal is off, the Curtis controller is in the neutral state and the main contactor being not pulled. The power bank of the controller is not powered and the motor is stopped. If the signal is on, the main contactor pulls and the Curtis controller is ready to drive the motor.

2.3 Battery Management System

The battery management system of EMUS type (Fig. 7) is used for batteries with more cells (like the battery cells mounted on the E-Smart vehicle) connected in series to form a higher voltage battery pack.

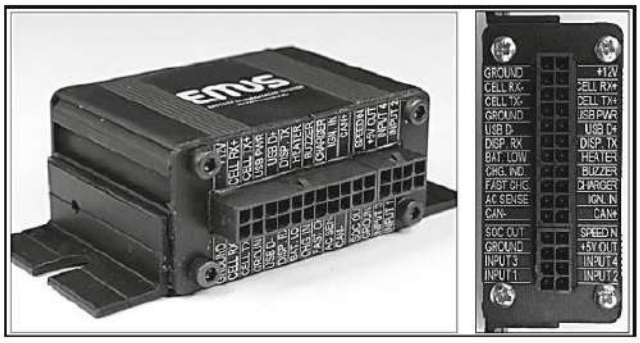

Fig. 7. The battery management system EMUS

Each cell of the battery has an electronic module which monitors cell's parameters, controls the balancing current and communicates with central control unit of the system. The control unit of EMUS battery management system is connected to cells electronic modules via double twisted-pair optically isolated interface over which it communicates and collects cell characteristic information and manages the battery [3]. The control unit of EMUS also has a USB interface for configuration, which is used to connect it to a PC to configure the battery management system via specific free downloadable software.

3 E-Smart Vehicle Functionality

3.1 E-Smart Driving Modes

E-Smart vehicle works just like any full electric vehicle. The electric current is drawn from the batteries pack and applied, under the management of the electronic control module E-Car-Box, to the electric motor. Inside the motor, this current is passed through a magnetic field, which results in a torque that is used to turn the vehicle's wheels [4].

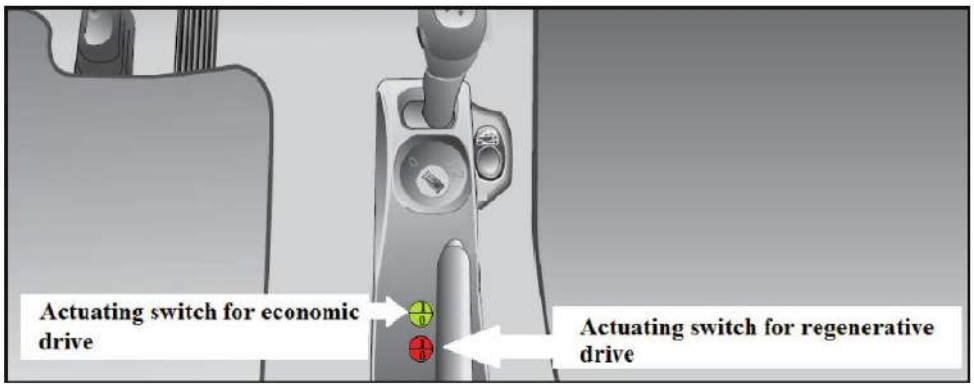

Fig. 8. The switches for enable and disable the regenerative or economic driving mode

This process can be reversed during braking of the vehicle. Effectively, the electronic control module converts the motor to a generator and the regenerative braking system can recapture kinetic energy and store it as electrical energy [5].

The regenerative driving mode can be enabled by switching the red button in 1 position (Fig. 8). Also, the regenerative driving mode can be disabled by switching the red button in 0 position. Another driving mode can be selected, the economic driving mode. In this mode the battery pack discharge is limited even if the accelerator pedal is fully pressed to save the energy and the vehicle speed is limited to 36 km/h. The economic driving mode can be enabled or disabled by switching the green button (Fig. 8).

3.2 E-Smart Motor Parameters

Using Curtis 840 display and Emus Evgui application were determined power, torque and motor speed of E-Smart vehicle. Measurements were made for both driving modes, regenerative and economic from vehicle starting, on straight road without slope (Fig. 9). AQ3

Fig. 9. The chosen road for tests

Table 1. Measured parameters for the economic and regenerative driving modes.

Motor speed [rpm]		Torque [Nm]		Power [kW]	
Economic drive	Regenerative drive	Economic drive	Regenerative drive	Economic drive	Regenerative drive
35	257	18	62	3.18	5.34
297	636	66	112	4.27	18.02
702	1214	68	93	10.34	17.58
907	1722	69	70	12.07	17.42
1257	1909	63	60	10.91	17.36
1451	2235	47	51	10.68	17.34
1672	2489	39	45	10.52	16.91
1798	2645	37	40	10.43	16.23
1880	2773	35	37	9.96	15.37
1929	2889	32	33	9.45	13.42
2154	2993	31	29	6.36	13.15
2224	3065	28	28	6.22	13.08
2310	3123	26	27	5.92	13.03
2375	3220	24	26	5.68	13.03
2415	3315	23	26	5.57	13.03
2472	3386	22	25	5.41	13.01
2522	3460	19	24	5.38	12.76
2565	3484	16	23	5.24	12.29

In Table 1 are displayed the consumed power and torque values depending on the motor speed for the both driving modes.

It should be mentioned that the E-Smart vehicle's acceleration pedal was fully pressed for all the road in both cases.

In Figs. 10 and 11 are showed the diagrams of power and torque in function with motor speed for the boat driving modes, economic and regenerative.

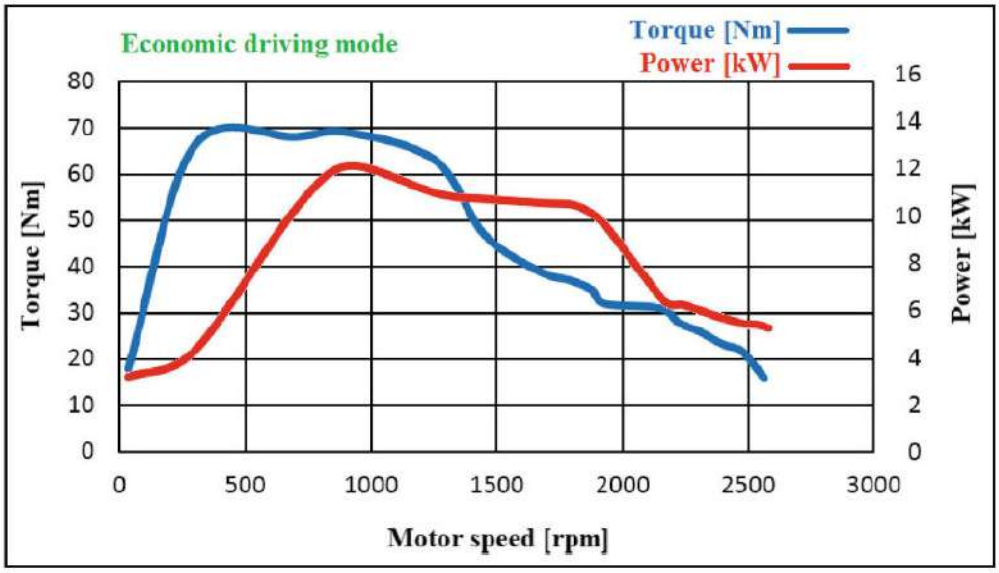

Fig. 10. The power and torque diagram for economic driving mode

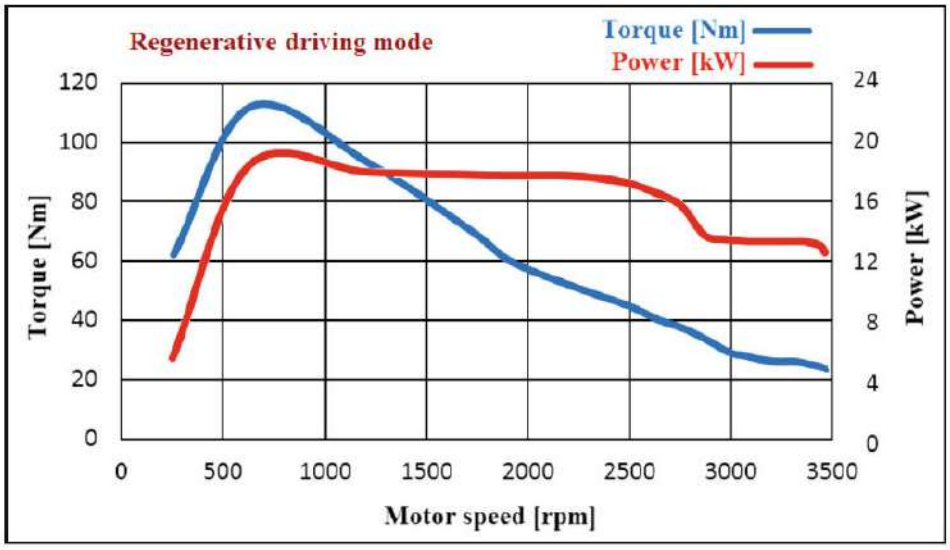

Fig. 11. The power and torque diagram for regenerative driving mode

The values obtained for the economic driving mode are lower because the limiting controlled from the E-Car-Box electronic control module. Instead, the traveled distance using this economic mode was nearly 15 km longer than the normal (approximatively 65 km starting with batteries fully loaded). With the regenerative mode the distance traveled with batteries pack fully loaded was approximatively 50 km, but with a top speed of 80 km/h.

4 Conclusions

Like all electric vehicles, the good functioning of E-Smart depends solely on the correct functioning of electronic control systems. The main role in this case is held by the controller Curtis 1238 controller, which is actually the "brain" of the entire system. Actually E-Smart vehicle, on operating mode, is very much like mobile robots [6]. This paper presents an overview of E-Smart, an old vehicle, pollutant, transformed into a modern vehicle, friendly with the environment, which should be implemented in a large city like Brasov.

References

1. Leitman, S., Brant, B.: Build Your Own Electric Vehicle, 3rd edn. McGraw-Hill Education Publishing, New York (2009) AQ4
2. Larminie, J., Lowry, J.: Electric Vehicle Technology Explained, 2nd edn. John Wiley & Sons, Ltd., Hoboken (2012)
3. EMUS Battery management system, User's manual, JSC Elektromotus (2011)
4. Soylu, S.: Electric Vehicles - the Benefits and Barriers. InTech Publishing (2011)
5. Stevic, Z.: New Generation of Electric Vehicles. InTech Publishing (2012)
6. Tarulescu, R.: Optimizarea Configuratiei Senzorilor Utilizati la Robotii Mobili. GlobeEdit Publishing (2016)

STEADY STATE ENGINE EFFICIENCY SPECIFIC TO SERIES HYBRID ELECTRIC VEHICLES

EFICIENȚA REGIMURILOR DE FUNCȚIONARE STABILIZATE, SPECIFICE MOTOARELOR CU ARDERE INTERNĂ CARE ECHIPEAZĂ AUTOVEHICULELE HIBRID ELECTRICE

REZUMAT

Regulamentele Comisiei Europene impun ca până în anul 2030 să se reducă în medie cu 30 % emisia de CO_2 provenită de la noile autoturisme și autovehicule comerciale ușoare, în raport cu valorile limită ale anului 2020. În acest context, autovehiculele hybrid electrice (AHE) devin un segment din ce în ce mai important din întreg parcul auto European. În cadrul AHE se poate realiza un management energetic cu mult mai eficient decât la autovehiculele clasice. De aceea AHE reprezintă o soluție prin care se poate reduce consumul de combustibil și emisiile poluante datorate transportului rutier. Autovehiculele clasice și AHE-paralel funcționează frecvent la regimuri tranzitorii, în schimb AHE-serie funcționează la regimuri stabilizate. Obiectivul principal al acestui articol este acela de a evidenția avantajele AHE-serie față de AHE-paralel sau cu alte cuvinte avantajele regimurilor stabilizate față de cele tranzitorii, prin cercetări experimentale. Regimurile tranzitorii ale motorului cu ardere internă sunt obținute succesiv prin variația turației, a sarcinii și a ambilor parametri în același timp. Valorile astfel obținute sunt comparate cu cele rezultate în timpul funcționării motorului cu ardere internă la regimuri stabilizate. Performanțele energetice și ecologice ale motorului obținute în cadrul regimurilor stabilizate sunt mai mari față de cele din regimurile tranzitorii, diferența cea mai mică observându-se la variația sarcinii.

Key-Words: *hybrid electric vehicle – HEV, engine, transient state, steady state.*

S.l. dr. ing.
Cristian-Ioan LEAHU
catalin.zaharia@upit.ro

Conf. dr. ing.
Stelian TARULESCU

S.l. dr. ing.
Sebastian RADU
dan.moldovanu@auto.utcluj.ro

Universitatea Transilvania din Brașov,
Str. Politehnicii, Nr. 1, 500024 Brașov, Romania

1. INTRODUCTION

At present are established EU fleet wide targets value for 2020 of 95 CO_2 g/km for passenger cars and 147 CO_2 g/km for light commercial vehicles. This values are based on the New European Driving Cycle test procedure (NEDC).

The European Commission regulatory proposed for the period after 2020 CO_2 emission targets for passenger cars and light commercial vehicles. Average CO_2 emissions of the EU fleet of new passenger cars and light commercial vehicles in 2025 will have to be 15 % lower than in 2020 [1]. For 2030, CO_2 targets value for both type vehicles are 30 % lower than in 2020. The values will be based on the Worldwide Harmonized Light Vehicle Test Procedure (WLTP).

These CO_2 limits values are almost impossible to meet if unless used the hybrid electric vehicle powertrain.

1.1 The Hybrid Electric Vehicle

Hybrid electric vehicles (HEV) are becoming a more and more important vehicle segment in the European car park. Based on the statistics from domain, in the year 2017, in Europe, 431.504 HEV (full and mild hybrids) have been registered. Which represent a 54.8% increase of new HEV registered in 2017 compared to the 2016.

HEVs can be classified based on the degree of hybridization: Micro-Hybrid, Mild-Hybrid and Strong-Hybrid. Depending on the way in which the energy flow is transmitted, the Strong-Hybrid type systems can be divided into three types: serial, parallel and Power Split HEV (Figure 1) [3] [4].In the case of HEV a more efficient energy management can be achieved compared to the conventional internal combustion engine powered vehicles (Figure 2). Due to this reason, HEV represent a viable solution throughout which a diminishing of the fuel consumption as well as vehicle emissions can be achieved [5] [6].

Energy management in case of HEV that use a parallel drivetrain is based on the fact that the mechanical energy of the engine is transmitted, based on requirements, to the vehicle's wheels and/or to the generator, and afterwards stored in batteries. Moreover, during vehicle deceleration, the generator creates electricity, which is then stored in batteries for future vehicle propulsion purposes.

Series HEV, are usually powered by electric traction motors. The mechanical energy produced by the engine is converted into electrical energy used to power the traction motors and eventually the wheels. The main advantage of series drivetrain HEV is that the engine operates in a steady regime compared to parallel HEV or even conventional internal combustion engine powered vehicles, where the engine operates frequently in transitory regimes [7].

The NEDC, is supposed to generally represent the typical usage of a vehicle in Europe. The performances of engines during transitory regime functioning are significantly superior compared to steady state regimes. The main objective of this paper is to emphasis this advantages of steady state engines throughout experimental researches compared to transitory regimes.

2. METHODOLOGY AND RESULTS OF EXPERIMENTAL RESEARCH

The experimental research was carried out at Transilvania University of Brasov, ICDT - Research & Development Institute. The engine used for experimental investigation is an AVL Single Cylinder Compression Ignition Engine type 5402.

For experimental the AVL engine, operated in two modes: at steady state (similar to the series HEV) and transient state (similar to the conventional vehicles and parallel HEV).

In stabilized regimes, the engine was run at three engine speeds: 1500, 1750, 2000 rpm's and three different engine loads: 20%, 30% and 40%. As shown in Table 1, the transient regimes were achieved with the following three scenarios: constant engine speed and variable engine load; constant engine load and variable engine speed; both, the load and the speed are variable. In fact, three situations were simulated

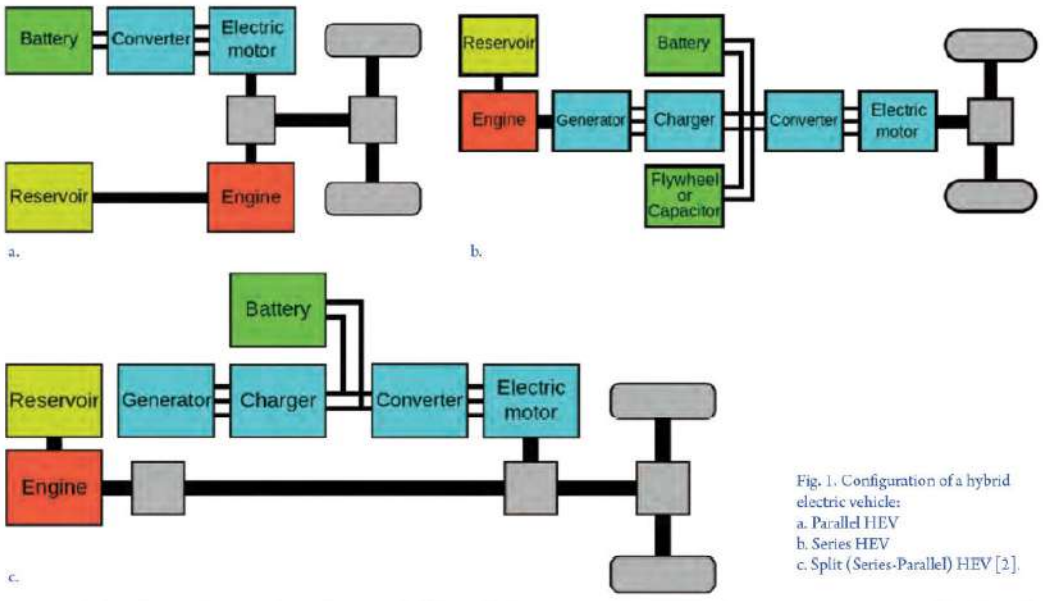

Fig. 1. Configuration of a hybrid electric vehicle:
a. Parallel HEV
b. Series HEV
c. Split (Series-Parallel) HEV [2].

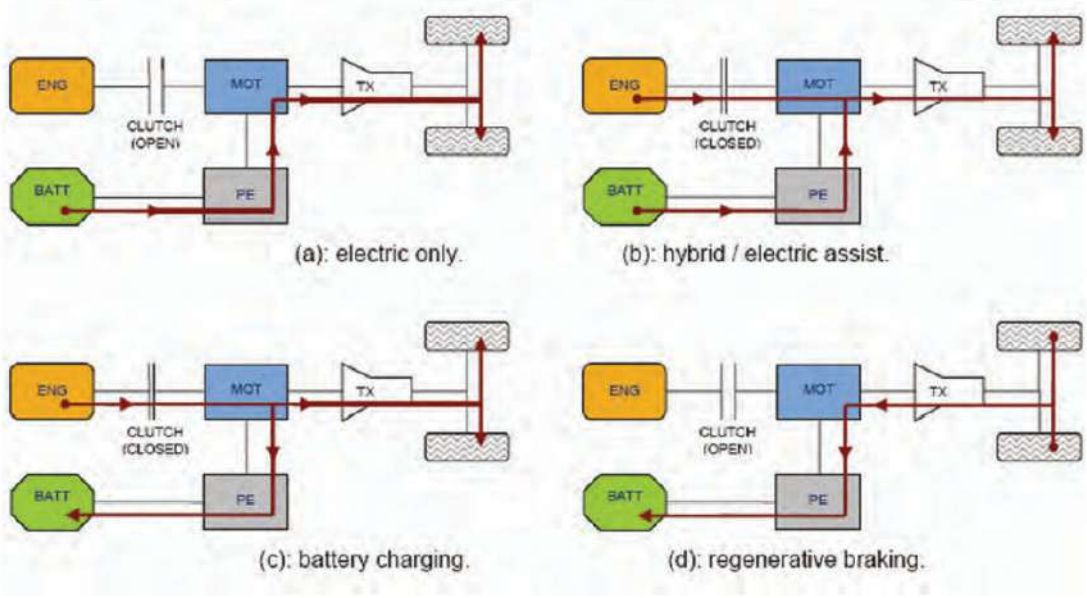

Fig. 2. Some representative modes for a parallel hybrid configuration [2].

Fig. 2. Some representative modes for a parallel hybrid configuration [2].

during the operation of the vehicle, namely:

1. Vehicle's resistances are increasing, but the engine acceleration remains unchanged, which means that the engine speed is reduced;
2. Vehicle's resistances are increasing, but engine speed remains quasi-constant due to engine acceleration;
3. The power surplus obtained through the engine acceleration is higher than the resistance level, so an engine speed increase occurs.

The experimental results obtained in the regimens expressed in Table 1 are shown in Figures 3-5. For example, Figure 3a, shows that the engine running successively at steady state: 1500 rpm / 20%, 1750

Table 1. Experimental research strategy

Comparison 1: constant speed and variable load		Comparison 2: variable speed and constant load		Comparison 3: variable speeds and loads
Speeds [rpm] / Loads % - Steady state				
1500 / 20	2000 / 20	1500 / 20	1500 / 40	1500 / 20
1500 / 30	2000 / 30	1750 / 20	1750 / 40	1750 / 30
1500 / 40	2000 / 40	2000 / 20	2000 / 40	2000 / 40
Speeds [rpm] / Loads % - Transient state				
1500 / 20-40	2000 / 20-40	1500-2000 / 20	1500-2000 / 20	1500-2000 / 20-40

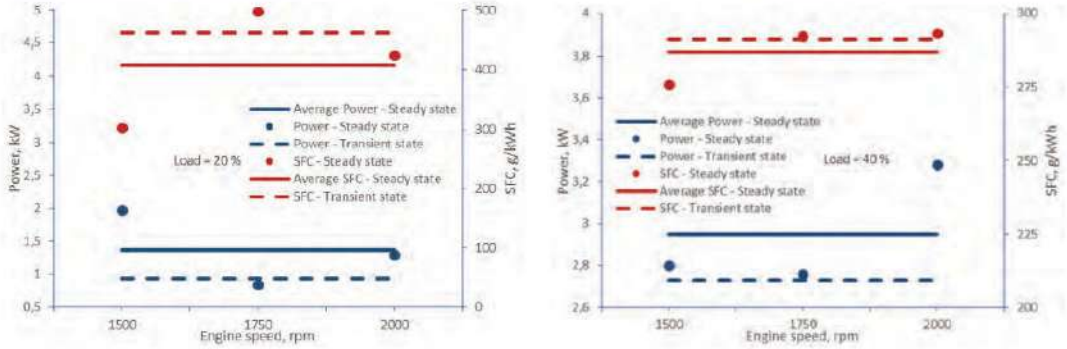

Fig. 3. The average and absolute value of the power and SFC of the engine operated at steady and transient state (variation speed: 1500-2000 rpm): a. 20 % load; b. 40 % load.

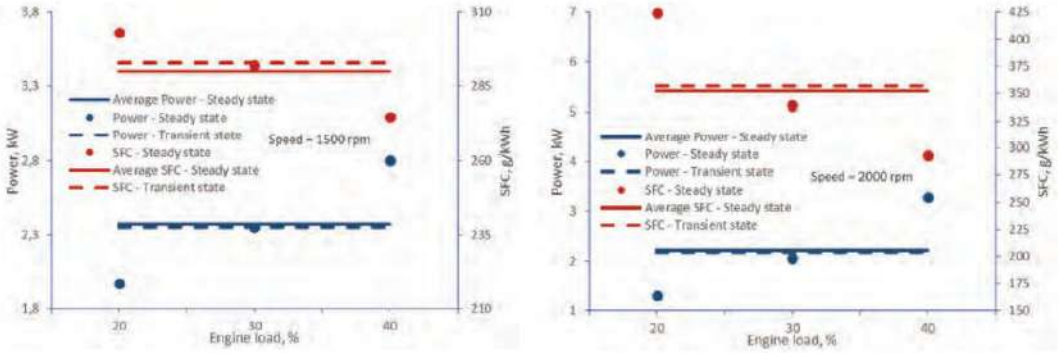

Fig. 4. The average and absolute value of the power and SFC of the engine operated at steady and transient state (variation load: 20-40 %): a. 1500 rpm engine speed; b. 2000 rpm speed.

rpm / 20% and 2000 rpm / 20% developed a power of 1.97 kW, 0.84 kW and 1.3 kW (the blue dots). Average power is considered to be 1.37 kW (the continuous blue line). Instead, if the engine is running at transient speed rising from 1500 rpm to 2000 rpm then the engine develops a power of 0.94 kW (the discontinuous blue line). At the same time, the engine has a fuel consumption of 203 g/kWh, 497 g/kWh and 424 g/kWh (the red dots) at steady state with a mean value of 408 g/kWh (the continuous red line). In transient state the consumption value is 460 g/kWh (the discontinuous red line). These experimentally obtained values highlight the advantages of series HEV engines compared to classic engines. A 46 % higher power and a lower specific fuel consumption (SFC) of 11% were obtained if the

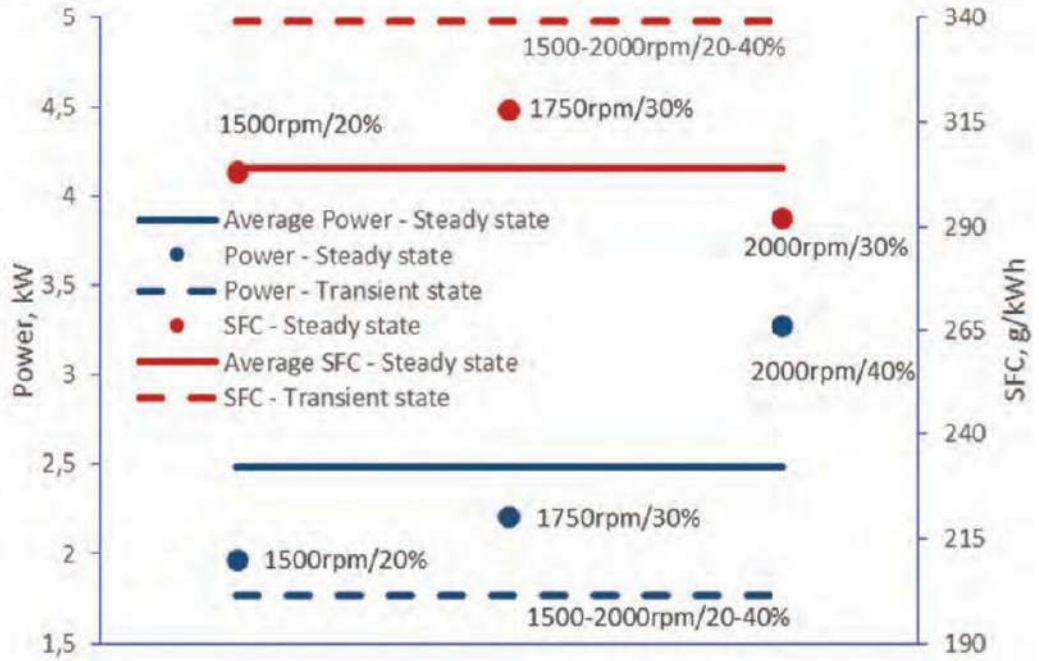

Fig. 5. The average and absolute value of the power and SFC of the engine operated at steady and transient state (20-40 % variation load and 1500-2000 rpm variation speed).operated at steady and transient state (variation load: 20-40 %): a. 1500 rpm engine speed; b. 2000 rpm speed.

engine functioning to steady state at series HEV.

If the Figures 3-5 are further analyzed is possible to identify the steady state the engine with the highest power and the lowest fuel consumption. Or in other words, the state at which series HEV would have maximum performance compared to conventional vehicles.

It can be noticed that the engine speed change has the greatest influence on engine power and SFC during the transient regimes. In particular, by increasing the engine speed, the inertia forces of the moving parts increases. The value of the inertia forces is higher during engine acceleration. It also increases the intake air speed entering the engine cylinders and reduces the intake time. Thus, fuel burning in cylinders is affected during transient regimes [8].

By increasing only the engine load, it will change the amount of diesel fuel injected into the cylinders. Thus, the ratio from the amount of intake air and the amount of fuel in the cylinders is different during the transitory regimes relative to the stable regimes, which may affect the quality of the combustion. The difference between this values obtained in the stabilized and transient regimes (as it can see in Figure 4) is minimal.

The series HEV equipped with a diesel engine that operates at steady state prove to be a viable solution that highest power, reduces the fuel consumption and, implicitly, the emission of CO_2.

5. CONCLUSION

In the case of steady regimes, the engine's performance and environmental characteristics are higher than for the transient regimes. The increase of engine speed in transient regimes mostly affects the engine's performance and environmental performance. One of the most important advantage of series drivetrain HEV is that the engine operates in a steady regime compared to parallel HEV or even conventional internal combustion engine powered vehicles, where the engine operates frequently in transitory regimes.

Lucrare prezentată în cadrul Congresului Internațional al SIAR de Inginerie a Autovehiculelor și Transporturilor – AMMA 2018, 17.10 – 19.10.2018, Cluj-Napoca, România, și publicată în volumul „AMMA 2018 – The IVth International Congress, Selection of Papers", UTPress, ISBN 978-606-737-314-1.

REFERENCES:

[1] *https://ec.europa.eu/clima/policies/transport/vehicles/proposal_en;*

[2] *https://en.wikipedia.org/wiki/Hybrid_vehicle_drivetrain#Parallel_hybrid;*

[3] Iota, C., *Bosch – Technology and Know-How for Hybrid Vehicles*, Ingineria Automobilului, vol. 6, no. 1, 11-13, 2012;

[4] http://www.toyota-global.com/innovation/environmental_technology/hybrid/;

[5] Varga, B.O.; Iclodean, C.; Mariasiu, F., *Electric and hybrid buses for urban transport*. Springer International Publishing, Switzerland, 2016;

[6] Ehsani, M.; Gao, Y.; Gay, S.E., *Modern Electric, Hybrid Electric, and Fuel Cell Vehicles, Fundamentals, Theory, and Design*. CRC Press, 2010;

[7] Dogariu, D.M.; Chiru, A.; Leahu, C.I.; Lazar, M., *Experimental Research on the Hybridization of a Road Vehicle*. Romanian Journal of Automotive Engineering – RoJAE, vol. 21, no.1, 15-20, 2015;

[8] Basshuysen, R.; Schäfer, F., *Internal combustion engine handbook: basics, components, systems, and perspectives*. SAE International, Warrendale, 2002.

International Journal of Automotive Technology, Vol. 17, No. 3, pp. 387–397 (2016)
DOI 10.1007/s12239–016–0040–y

pISSN 1229–9138/ eISSN 1976–3832

IMPACT PHASE IN FRONTAL VEHICLE-PEDESTRIAN COLLISIONS

A. SOICA* and S. TARULESCU

Automotive and Transport Department, Transilvania University of Braşov, Braşov 500036, Romania

(Received 11 July 2014; Revised 4 August 2015; Accepted 19 October 2015)

ABSTRACT–The paper presents an alternative model developed in order to determine the pedestrian throw distance, taking into account ten distinct parameters. The collision dynamics, after the primary and secondary impact (pedestrian's head hitting the vehicle windshield-hood area) between the vehicle and the pedestrian, entails the pedestrian 'carrying' phase onto the vehicle hood-windshield. Other parameters influencing the pedestrian throw distance, such as road inclination, friction coefficient between the pedestrian and the ground, vehicle and pedestrian mass, pedestrian launch angle are considered for the analysis. A comparison between the results obtained through the formula proposed in this paper and the results obtained by other researchers as well as a comparison with the results extracted from the casuistry analyzed by the authors on both accident reconstruction and laboratory tests is carried out.

KEY WORDS : Vehicle-pedestrian impact, Model, Pedestrian throw distance, Accident reconstruction, Pedestrian impact phase

NOMENCLATURE

v_o' : vehicle speed at the moment of the first contact with the pedestrian, m/s
v_o : speed of the vehicle-pedestrian assembly, immediately after the first contact, m/s
v : vehicle velocity at the the moment of secondary impact, m/s
v_p : pedestrian speed at the moment of launching phase, m/s
v_{px} : pedestrian speed on X axis at the moment of launching phase, m/s
v_{py} : pedestrian speed on Y axis at the moment of launching phase, m/s
a : average brake deceleration from the moment prior to the first impact with the pedestrian m/s^2
a_{px} : pedestrian acceleration on X axis at the moment of launching phase, m/s^2
a_{py} : pedestrian acceleration on Y axis at the moment of launching phase, m/s^2
m_v : vehicle mass, kg
m_p : pedestrian mass, kg
h : height at which the pedestrian is launched off the vehicle, m
t_0 : time at which the pedestrian is hitted by the vehicle, s
t_1 : time at which the pedestrian hits the hood-windshield area with the head, s
t_1' : time at which the pedestrian is lauched in flying phase, s
t_2 : time at which the pedestrian hits the ground, s
t_3 : time at which the pedestrian stops on the ground, s
x_1 : the space covered by the vehicle-pedestrian assembly in the sub-phase 1.1, m
x_1' : the space covered by the vehicle-pedestrian assembly in the sub-phase 1.2, m
x_2 : the space covered by the pedestrian in the flying phase, m
x_3 : the space covered by the pedestrian in the sliding phase, m
D : pedestrian throw distance, the total space covered by the pedestrian, m
S_{aut} : the space covered by the pedestrian in the contact phase with vehicle, phase 1, m
Dk : pedestrian throw distance according to Kuhnel-Schultz law, m
β : road inclination angle, degree
α : pedestrian launch angle, degree
μ : friction coefficient between the pedestrian and the ground
η : pedestrian impact factor

1. INTRODUCTION

The irremediable losses of human lives as well as the other consequences of a road traffic accident call for a common effort to identify and acknowledge by all the participants in traffic some intelligent solutions in order to diminish the consequences of this millennium immense problem.

Children are vulnerable pedestrians due to the fact that

*Corresponding author. e-mail: a.soica@unitbv.ro

the vehicle driver finds it more difficult to perceive them in his visual angle and, the other way around, children, due to their low visual position, do not observe or do not estimate correctly the vehicle motion. Similarly, the elderly are the most frequent victims among the pedestrians. They are extremely vulnerable due to the decrease in their capacity to observe approaching vehicles as well as due to the reduced agility and walking speed to avoid the vehicles or to cross the road at a faster pace.

The advancement of some measures aiming at traffic safety at a low cost demands for the necessity to establish the priority order, taking into account the "costs-advantages" analysis, by introducing the efficiency criterion when drawing up working programmes.

The expense categories related to road traffic accidents include the following;

- Medical expenses, material damages and general losses;
- Administrative expenses (police, insurances ect);
- Evaluation of personal suffering, damage;
- Damages following less serious road traffic accidents, with reduced material losses (these damages are not recorded in the statistical reports drawn up by the police);
- Pretium vivendi (OCDE, 2000) = cost of life, calculated on the basis of the value assigned to average life expectancy.

Countries all over the world take into account expenses from the first two categories; in addition, some countries also consider the other expense categories.

Originating their initiatives in the information about road traffic accidents involving pedestrians, various organizations and researchers all over the world have established a research and development programme with a view to reducing the consequences of damages following the vehicle-pedestrian collisions and to analyze and accurately reconstruct the road traffic accidents. Researches in the field of road traffic accidents reconstruction and analysis have been carried out by Searle, Collins, Wood, Simms, Batisa, Han, Kuhnel, Schulz, Rau, Otte, Moser, Evans, Smith, Hill, Dettinger, Eubanks, Limpert, Araszewski, Toor, Oh, C., Kang, Y-s. and so on and so forth. Specialised programmes designed for reconstructing road traffic accidents are available at present, in all cases the expert must introduce the input data needed to establish as accurately as possible the accident dynamics, for example PC-CRASH (2008).

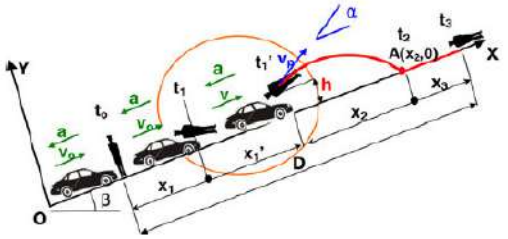

Figure 1. Pedestrian throw diagram.

In case of road traffic accidents involving pedestrians, the pedestrian throw distance is defined by a series of factors such as impact speed, vehicle type (geometry), vehicle and pedestrian motion conditions as well as the friction parameter between the pedestrian and the vehicle, and between the pedestrian and the ground (Wood and Simms, 2000). Determining the speed at which the impact between the vehicle and the pedestrian occurs stands for an important requirement when analyzing and reconstructing road traffic accidents (Wood *et al*., 2005; Hill, 1984; Jun *et al*., 2009). Along the years many researchers have analyzed this aspect and have advanced various formulae and models in order to determine the pedestrian throw distance after the collision with the vehicle, (Searle and Searle, 1983; Searle, 1993; Kuhnel, 1980, Wood and Simms, 2005; Collins and Moris, 1979; Batista, 2008; Han and Brach, 2001). The methods used to predict speed from the throw distance may be categorised as empirical (Evans and Smith, 1999; Rau *et al*., 2000), deterministic (Searle and Searle, 1983; Searle, 1993; Toor and Araszewski, 2003) or statistical (Han and Brach, 2001; Wood *et al*., 2005; Simms *et al*., 2004; Oh *et al*., 2005). This paper is grounded in the studies carried out by Han and Brach (2001) and Batista (2008), the novelty of this work and the difference from another paper consisting in the the fact that the duration of the contact phase between the vehicle and the pedestrian is divided into two sub-phases. The first sub-phase, from the primary vehicle-pedestrian impact to the secondary impact, when the pedestrian's upper body hits the hood-windshield area. The second sub-phase, defined to a certain extent by Han and Brach (2001) represents the pedestrian carrying phase onto the hood until the moment the pedestrian falls off the vehicle, on the ground. This sub-phase was not studied in their paper.

The aim of this paper is to determine an alternative pedestrian throw model on a road with different inclination, according to the impact speed, braking deceleration at the impact moment and other eight parameters. It is known that at the place of the accident the investigators record braking traces, the pedestrian position, technical data of the vehicle, anatomic characteristics of the pedestrian as well as other elements. Likewise, the influence of various factors upon the pedestrian throw distance is also noticed.

2. DYNAMICS OF THE ROAD TRAFFIC ACCIDENT INVOLVING PEDESTRIANS

Five categories of vehicle – pedestrian collisions are described by Ravani *et al*. (1981) and Brooks *et al*. (1987). These are wrap, forward projection, fender vault, roof vault and somersault collisions (Han and Brach, 2001). The model suggested may be applied in wrap and fender vault collisions.

The analysis of data, diagrams and photo-video recordings shows the three typical phases of a motor vehicle-

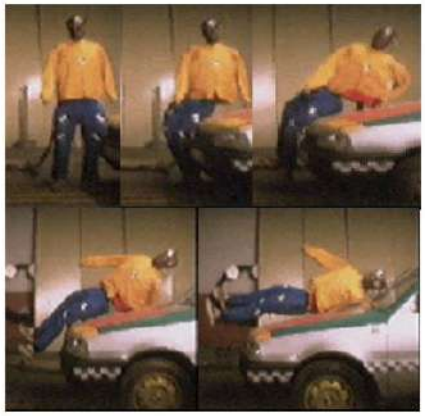

Figure 2. Sub-phase 1.1 of the impact until the "t_1" moment. Frames at 0, 50, 100, 150 and 200 ms, test 1 at 29.58 km/h.

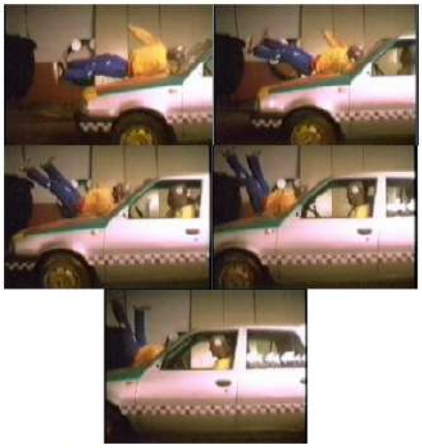

Figure 3. Sub-phase 1.2 – Carrying the pedestrian on the hood until the flight phase. Frames at 200, 250, 300, 350, 400 ms.

pedestrian impact (Eubanks and Haight, 1992). In 1998 Limpert also splits a vehicle-pedestrian collision into 3 phases, the impact phase, the flight phase and the sliding and/or rolling phase (Han and Brach, 2001).

The authors of this paper decomposed the impact phase into two sub-phases. **Phase 1.** The contact with the motor vehicle, which lasts from the initial contact between the vehicle and the pedestrian until the moment the pedestrian falls off (is launched from) the vehicle. This phase is divided into two sub-phases;

- **Sub-phase 1.1.** lasts from the primary impact to the moment the pedestrian's head hits the vehicle hood-windshield, see Figure 2. The corresponding time is (t_0-t_1), according to Figure 1.
- **Sub-phase 1.2.** from the moment the pedestrian hits the hood-windshield until the moment the pedestrian falls off the vehicle, see Figure 3. The second sub-phase is "carry" phase of the pedestrian on the hood. This phase is better emphasized in case of collisions at low speeds. Yet, in case of greater impact speeds, about 40 km/h, this phase is detectable with high-speed cameras. The corresponding time is (t_1-t_1'), according to Figure 1.

There are some exception in accident dynamics; An example of this category is where a pedestrian rises up onto the hood, perhaps suffers a secondary collision, and remains on the hood without being thrown forward. In cases such as these, the pedestrian typically slides from the hood either to the side or forward, depending on the braking and steering of the vehicle. In this case there is a "carry" phase between impact and flight (Han and Brach, 2001).

The two sub-phases, cumulated as time and distance covered, make up the "total carry" phase or pedestrian contact phase with the vehicle.

Phase 2. The flight phase, which lasts from the moment that pedestrian falls off the vehicle until the contact with the ground. We notice the fact that for low impact speeds, the flight phase is almost neglectable; it implies the pedestrian's body fall off the vehicle on the ground. During the experimental tests carried out by the authors, the pedestrian was imprinted an horizontal launch not an oblique launch motion. The corresponding time is (t_1'-t_2), see Figure 1.

Phase 3. The contact with the ground, which lasts from the moment the pedestrian hits the ground until the final position. The corresponding time is (t_2-t_3), see Figure 1.

It follows that the pedestrian throw distance stands for the sum of the four distances covered by the pedestrian during the collision with the vehicle.

$$D = x_1 + x_1' + x_2 + x_3 \quad (1)$$

2.1. Work Hypotheses

We consider as working hypotheses the following;

- The vehicle travels on a road with a "β" inclination and enters the braking phase at the very moment of the impact with the pedestrian.
- Vehicle speed before the first contact with the pedestrian "v_o' ".
- The duration of sub-phase 1.1 of the collision between the vehicle and the pedestrian (t_0-t_1), until the secondary impact is known.
- The average braking deceleration "a" is known. This is constant throughout the whole sub-phase 1.1 and the sub-phase 1.2. of the impact.
- The pedestrian has zero speed and the impact occurs in XOY plan.

• Air resistance is not taken into account.

2.2. Phase 1 – Primary Impact, Secondary Impact and Pedestrian Carrying on the Vehicle

Considering the vehicle-pedestrian impact as a plastic collision, the post impact speed "v_o" of the vehicle-pedestrian assembly, immediately after the first contact, is given by;

$$v_o = \frac{v_o'}{1+\frac{m_p}{m_v}} \tag{2}$$

After the impact between the vehicle and the pedestrian, considering the braking motion of the vehicle-pedestrian assembly, with the deceleration "a", we obtain the velocity at the the moment "t_1" (secondary impact) which may be expressed through;

$$v = v_o + a \cdot t_1 \tag{3}$$

$$v^2 = v_o^2 + 2 \cdot a \cdot x_1 \tag{4}$$

For sub-phase 1.1 of the vehicle-pedestrian impact, until the secondary impact the space covered by the vehicle-pedestrian assembly results from the Equation (4);

$$x_1 = \frac{v^2 - v_o^2}{2 \cdot a} \tag{5}$$

By combining Equations (2), (3) şi (5) we obtain the distance covered by the vehicle during the sub-phase 1.1;

$$x_1 = -\frac{\left(\frac{v_o'}{1+\frac{m_p}{m_v}} + a \cdot t_1\right)^2 - \left(\frac{v_o'}{1+\frac{m_p}{m_v}}\right)^2}{2 \cdot a} \tag{6}$$

Where "a" stands for the braking deceleration, which may be determined e.g. from the skid marks or from the on board vehicle computer, "v" stands for the vehicle speed at the moment the pedestrian hits the hood-windshield with the head (secondary impact), and "t_1" stands for the time at the secondary impact. Throughout the sub-phase 1.1 the pedestrian is hit, accelerated and, at the moment of the secondary impact with the hood-windshield he/she finally has a speed proportional with the speed of the vehicle at this moment "v".

The high speed video camera shows that after the secondary impact, that is time "t_1" the pedestrian is carried on the vehicle for a time (t_1-t_1'). We deduce that the speed at which the pedestrian is thrown during the flight phase, "t_1' ", is lower than the speed of the vehicle at moment "t_1". We express this through the pedestrian impact coefficient "η", coefficient that also occurs in Batista (2008) and Han and Brach (2001); yet, we state that in the model proposed in this paper the speed of the vehicle untill the secondary impact "t_1" is variable, the vehicle-pedestrian assembly is under brake state with average deceleration "a" from the initial speed "v_o" to speed "v". The pedestrian speed is given by;

$$v_p = \eta \cdot v \tag{7}$$

From Equations (7) and (3)

$$v_p = \eta \cdot (v_o + a \cdot t_1) \tag{8}$$

And considering the Equation (2)

$$v_p = \eta \cdot \left[\left(\frac{v_o'}{1+\frac{m_p}{m_v}}\right) + a \cdot t_1\right] \tag{9}$$

The pedestrian speed was related to the vehicle speed from the moment of the secondary impact. This is based on the recordings with the high speed camera. Thus, following the first contact with the pedestrian's lower limbs, the pedestrian is imprinted a rotation and bending movement of the body to the hood-windshield area of the vehicle. At the time of secondary impact a new tendency for the pedestrian body to rotate around the contact point between his head and the vehicle surface occurs, due to the inertia of human body segments masses (lower limbs and torso). The pedestrian falls off the vehicle when the pedestrian speed is higher than the vehicle speed.

The vehicle-pedestrian assembly is still in braking motion, therefore the pedestrian falls off the vehicle at time "t_1' ", after he has covered the space (x_1+x_1'), when the pedestrain speed becomes greater than or equal to the vehicle speed. Given the Equation (7) the speed is expressed through;

$$(\eta \cdot v)^2 = v'^2 = v^2 + 2 \cdot a \cdot x_1' \tag{10}$$

Resulting the space covered in sub-phase 1.2 of the impact;

$$x_1' = -\frac{(\eta \cdot v)^2 - v^2}{2 \cdot a} = \frac{v^2 \cdot (\eta^2 - 1)}{2 \cdot a} \tag{11}$$

And by replacing "v" with the Equations (3) and (2)

$$x_1' = -\frac{\left[\left(\frac{v_o'}{1+\frac{m_p}{m_v}}\right) + a \cdot t_1\right]^2 \cdot (\eta^2 - 1)}{2 \cdot a} \tag{12}$$

During the phase 1 the pedestrian in contact with the vehicle covers the space;

$$S_{aut} = x_1 + x_1' \tag{12'}$$

During phase 1, throughout the two sub-phases we can particularize the movement by modifying the value of the average deceleration "a", which may be divided in deceleration "a_1" on sub-phase 1.1. and another deceleration "a_2" on sub-phase 1.2. These situations are encountered in real situations by modifying the time when the brakes are applied by the driver, who seized the danger before hittimg the pedestrian, according to the reaction speed as well as to the brake actuating system.

If throughout phase 1.1 the vehicle speed was constant,

then a = 0 and consequently the speed of the vehicle-pedestrian assembly at the moment "t_1" would be $v = v_o$ and the pedestrian speed would be $v_p = \eta \cdot v_o$, as in relations from Batista (2008) and Han and Brach (2001).

2.3. Phase 2 – Pedestrian Flying Phase

The oblique throw motion with speed "v_p" determined with the Equation (7) is characterized through the pedestrian flight until the contact with the ground.

By decomposing the movement on the two axes OX and OY and through particularization we obtain the initial throw speed of the pedestrian, knowing that on OX axis we have $a_{px} = -g\sin(\beta)$, on axis OY we have $a_{py} = -g\cos(\beta)$, and the height at which the pedestrian hits the ground $y_0 = h$.

At the launch moment we have;

$$v_{px}(0) = v_p \cdot \cos(\alpha)$$
$$v_{py}(0) = v_p \cdot \sin(\alpha) \quad (13)$$

And at the moment "t_2";

$$v_{px}(t_2) = v_p \cdot \cos(\alpha) - g \cdot \sin(\beta) \cdot t_2$$
$$v_{py}(t_2) = v_p \cdot \sin(\alpha) - g \cdot \cos(\beta) \cdot t_2 \quad (14)$$

The motion equations on the two axes;

$$x_2 = v_p \cdot \cos(\alpha) \cdot t_2 - \frac{g \cdot \sin(\beta) \cdot t_2^2}{2}$$
$$y = h + v_p \cdot \sin(\alpha) \cdot t_2 - \frac{g \cdot \cos(\beta) \cdot t_2^2}{2} \quad (15)$$

From the motion equation on axis OY and considering the motion particularization conditions, we determine the flight time from the vehicle on the ground, coordinates point A(x_2,0), where $y = 0$

$$t_2 = \frac{v_p \cdot \sin(\alpha) + \sqrt{v_p^2 \cdot \sin^2(\alpha) + 2 \cdot g \cdot h \cdot \cos(\beta)}}{g \cdot \cos(\beta)} \quad (16)$$

The general solution of the trajectory is given by the relation by replacing Equation (16) in (15).

2.4. Phase 3 – Pedestrian Sliding on the Ground

At this stage of the impact the body falls on the ground with speeds on axes OX and OY. An important part of this speed is lost due to the contact with the ground. The human body will have aleatory rolling and sliding movements, with different intensities at each bounce. These are beyond the topic of this study. When sliding on the ground we have, considering the study dealt with by Han and Brach (2001), a pedestrian slide distance defined through coulombian friction.

$$x_3 = \frac{(v_p(t_2))^2}{2 \cdot [\mu \cdot \cos(\beta) + \sin(\beta)] \cdot g} \quad (17)$$

$$v_p(t_2) = v_{px}(t_2) + \mu \cdot v_{py}(t_2) \quad (18)$$

Where

$$v_{px}(t_2) = v_p \cdot \cos(\alpha) - g \cdot \sin(\beta) \cdot t_2$$
$$v_{py}(t_2) = v_p \cdot \sin(\alpha) - g \cdot \cos(\beta) \cdot t_2 \quad (19)$$

$$t_2 = \frac{v_p \cdot \sin(\alpha) + \sqrt{v_p^2 \cdot \sin^2(\alpha) + 2 \cdot g \cdot h \cdot \cos(\beta)}}{g \cdot \cos(\beta)} \quad (20)$$

By replacing Equations (9), (17), (18) and (19) in (1) there results the formula of the distance covered by the pedestrian when sliding/rolling on the ground. The total pedestrian throw distance is thus made up of $D = x_1 + x_1' + x_2 + x_3$, which, under the form of a law dependent on the parameters enumerated, is given by the Equation (21)

$$D(v_o', a, t_1, \eta, h, m_v, m_p, \mu, \alpha, \beta) =$$
$$= x_1(v_o', a, t_1, m_v, m_p) +$$
$$+ x_1'(v_o', a, t_1, \eta, m_v, m_p) + \quad (21)$$
$$+ x_2(v_o', a, t_1, \eta, h, m_v, m_p, \mu, \alpha, \beta) +$$
$$+ + x_3(v_o', a, t_1, \eta, h, m_v, m_p, \mu, \alpha, \beta)$$

3. DISCUSSIONS AND LIMITS OF THE PROPOSED MODEL

For a deceleration a = 0 in sub-phase 1.1 the following relation would result

$$x_1 = v_o \cdot t_1 \quad (22)$$

In sub-phase 1.2. the formula proposed would not give results, it should be ignored.

Through successive modification of the above-mentioned parameters and constant maintenance of the other parameters we obtain the influence of each parameter. Thus, we notice the significant influence of the vehicle deceleration, friction coefficient between the pedestrian and the ground, road inclination, vehicle mass and pedestrian mass and to a lesser extent the pedestrian throw angle off the vehicle. The impact time, the height at which the pedestrian is thrown during the flight phase and the pedestrian impact coefficient have minor influences upon the pedestrian throw distance.

As a result, the input date recorded in diagrams, for each case, at a 25 m/s speed, are as follows;

- Doubling the deceleration during braking lead to a decrease in the throw distance by 16 %.
- Doubling the friction coefficient between the pedestrian and the ground leads to a decrease in the throw distance by 29 %.
- The increase of the road inclination from 0 to 10 degrees leads to a decrease in the throw distance by 20 %.
- Doubling the vehicle mass leads to an increase in the throw distance by 20 %.

4. COMPARING THE PROPOSED MODEL WITH OTHER MODELS

Testing experiments regarding the throw distance recorded

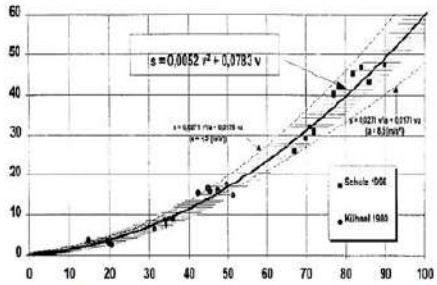

Figure 4. Kuhnel-Schulz model on pedestrian throw distance.

during the reconstruction of road traffic accidents involving pedestrians were carried out by Kuhnel (1980), Rau *et al.* (2000), Dettinger (1996, 1997), Moser *et al.* (1999, 2000) and so on.

4.1. Comparison with Different Models

In the first analysis we make reference to the pedestrian throw model designed by Kuhnel-Schulz, Figure 4.

This model was experimentally determined by Kuhnel-Schulz, but we do not have enough data regarding certain parameters that must be initialized in the model proposed by the authors; this is the reason why the comparison has certain limits.

This is defined through;

$$D_k(v) = 0.0052 \cdot v^2 + 0.0783 \cdot v, \tag{23}$$

where speed is recorded in km/h, or if the vehicle deceleration is taken into account;

$$D_{k\_a}(v, a) = 0.0271 \cdot \frac{v^2}{a} + 0.0178 \cdot v \cdot a \tag{24}$$

By choosing an investigation case submitted to research by the author a similitude results from the model proposed by

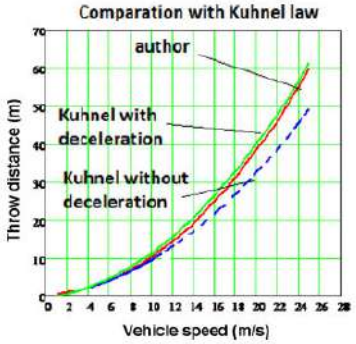

Figure 5. Comparison between the formula proposed and Kuhnel-Schulz model, for a case of a road traffic accident reconstruction.

Kuhnel-Schulz and the model proposed by authors, i.e. the green and the red curvature in the diagram below;

A road traffic accident was submitted to analysis taking into account the following input data;

- a = – 4 m/s² – average brake deceleration from the moment prior to the first impact with the pedestrian;
- m_v = 1040 kg – vehicle mass;
- m_p = 75 kg – pedestrian mass;
- h = 1 m – height at which the pedestrian falls off the vehicle;
- t_1 = 0.2 s – time at which the pedestrian hits the hood-windshield area with the head;
- α = 16 degrees – pedestrian launch angle off the vehicle;
- μ = 0.75 – friction coefficient between the pedestrian and the ground;
- η = 0.75 – pedestrian impact factor.
- D = 34 m – pedestrian throw distance measured at the place of the accident

We determined the v_o' – vehicle speed at the moment of the first contact with the pedestrian, which is 18.76 m/s, according the proposed model, and 18.28 m/s according to Kuhnel-Schulz model. The error is 2.6 % or 0.48 m.

The following comparison focuses on our results as related to those provided by Batista (2008) as well as to those resulting from Kuhnel-Schulz model, for another casuistry. The input data are;

- v_o' = 13.89 m/s = vehicle speed at the moment of the first contact with the pedestrian;
- a = – 8.5 m/s² – average brake deceleration beginning with the moment prior to the first impact with the pedestrian, approached by the authors. The data recorded in Batista (2008) do not include references to the braking deceleration.
- m_v = 1,460 kg – vehicle mass;
- m_p = 80 kg – pedestrian mass;
- h = 1 m – height at which the pedestrian falls off the vehicle;
- t_1 = 0.2 s – time at which the pedestrian hits the hood-windshield area with the head; impact time in Batista (2008);
- α = 16 degrees – pedestrian launch angle;
- μ = 0.6 – friction coefficient between the pedestrian and the ground;
- η = 0.9 – pedestrian impact factor.

As output parameter we considered the pedestrian throw distance "D", on road with 8 % inclination.

As noticed, the same impact-related data were used as in the analysis in Batista (2008). For the same impact speed of 13.89 m/s, the throw distance was compared with the throw distance obtained by Kuhnel (1980) and Rau *et al.* (2000).

Therefore, the throw distance indicated by professor Batista was of 16 m, with a road inclination of 8 %.

Kuhnel-Schulz model shows, on the one hand, a throw space of 16.61 m for a model that take account of the braking deceleration and, on the other hand, a throw space

of 15.53 m for a model that does not take account of deceleration.

The model proposed by the authors of this study shows a throw distance of 14.7 m. The error is 8.8 % for Batista model, 12.9 % for Kuhnel law with deceleration and 5.6 % for Kuhnel law without deceleration.

Differences are marked by the fact that in Batista (2008) the contact time between the vehicle and the pedestrian is of only 0.2 seconds and the distance covered by the pedestrian is of 2 m, these data being approximated as input data, whereas in the proposed model the total contact time between the vehicle and the pedestrian is $t_1 + t_1' = 0.2+0.135 = 0.335$ seconds. The space covered by the pedestrian during this phase is $x_1+x_1' = 2.46+1.47 = 3.93$ m. The distance covered during the flight phase is $x_2 = 7.96$ m, and the sliding distance on the ground is $x_3 = 2.97$ m.

4.2. Comparison with Accident Reconstruction Software

Grounded on the model proposed by the authors of this paper, the analysis of this case leads to a pedestrian throw distance of 34.43 m, at an impact speed of 68 km/h. Using the PC-Crash (2008) application which is based on a multibody pedestrian model (Moser *et al.*, 1999, 2000), the pedestrian throw distance is 34 m for the same impact speed.

The input data were the following;

- a = – 4 m/s^2 – average brake deceleration from the moment prior to the first impact with the pedestrian;
- m_v = 1,040 kg – vehicle mass;
- m_p = 75 kg – pedestrian mass;
- h = 1 m – height at which the pedestrian falls off the vehicle;
- t_1 = 0.2 s – time at which the pedestrian hits the hood-windshield area with the head;
- α = 16 degrees – pedestrian launch angle;
- μ = 0.75– friction coefficient between the pedestrian and the ground;
- η = 0.75 – pedestrian impact factor.
- D = 34 m – pedestrian throw distance measured at the place of the accident.

The calculated error is 1.2 % or 0.43 m.

4.3. Comparison of Pedestrian Throw Distance with the Data Experimentally Obtained

Taking into account that some input parameters cannot be but approximated and previously analyzing their influence upon the pedestrian throw distance, friction coefficient between the pedestrian and the ground hold a major influence. Thus, we extracted limits of this coefficient from the specialist literature, as shown in Table 1.

In our analysis we choose a coefficient value of 0.52, being known that fact that the testing experiments took place on a dry concrete track. A zero value was chosen at the end of phase 1 for the pedestrian launch angle off the vehicle, the analysis of impact video recordings leading to this conclusion.

Table 1. After (Stevenson, 2006).

Author	Friction coefficient	Type of surface
Searle (1983)	0.66	Asphalt
	0.79	Grass
Collins (1979)	1.1	
Severy (1966)	0.4 ~ 0.75	
Fricke (1990)	0.45 ~ 0.6	Asphalt
	0.4 ~ 0.65	Concrete
	0.45 ~ 0.7	Grass
Stevenson (2006)	0.57 ~ 0.58	Asphalt
	0.54 ~ 0.6	Grass

Time "t_1" of 0.195 s was obtained from the recordings on deceleration diagrams of the dummy pedestrian head, Figure 6.

Input data;

- v_0' = 8.216 m/s^2 = vehicle speed at the moment of the first contact with the pedestrian
- a = – 4 m/s^2 – average brake deceleration from the moment prior to the first impact with the pedestrian;
- m_v = 1,024 kg – vehicle mass;
- m_p = 73 kg – pedestrian mass;
- h = 1 m – height at which the pedestrian falls off the vehicle;
- t_1 = 0.195 s – time at which the pedestrian hits the hood-windshield area with the head;
- α = 0 degrees – pedestrian launch angle;
- μ = 0.52 – friction coefficient between the pedestrian and the ground;
- η = 0.883 – pedestrian impact factor.

There follows;

- D = 7.01 m – pedestrian throw distance measured at the place of the accident, at the dummy's hip, as compared to the initial contact point.

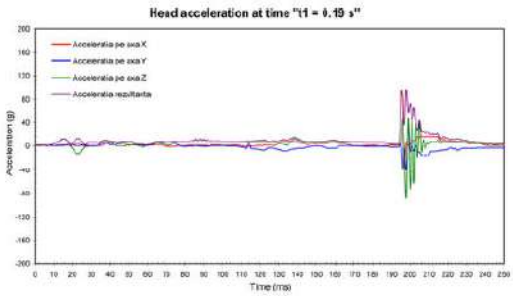

Figure 6. End time of sub-phase 1.1 – The pedestrian hits the windshield with the head, experimental data.

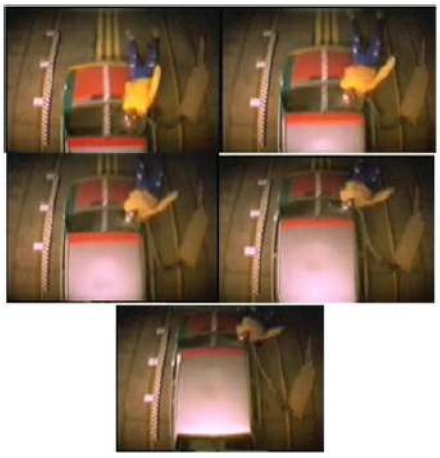

Figure 7. Sub-phase 1.2 – Carrying the pedestrian on hood until the launch in the flight phase. Frames at 200, 250, 300, 350, 400 ms, recording from above.

The formula proposed showed a pedestrian throw distance of 6.87 m, with the contact time $t_1 + t_1' = 0.195 + 0.202 = 0.397$ seconds. The space covered by the pedestrian during this phase is $x_1 + x_1' = 1.42 + 1.307 = 2.73$ m. The distance covered during the flight phase is $x_2 = 2.75$ m, and the sliding distance on ground is $x_3 = 1.4$ m. The calculated error is 2 % or 0.14 m.

Likewise, the high speed camera recordings show the existance of sub-phase 1.2 of the primary impat; during this phase the pedestrian is carried on the vehicle hood, Figures 3 and 7.

The length of time when the pedestrian is carried on the vehicle may be determined with

$$\eta \cdot v = v + a \cdot t_1' \tag{25}$$

$$t_1' = \frac{v \cdot (\eta - 1)}{a} \tag{26}$$

The model proposed for the impact characteristics previously enumerated shows a time, "t_1' " of 0.202 seconds, comparable with the time of approximately 0.208 seconds resulted from the analysis of high speed recordings.

4.4. Identification of Sub-phase 1.2. by Other Experimental Data

For lower vehicle speeds, and not only, the authors argue that the model presented may help determine the distance covered by the pedestrian during the contact with the vehicle. As determined from experimental researches, by analyzing the high-speed films, the distance covered by the pedestrian during the contact with the touring car, distance that is made up of distances $x_1 + x_1'$, is greater than the

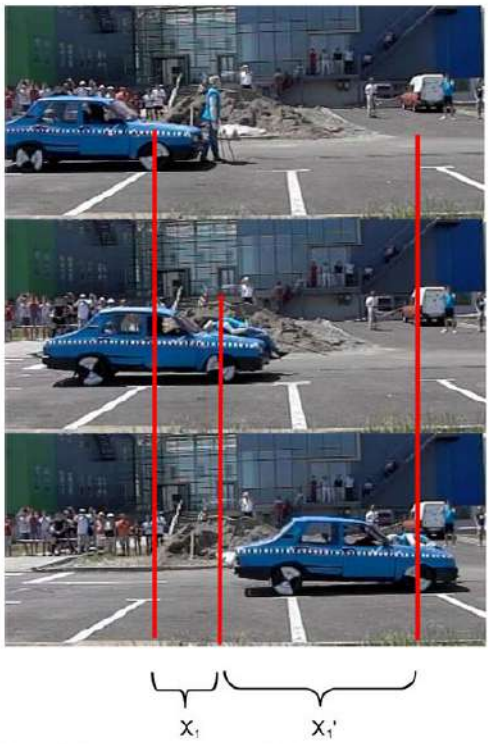

Figure 8. Sub-phases 1.1 and 1.2 – Carrying the pedestrian on hood, test no. 4.

distance approximated through the bilinear function presented in Han and Brach (2001).

The pedestrian "carry" sub-phase has not been considered by the specialist literature reviewed. Together with the sub-phase between the first and secondary impact, the distance covered by the vehicle-pedestrian assembly until the pedestrian falls off the vehicle is greater than the approximations given by the bilinear law (0.5 m ~ 1.5 m). This contention is confirmed through experimental determinations presented in Figures 8 – 11 and Table 2. The experimental determinations undertook tests with adult pedestrians in different positions at the moment of the primary impact: hit while standing still, hit on the side, hit while walking, hit when wearing special harness.

Vehicles front geometry varied, the tests were carried out on 6 types of vehicles with different front profiles. The collision speeds ranged between 20 km/h and 40 km/h, except for case number 9 for which we do not have information on impact speed. In the cases subjected to analysis the distance covered by the pedestrian between the primary and secondary impact ranged between 0.8 ~ 1.7 meters, distance at the upper limit or greater than the one considered in the bilinear model, Figure 11. After the

Table 2. Distance covered in total pedestrian carry phase.

Case no.	Vehicle/ test no.	Vehicle speed (m/s)	X_1 (m)	X_1' (m)	X_1+X_1' (m)
1	V1_t1	8.21	1.40	1.30	2.70
2	V1_t2	8.36	1.00	2.25	3.25
3	V2	8.05	1.70	2.75	4.45
4	V3_t1	5.86	1.20	3.60	4.80
5	V3_t2	8.08	1.45	2.65	4.10
6	V3_t3	8.88	1.35	3.50	4.85
7	V4	6.94	1.10	2.70	3.80
8	V5	~ 10.66	1.20	2.40	3.60
9	V6	n.a.	0.80	1.20	2.00

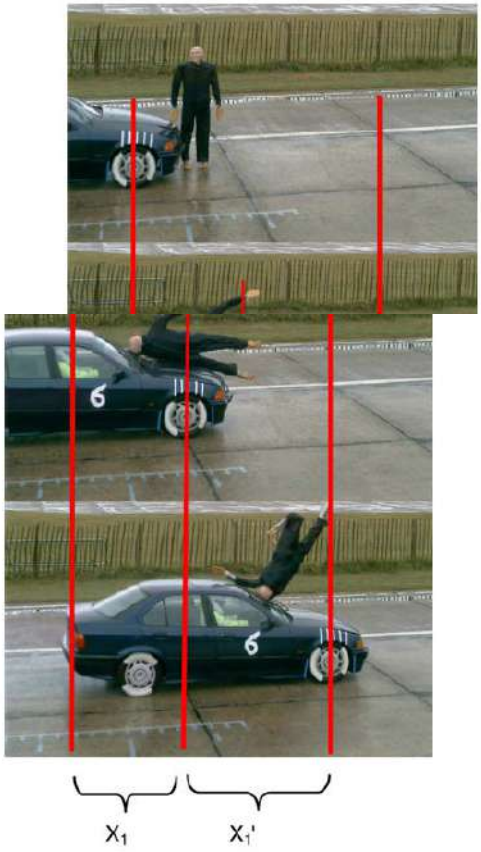

Figure 9. Sub-phases 1.1 and 1.2 – Carrying the pedestrian on hood, test no. 8 (Pedestrian Accident Demonstration, 2013).

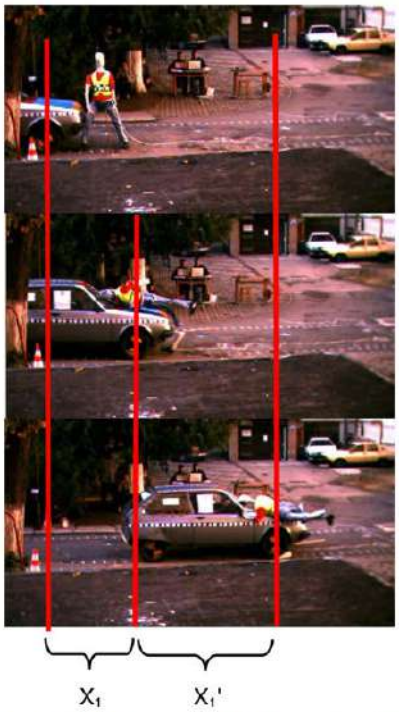

Figure 10. Sub-phases 1.1 and 1.2 – Carrying the pedestrian on hood, test no. 3 (Togănel, 2008).

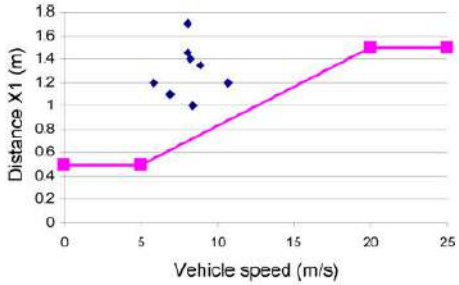

Figure 11. Comparison between carry distance on vehicle, sub-phases 1.1, and bilinear function.

secondary impact some pedestrians were carried on the hood, others rolled down and fell along the side of the vehicle and others were projected up in the air when the vehicle had high speed. The distance covered by the vehicle from the secondary impact to the moment the pedestrian fell off the vehicle varied between 1.20 and 3.60 meters. As a consequence, the total distance covered by the pedestrian during the contact phase with the vehicle ranges

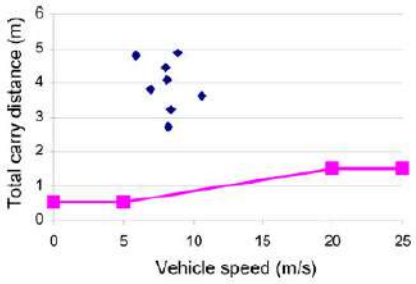

Figure 12. Comparison between total carry distance on vehicle, sub-phases 1.1 and 1.2, and bilinear function.

between 2.00 m ~ 4.85 m, see Figure 12 where all the points experimentally obtained were marked, as compared to the distance covered by the pedestrian as proposed through the bilinear law.

For lower impact speeds the flight phase is almost undetectable, at the end of the contact phase with the vehicle the pedestrian falls off in front or along the side of the vehicle, depending on the movement generated after the first contact.

Although the total projection distance of the pedestrian does not modify through the model proposed, the share of the distances covered by the pedestrian during each phase varies. Thus, the distance covered during the contact phase with the vehicle increases while the distance covered during the flight phase diminishes. For impact speeds of about 30 km/h, the distance covered by the pedestrian during the contact phase may amount to 50 % of the total projection distance, as can be seen from the graph in Figure 4.

At the speed of 40 km/h a 30 % ratio between the distance covered by the pedestrian during the contact phase with the vehicle and the total projection phase, in line with the graph from Figure 4, may be observed.

5. CONCLUSION

The model presented shows results comparable with those in current models e.g. (Kuhnel-Schulz, PC-Crash, Batista, Han), with the data resulted from the casuistry submitted to analysis by the authors of this research, as well as with those experimentally obtained.

In-depth research is called for with regard to the distance covered by the pedestrian on the vehicle during the contact phase as the real cases show that the approximation bilinear function does not provide sufficiently accurate results.

Vehicle-pedestrian collisions are governed by complex phenomena and are influenced by many factors that cannot be modelled with precision. Decomposing the pedestrian-vehicle contact phase into two sub-phases and generalizing formulae for the vehicle motion (constant or under brake) during this phase, gives the possibility ro reconstruct various typologies of road traffic accidents, within precision limits comparable with other methods and models.

Future research upon a good corelation between the carryng time of pedestrian and the impact coefficent η should be conducted.

REFERENCES

Batista, M. (2008). A simple throw model for frontal vehicle pedestrian collisions. *Promet-Traffic & Transportation* **20**, 6, 357–368.

Brooks, D., Wiechel, J., Sens, M. and Guenther, D. A. (1987). A comprehensive review of pedestrian impact reconstruction. *SAE Paper No.* 870605.

Oh, C., Kang, Y-S., Kim, B. and Kim, W. (2005). Analysis of Pedestrian-vehicle Crashes in Korea: Focused on Developing Probabilistic Pedestrian Fatality Model, http://www-nrd.nhtsa.dot.gov/pdf/esv/esv19/05-0131-w.pdf

Collins, J. C. and Moris. J. L. (1979). *Highway Collision Analysis*. Thomas Publishing. Springfield, Illinois.

Dettinger, J. (1996). *Methods of Improving the Reconstruction of Pedestrian Accidents: Development Differential, Impact Factor, Longitudinal Forward Trajectory, Position of Glass Splinters (in German)*. Verkehrsunfall und Fahrzeugtechnik. München, Germany, 324–330.

Dettinger, J. (1997). *Methods of Improving the Reconstruction of Pedestrian Accidents: Development Differential, Impact Factor, Longitudinal Forward Trajectory, Position of Glass Splinters (in German)*. Verkehrsunfall und Fahrzeugtechnik. München, Germany, 25–30 (Two Parts).

Eubanks, J. J. and Haight, W. R. (1992). Pedestrian involved traffic collision reconstruction methodology. *SAE Paper No.* 921591.

Evans, A. K. and Smith, R. (1999). Vehicle speed calculation from pedestrian throw distance. *Proc. Inst. Mech. Engrs. Part D*, **213**, 441–447.

Fricke, L. B. (1990). Traffic Accident Reconstruction. Vol. 2 of the Traffic Accident Investigation Manual.

Han, I. and Brach, R. M. (2001). Throw model for frontal pedestrian collisions. *SAE Paper No.* 2001-01-0898.

Hill, G. S. (1984). Calculations of vehicle speed from pedestrian throw, *Impact*, 18–20.

Jun, X., Yibing, L., Guangquan, L. and Wei, Z. (2009). Reconstruction model of vehicle impact speed in pedestrian – Vehicle accident. *Int. J. Impact Engineering*, **36**, 783–788.

Kuhnel, A. (1980). *Der Fahrzeug Fussganger Unfall und seine Rekonstruktion*. Dissertation. TU-Berlin. Berlin, Germany.

Limpert, R. (1999). *Motor Vehicle Accident Reconstruction and Cause Analysis*. 5th edn. Lexis Publishing. Charlottesville, Virginia, USA, 539–554.

Moser, A., Hoschopf, H., Steffan, H. and Kasanicky, G. (2000). Validation of the PC-crash pedestrian model. *SAE Paper No.* 2000-01-0847.

Moser, A., Steffan, H. and Kasanicky, G. (1999). The pedestrian model in PC-crash – The introduction of a multi body system and its validation. *SAE Paper No.* 1999-01-0445.

OCDE (2000). Report of the Hundred and Seventeenth Round Table on Transport Economics Held in Paris on 26th-27th October 2000 on the following topic: Economic Evaluation Of Road Traffic Safety Measures.

PC-CRASH (2008). A Simulation Program for Vehicle Accidents. Technical Manual. Version 8.1, March.

Pedestrian Accident Demonstration (2013). http://www.youtube.com

Rau, H., Otte, D. and Schulz, B. (2000). Pkw-fußgangerkollisionen im hohen geschwindigkeitsbereich ergebnisse von dummyversuchen mit kollisions-geschwindigkeiten zwischen 70 and 90 km/h. *Verkehrsunfall und Fahrzeugtechnik*, **12**, 341–350.

Ravani, B., Brougham, D. and Masson, R. T. (1981). Pedestrian post impact kinematics and injury pattern. *SAE Paper No.* 811024.

Searle, J. A. (1993). The physics of throw distance in accident reconstruction. *SAE Paper No.* 930659.

Searle, J. A. and Searle, A. (1983). The trajectories of pedestrians, motorcycles, motorcyclists, etc., following a road accident. *SAE Paper No.* 831622.

Severy, D. and Brink, H. (1966). Auto-pedestrian collision experiments using full-scale accident simulation. *SAE Paper No.* 660080.

Simms, C., Wood, D. and Walsh, D. (2004). Confidence limits for impact speed estimation from pedestrian, projection distance. *IJCrash* **9**, **2**, 219–228.

Stevenson, T. J. (2006). *Simulation of Vehicle-Pedestrian Interaction.* Ph. D. Dissertation. University of Canterbury. Canterbury, New Zealand.

Toor, A. and Araszewski, M. (2003). Theoretical vs. empirical solutions for vehicle/pedestrian collisions. *SAE Paper No.* 2003-01-0883.

Togănel, G. (2008). *Cercetări Privind Influenta Designului Caroseriei Asupra Sigurantei Pasive a Automobilelor.* Ph. D. Dissertation. Transilvania University of Brasov. Brasov, Romania.

Wood, D. and Simms, C. (2000). Coefficient of friction in pedestrian throw. *Impact – J. ITAI* **9**, **1**, 12–14.

Wood, D., Simms, C. and Walsh, D. G. (2005). Vehicle-pedestrian collisions: Validated models for pedestrian impact and projection. *Proc. IMechE, Part D: J. Automobile Engineering* **219**, **2**, 183–195.

Optimization of Cooling System for Internal Combustion Engines

Radu Tarulescu[1], Stelian Tarulescu[1], Adrian Soica[1]

[1] Transilvania University of Brasov, Brasov, Romania
s.tarulescu@unitbv.ro, radu.tarulescu@unitbv.ro,
a.soica@unitbv.ro

Abstract. In this paper, the authors tackle the problem of energetic optimization of the cooling system of internal combustion engines (heat exchanger, water pump, air ventilator, hydraulic transport installation and thermostat) by the adjustment of fluid flows and their economic correlation. The adjustments can be primary, secondary and combined, resulting different characteristics, emphasized by numeric application. The increase of economic efficiency ε_{ec} (indicator defined by authors), for imposed thermal efficiency ε_t, leads to energetic savings due to the reduction of driving power and fuel consumption.

Keywords: Mass Flow, Coolant, Energetic Efficiency, Heat exchanger

1 Introduction

The paper tackles the problem of energetic optimization of the cooling system of internal combustion engines by the adjustment of fluid flows, namely the coolant and air. The adjustment will be carried out by modifying the revolution speed of water pump and ventilator. The adjustment can be:

- Primary, with the variable mass flow of coolant $\dot{m}_{coolant}$ and constant mass flow of air $\dot{m}_{air}$;
- Secondary, with the constant mass flow of coolant $\dot{m}_{coolant}$ and variable mass flow of air $\dot{m}_{air}$;
- Combined, with the variable mass flow of coolant $\dot{m}_{coolant}$ and variable mass flow of air $\dot{m}_{air}$, with the optimum ratio between them $R_{\dot{m}} = \frac{\dot{m}_{coolant}}{\dot{m}_{air}}$.

Different characteristics result in each case. The increase of economic efficiency ε_{ec}, considering the imposed thermal efficiency ε_t, leads to energetic savings due to the reduction of driving power and fuel consumption.

2 Theoretical considerations

The heat exchanger transfers the heat flow Φ[W] from the primary hot fluid (coolant) to the secondary cold fluid (air), consuming the hydraulic $N_{coolant}$[W] and air power N_{air}[W] from the pump and fan, both driven by the internal combustion engine [1].
The total fluid drive power N_{drive}[W] has the following expression:

$$N_{drive} = N_{coolant} + N_{air} = K_1 \cdot \dot{m}^3_{coolant} + K_2 \cdot \dot{m}^3_{air}\,[\mathrm{W}], \tag{1}$$

where K_1 and K_2 are dimensional constant values which express the linear and local resistance to the flow of fluids (coolant and air) through the heat exchanger.
The authors define the economic/energetic efficiency of the cooling system from the relation:

$$\varepsilon_{ec} = \frac{\Phi}{N_{drive}} = \frac{\Phi}{N_{coolant} + N_{air}} = \frac{\Phi}{K_1 \cdot \dot{m}^3_{coolant} + K_2 \cdot \dot{m}^3_{air}}, \tag{2}$$

as a functional, dimensionless, energetic and performance indicator. The aim is that the drive power N_{drive} should be as low as possible so that the economic efficiency ε_{ec} may be as high as possible, which can be obtained by the optimum ratio:

$$R_{\dot{m}} = \frac{\dot{m}_{coolant}}{\dot{m}_{air}}, \tag{3}$$

and by reducing the values of hydraulic resistances $K_1 \rightarrow$ min and $K_2 \rightarrow$ min.
The thermal, dimensional capacities are given by the relations [2]:

$$W_{coolant} = \dot{m}_{coolant} \cdot c_{coolant} \text{ and } W_{air} = \dot{m}_{air} \cdot c_{air}\,[\mathrm{W/K}], \tag{4}$$

where $c_{coolant}$[kJ/kg·K] and c_{air}[kJ/kg·K] are the specific mass heats of the two fluids.
The thermal efficiency of the heat exchanger is defined as the ratio of heat loads of the two fluids:

$$\varepsilon_t = \frac{W_{coolant} \cdot (T_1 - T_2)}{W_{\min} \cdot (T_1 - T_1')} = \frac{W_{air} \cdot (T_2' - T_1')}{W_{\min} \cdot (T_1 - T_1')}, \tag{5}$$

where T_1[K] and T_2[K] are the inlet and outlet temperatures of the coolant from the heat exchanger, T_1'[K] and T_2'[K] are the inlet and outlet temperatures of the air from the heat exchanger and W_{min}[W/K] is the minimum flow of thermal capacity between $W_{coolant}$[W/K] and W_{air}[W/K]. The counter-flow device with the infinite heat exchanger surface S[m^2] has $\varepsilon_t = 1$.

As thermal, dimensionless, performance indicator, the aim is to obtain $\varepsilon_t \rightarrow$ max, which leads to the optimum ratio $R_{\dot{m}} = \frac{\dot{m}_{coolant}}{\dot{m}_{air}}$, the specific temperatures and heats being known.

In the case of more complex heat exchangers, such as the case with crossed circulation of fluids, the calculation of heat load can be carried out with the method suggested by Nusselet, according to which [3]:

$$\Phi = F \cdot k \cdot S \cdot \Delta T_{med}, \tag{6}$$

where F[-] is the sub-unitary correction factor, S[m^2] is the total surface of heat exchange, k[W/m^2K] is the global coefficient of heat exchange and ΔT_{med} is the average logarithmic difference of temperatures.

$$\Delta T_{med} = \frac{\Delta T_{\max} - \Delta T_{\min}}{\ln \frac{\Delta T_{\max}}{\Delta T_{\min}}} \text{ [K]}, \tag{7}$$

in which

$$\Delta T_{\max} = T_2 - T_1' \text{ [K] and } \Delta T_{\min} = T_1 - T_2' \text{ [K]} \tag{8}$$

The sub-unitary, dimensionless correction factor, determined experimentally or theoretically, is expressed as a function:

$$F = f(P, R), \tag{9}$$

where

$$P = \frac{T_2' - T_1'}{T_1 - T_1'} \text{ and } R = \frac{T_1 - T_2}{T_2' - T_1'} \tag{10}$$

The correction factor F can be calculated using the relations specific to every type of exchanger or can be determined from diagrams set out with their help [4].

The thermal efficiency, defined by relation (5) has the expression:

$$\varepsilon_t = \frac{1 - \exp\left[-\frac{k \cdot S}{W_{\min}} \cdot \left(1 - \frac{W_{\min}}{W_{\max}}\right)\right]}{1 - \frac{W_{\min}}{W_{\max}} \cdot \exp\left[-\frac{k \cdot S}{W_{\min}} \cdot \left(1 - \frac{W_{\min}}{W_{\max}}\right)\right]}, \tag{11}$$

Noting down the dimensionless expression $kS/W_{min} = HTU_{max}$ (The number of heat transfer units), the following general relation is obtained [5]:

$$\varepsilon_t = \frac{1-\exp\left[-HTU_{max}\cdot\left(1-\frac{W_{min}}{W_{max}}\right)\right]}{1-\frac{W_{min}}{W_{max}}\cdot\exp\left[-HTU_{max}\cdot\left(1-\frac{W_{min}}{W_{max}}\right)\right]}, \quad (12)$$

For the constant values K_1 and K_2 from relation (2), the authors obtained the expression:

$$K_i = \left(\frac{\Sigma\xi+\lambda\cdot\frac{l}{4\cdot R_h}}{2\cdot\rho^2\cdot A^2}\right)_i, i=1,2, \quad (13)$$

in which ρ_i[kg/m^3] are the densities of the two fluids, A_i[m^2] are the flow areas through the heat exchanger of the two fluids, $R_{h,i}$[m] are the equivalent hydraulic radiuses, l[m] is the total length of hydraulic and air pipes, λ is the coefficient of linear losses and $\Sigma\xi$ is the sum of coefficients of local losses.

3 Numerical application

We consider that the internal combustion engine, with the nominal power N_{nom} = 100hp = 73kW, has the capacity to carry out overloads of up to 25%. We suggest the conventional heat exchanger, for the maximum load of the internal combustion engine, which ensures: T_1 = 95[°C] (constant value by thermostat adjustment), T_2 = 80[°C], T_1' = 15[°C], T_2' = 40[°C]. It results that $\Delta T_{coolant}$ = 15[K], and ΔT_{air} = 25[K].
ΔT_{max} = 338.15[K], ΔT_{min} = 328.15[K], P = 0.313, R = 0.6, F = 0.98, ΔT_{med} = 333.33[K] were calculated.

Table 1. Computed values of the conventional heat exchanger parameters

N_{nom}	Φ	$\dot{m}_{cool}$	$\dot{m}_{air}$	N_{cool}	N_{air}	$R_{\dot{m}}$	ε_t	ε_{ec}
[kW]	[kW]	[kg/s]	[kg/s]	[kW]	[kW]	[-]	[-]	[-]
73.5	25.8	0.41	1.03	1.8	0.252	0.4	0.31	10.0
84.5	25.8	0.41	1.03	1.8	0.252	0.4	0.31	11.5
92.0	25.8	0.41	1.03	1.8	0.252	0.4	0.31	12.5

The following dimensions were obtained (dimensioned): S = 0.65[m^2], $c_{coolant}$ = 4.187[kJ/kg·K], c_{air} = 1[kJ/kg·K] and k = 120[W/m^2·K].

$K_1 = 26[W \cdot s^3/kg^3]$ and $K_2 = 230[W \cdot s^3/kg^3]$ were calculated for the heat exchanger geometry $A_{coolant} = 4.18 \cdot 10^{-4}[m^2]$, $l_{coolant} = 7[m]$, $A_{air} = 2.78 \cdot 10^{-2}[m^2]$ and $l_{air} = 10[m]$. The results presented in Table 1 correspond to the conventional heat exchanger, dimensioned for the maximum allowed overload (at the maximum revolution speed of the internal combustion engine). The rate flows of coolant and air are constant, in an optimized ratio $R_{\dot{m}} = \frac{\dot{m}_{coolant}}{\dot{m}_{air}} = 0.4 = const.$. The drive powers $N_{coolant}$ and N_{air} are in proportion to the revolution speed of the internal combustion engine. The cooling system has the constant thermal efficiency ε_t and economic efficiency which increases along with the load. The values obtained are acceptable, conventional.

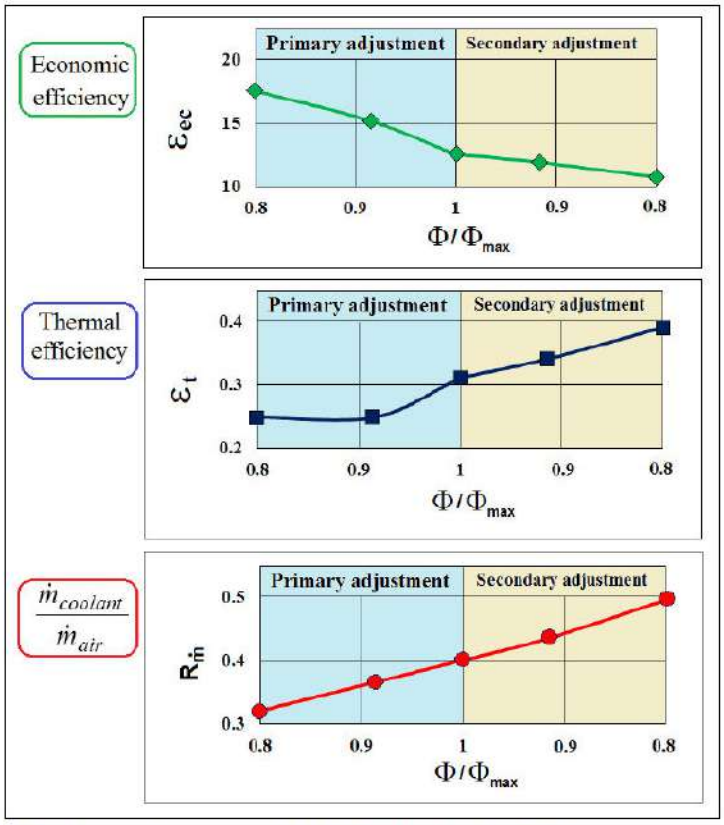

Fig. 1. Dimensional characteristic of primary and secondary adjustments

Table 2, Fig. 1 and Fig. 2 presents the modified characteristics of the heat exchanger in case of primary adjustment, which enables independent driving of the internal combustion engine, for example by means of an electric motor with a constant speed of the fan. The ratio $R_{\dot{m}}$ becomes variable, along with the drive revolution speed of the pump. The power N_{air} is constant and power $N_{coolant}$ is variable, in proportion to the revolution speed of the pump.

Table 2. Computed values of the heat exchanger in case of primary adjustment

N_{nom}	Φ	Φ/Φ_{max}	$\dot{m}_{cool}$	$\dot{m}_{air}$	N_{cool}	N_{air}	$R_{\dot{m}}$	ε_t	ε_{ec}
[kW]	[kW]	[-]	[kg/s]	[kg/s]	[kW]	[kW]	[-]	[-]	[-]
73.5	20.6	0.8	0.328	1.03	0.92	0.25	0.32	0.24	17.5
84.5	23.6	0.915	0.377	1.03	1.4	0.25	0.36	0.24	15.1
92.0	25.8	1	0.410	1.03	1.8	0.25	0.40	0.31	12.5

The thermal efficiency of the heat exchanger ε_t becomes variable, maximum at the maximum overload of the engine. The economic efficiency ε_{ec} is increased, a lot higher than in the case from Table 1, especially at the nominal power and partial overloads of the internal combustion engine.

Table 3. Computed values of the heat exchanger in case of secondary adjustment

N_{nom}	Φ	Φ/Φ_{max}	$\dot{m}_{cool}$	$\dot{m}_{air}$	N_{cool}	N_{air}	$R_{\dot{m}}$	ε_t	ε_{ec}
[kW]	[kW]	[-]	[kg/s]	[kg/s]	[kW]	[kW]	[-]	[-]	[-]
73.5	20.6	0.8	0.41	0.825	1.8	0.12	0.49	0.39	10.7
84.5	23.6	0.915	0.41	0.94	1.8	0.19	0.43	0.34	11.8
92.0	25.8	1	0.41	1.03	1.8	0.25	0.4	0.31	12.5

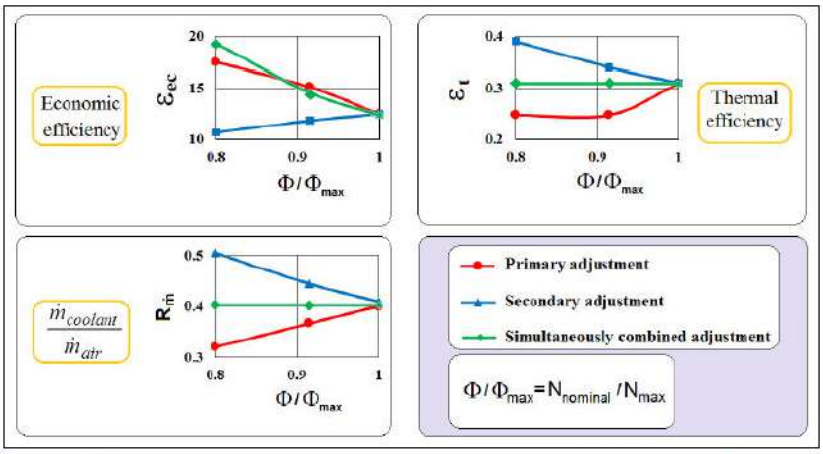

Fig. 2. Differences between the primary, secondary, and simultaneously combined adjustments

Table 3, Fig. 1 and Fig. 2 presents the modified characteristics of the heat exchanger in case of the secondary adjustment, with the variable ratio $R_{\dot{m}}$, decreasing along with the revolution speed of the internal combustion engine. The power $N_{coolant}$ is constant and the power N_{air} is variable increasing along with the revolution speed ventilator. The thermal efficiency of the heat exchanger ε_t becomes higher at nominal power and partial overloads. The economic efficiency ε_{ec} is slightly increased compared to the case presented in Table 1, increasing along with the heat load.

Table 4. Computed values of the heat exchanger in case of simultaneously combined adjustment

N_{nom}	Φ	Φ/Φ_{max}	$\dot{m}_{cool}$	$\dot{m}_{air}$	N_{cool}	N_{air}	$R_{\dot{m}}$	ε_t	ε_{ec}
[kW]	[kW]	[-]	[kg/s]	[kg/s]	[kW]	[kW]	[-]	[-]	[-]
73.5	20.6	0.8	0.328	0.825	0.923	0.129	0.4	0.31	19.5
84.5	23.6	0.915	0.377	0.94	1.4	0.190	0.4	0.31	14.8
92.0	25.8	1	0.410	1.03	1.8	0.252	0.4	0.31	12.6

Table 4 and Fig. 2 presents the modified characteristics of the heat exchanger in case of the simultaneously combined adjustment, with variable mass flows of both fluids, increasing in proportion to the load, but in an optimized ratio, $R_{\dot{m}} = \frac{\dot{m}_{coolant}}{\dot{m}_{air}} = 0.4 = const.$. The drive powers $N_{coolant}$ and N_{air} are variable, increasing proportionally with the load. The thermal efficiency ε_t remains constant, having the same value as in the case presented in Table 1. The economic efficiency ε_{ec} becomes efficient and higher than in the cases above, decreasing along with the load increase.

4 Conclusions

The analysis carried out shows a way of optimizing the cooling system of internal combustion engines by adjusting the flow rates according to the speed of the water pump and the air fan. Three different settings were performed, one primary with the variable mass flow rate of coolant and the constant air mass flow rate, a secondary one with the constant mass flow rate of coolant and the variable air mass flow and a mixed one with both variable. In the first two cases the thermal efficiency of the heat exchanger and the economic efficiency increase, and in the third case the thermal efficiency remains constant and the economic efficiency increases considerably.

The cooling system presented in this paper can be implemented on a vehicle with average power, with nominal consumption of 5.5 liters of fuel at 100 km and overload consumption (of up to 25% of the total available time) of 7 liters of fuel at 100 km.

For the covered distance of 200.000 km, according to calculations, the double adjustment of the cooling system of the internal combustion engine leads to the fuel saving of 1340 liters.

References

1. Bohacz, R. T., Engine cooling systems. Penguin Press, (2007).
2. Heat Exchanger Design Handbook. Second Edition, Taylor & Francis Inc Publisher, Bosa Roca, United States, (2013).
3. Lin, W., Sunden, B., Vehicle Cooling Systems for Reducing Fuel Consumption and Carbon Dioxide. Literature Survey, SAE Technical Paper, (2010).
4. Annaratone, D., Handbook for Heat Exchangers and Tube Banks design. Springer Berlin Heidelberg Publisher, (2010).
5. Tarulescu, R., Benche, V., Horizontal micro-carrier of heat and mass. Annals of the Oradea University, Oradea University Press, ISSUE 1, pp. 397-400, (2013).